OSCILLATING FIELD CURRENT DRIVE EXPERIMENTS IN THE MADISON SYMMETRIC TORUS

by

Arthur P Blair Jr

A dissertation submitted in partial fulfillment of
the requirements for the degree of

Doctor of Philosophy

(Physics)

at the

UNIVERSITY OF WISCONSIN–MADISON

2006

Dedicated to the memory of my father, for his unending words of encouragement: "So when are you graduating already?"

ACKNOWLEDGMENTS

I thank John Sarff, Karsten McCollam, Paul Nonn, Stewart Prager, and the entire MST gang for making OFCD the grand(ish) success it is.

DISCARD THIS PAGE

TABLE OF CONTENTS

Page

ABSTRACT v

1 Introduction 1

1.1 Motivation 1
1.2 Oscillating Field Current Drive 2
1.3 History 3
1.4 Summary of Experimental and Theoretical Results 4
1.5 Outline 6

2 Review of magnetic helicity and relaxation 7

2.1 The Reversed Field Pinch 7
2.2 Magnetic Helicity 9
2.3 Taylor's theorem and relaxation 11
2.4 Magnetic and Current Profile Models 13
2.5 Rational Surfaces, fluctuations, and instabilities 14
2.6 MHD dynamo 17
2.7 Reconnection 18
2.8 Dynamics of RFP relaxation 21

3 The Physics and Modelling of OFCD 26

3.1 Helicity Injection 26
3.2 Oscillating Field Current Drive 28
3.3 Numerical Studies 30
3.3.1 The 1D model 31
3.4 Summary 61

4 Experimental Setup 66

4.1 The Madison Symmetric Torus 66
4.2 The Ignitron Oscillator 67

Page

4.3 Diagnostics . . . 78
4.3.1 Edge magnetic probes . . . 78
4.3.2 Rutherford Scattering . . . 79
4.3.3 FarInfraRed interferometer . . . 80
4.3.4 Thomson scattering . . . 80
4.3.5 CHERS/IDS . . . 81
4.3.6 Edge probe . . . 81

5 The Experiments . . . 83

5.1 OPCD . . . 84
5.1.1 Sawtooth Entrainment . . . 88
5.1.2 Mode Spectra . . . 93
5.1.3 Anomalous Ion Heating . . . 102
5.2 OTCD . . . 109
5.2.1 Mode Spectra . . . 113
5.3 OFCD . . . 116
5.3.1 280 Hz . . . 116
5.3.2 530 Hz . . . 142
5.3.3 Anomalous Ion Temperature Modulation . . . 142
5.3.4 Temperature profiles . . . 148
5.3.5 Resistivity profile . . . 152
5.3.6 Penetration . . . 152
5.3.7 What happens if $F > 0$? . . . 157

6 Summary and Conclusions . . . 169

6.1 Future plans . . . 173

LIST OF REFERENCES . . . 175

OSCILLATING FIELD CURRENT DRIVE EXPERIMENTS IN THE MADISON SYMMETRIC TORUS

Arthur P Blair Jr

Under the supervision of Professor Stewart Prager

At the University of Wisconsin-Madison

Oscillating Field Current Drive (OFCD) is an inductive current drive method for toroidal pinches. To test OFCD, two 280 Hz 2 MVA oscillators were installed in the toroidal and poloidal magnetic field circuits of the Madison Symmetric Torus (MST) Reversed Field Pinch (RFP.) Partial sustainment experiments were conducted where the two voltage oscillations were superimposed on the standard MST power supplies. Supplementary current drive of about 10% has been demonstrated, comparable to theoretical predictions. Maximum current drive does not coincide with maximum helicity injection rate - possibly due to an observed dependence of core and edge tearing modes on the relative phase of the oscillators. A dependence of wall interactions on phase was also observed. Experiments were conducted at 280 and 530 Hz. 530 Hz yielded little or no net current drive. Experiments at 280 Hz proved more fruitful. A 1D relaxed state model was used to predict the performance of OFCD and to optimize the design of hardware. Predicted current drive was comparable to experimental values, though the aforementioned phase dependence was not. Comparisons were also made with a more comprehensive 3D model which proved to be a more accurate predictor of current drive. Both 1D and 3D models predicted the feasability of full sustainment via OFCD. Experiments were also conducted with only the toroidal field oscillator applied. An entrainment of the natural sawtooth frequency to our applied oscillation was observed as well as a slow modulation of the edge tearing mode amplitudes. A large modulation (20 to 80 eV) of the ion temperature was also observed that can be partially accounted for by collisional heating via magnetic pumping. Work is in progress to increase the power of the existing OFCD hardware.

Stewart Prager

ABSTRACT

Oscillating Field Current Drive (OFCD) is an inductive current drive method for toroidal pinches. To test OFCD, two 280 Hz 2 MVA oscillators were installed in the toroidal and poloidal magnetic field circuits of the Madison Symmetric Torus (MST) Reversed Field Pinch (RFP.) Partial sustainment experiments were conducted where the two voltage oscillations were superimposed on the standard MST power supplies. Supplementary current drive of about 10% has been demonstrated, comparable to theoretical predictions. Maximum current drive does not coincide with maximum helicity injection rate - possibly due to an observed dependence of core and edge tearing modes on the relative phase of the oscillators. A dependence of wall interactions on phase was also observed. Experiments were conducted at 280 and 530 Hz. 530 Hz yielded little or no net current drive. Experiments at 280 Hz proved more fruitful. A 1D relaxed state model was used to predict the performance of OFCD and to optimize the design of hardware. Predicted current drive was comparable to experimental values, though the aforementioned phase dependence was not. Comparisons were also made with a more comprehensive 3D model which proved to be a more accurate predictor of current drive. Both 1D and 3D models predicted the feasability of full sustainment via OFCD. Experiments were also conducted with only the toroidal field oscillator applied. An entrainment of the natural sawtooth frequency to our applied oscillation was observed as well as a slow modulation of the edge tearing mode amplitudes. A large modulation (20 to 80 eV) of the ion temperature was also observed that can be partially accounted for by collisional heating via magnetic pumping. Work is in progress to increase the power of the existing OFCD hardware.

Chapter 1

Introduction

1.1 Motivation

Like most toroidal plasma confinement schemes, the Reversed Field Pinch relies on induction to provide the toroidal current, which in turn provides the poloidal magnetic field that aids confinement. A large magnetic flux, ϕ, is driven through the region that threads the center of the torus. Growing with time it induces a toroidal loop voltage via Faraday's law ($\dot{\phi} = -V$), which in turn drives the toroidal current, which in turn provides the poloidal field. But the current that creates the flux cannot ramp up forever, so eventually the flux stops growing, the toroidal electric field and current die off, and the plasma is quenched. Transformers don't work at DC. So a tractable pulsed or steady-state current drive scheme is needed if the RFP is to become a viable candidate in the quest for fusion. RF and neutral beam injection current drive may provide solutions but are invasive, inefficient in reactor regimes, and expensive.

Bevir and Gray [3] first suggested that applying AC toroidal and poloidal loop voltages to the plasma could overcome the natural resistive decay of helicity, an important geometric attribute of the field lines. Helicity is a measure of the 'knottedness' of the magnetic field lines within some volume. Maintaining global helicity would, presumably, translate into maintaining the current in the plasma. The result would thus provide a more-or-less steady-state solution. On the physics end, the usual fields that maintain the RFP are static. Time varying magnetic fields, especially fields that oscillate on a time scale between the extremes of Alfvenic propagation and resistive dissipation, provide a new avenue for studying reconnection, transport, and the MHD dynamo in the RFP. The oscillating edge fields are expected to have a significant impact on the current profile that drives tearing instabilities, pushing the dynamics of RFP plasma's into unexplored territory.

1.2 Oscillating Field Current Drive

In Oscillating Field Current Drive(OFCD), also known as AC helicity injection, two oscillating electric fields, one toroidal and one poloidal, are applied to the surface of the plasma. Together, they drive a current in the edge with a significant DC component, altering the radial current profile. The plasma responds to this imposed current gradient by exciting tearing fluctuations near the core which feed an MHD dynamo ($\tilde{v} \times \tilde{B}$) that drives current in the core, thus redistributing the parallel current from the edge to the core of the plasma. The long term hope is that this injected current can take over as the power supply after the conventional power supply saturates.

Figure 1.1 shows a high level diagram of how OFCD is implemented on MST. Two high-power audio-frequency oscillators are magnetically coupled to the toroidal and poloidal field circuits. They are tuned to the same frequency. The phase difference between them is adjusted for maximum current drive.

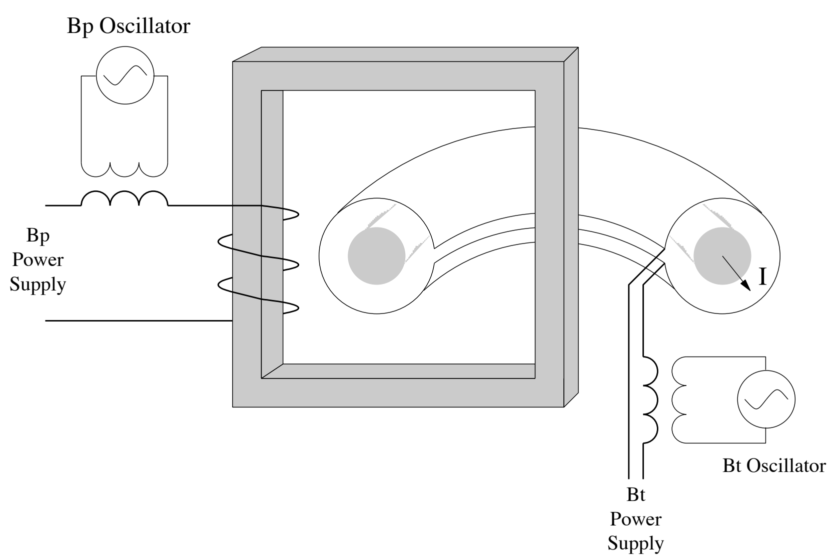

Figure 1.1 OFCD schematic

1.3 History

OFCD was first proposed by Bevir and Gray [3] in 1981 as a means of overcoming the transient nature of toroidal pinches. Theoretical and computational studies by Jensen and Chu[7] showed that a consequence of injecting helicity (by any means) is the generation of parallel current. In 1984 Schoenberg[5] et al reported numerical studies supporting Bevir and Gray using a 0-D model. Also reported was initial experimental data from the ZT-40 RFP but oscillating only one loop voltage at a time. In 1984 Schoenberg et al [14] further described computational studies detailing the nonlinear interactions between the toroidal and poloidal loop voltages and the ramifications for OFCD. In 1985 Bevir[8] reported optimistic results of a 0-D RFP model and a 1-D resistive diffusion model and even provided a prediction of the additional current drive assuming OFCD is turned on after the usual starting voltage. In 1985 Bellan[9] disputed Bevir and Grays contention that relaxation (described in chapter 2) was necessary for helicity injection but that it was necessary for redistribution of the edge current to the core. Bellan argued that the helicity injection resulted from a beating of a compressional Alfvén mode with a resistive diffusion mode in the edge. In 1986 Finn[11] reported still more optimistic results using a 1-D model assuming relaxation within the plasma and a resistive decay of skin currents in the edge. Not to be outdone, Nebel[12] and crew instilled even more theoretical confidence in OFCD by using six (count em six) different models including a hyper-resistivity model that included the effects of tearing mode interactions. Finally, inspired by the unending optimism of all these theorists, Schoenberg[14] et al tested OFCD with real hardware in the ZT-40 RFP at Los Alamos. They met with mixed results. Some effects as predicted by theory were experimentally verified. As much as 5% current drive was observed at low power operation. But no positive current drive was observed at higher power levels, precluding full sustainment by OFCD. This was probably due to wall interactions driving the resistivity up and a frequency of applied oscillation that was too high. These are problems we hope to avoid on MST. MST is better suited for OFCD experiments since the plasma is larger and hotter which translates into lower required voltages. MST has the added advantage of being well instrumented in the diagnostics most relevant to studying OFCD physics.

OFCD is not the only way to inject helicity into a toroidal plasma. Any scheme that drives current will inject helicity. In electrostatic helicity injection[16], the intersection of the magnetic field and two electrodes is explicitly controlled so that $\mathbf{B} \cdot \hat{\mathbf{n}} \neq 0$ at the probes. The probes are biased with a fixed potential, driving a current across the field lines. The obvious disadvantage of electrostatic helicity injection is that hot particles will follow the field lines into the probes. A variation of electrostatic heicity injection is coaxial helicity injection[17]. A small blob of plasma with a spheromak-like magnetic field is fired into the plasma from a coaxial gun. The blob carries its own field line knottedness adding to that of the torus. The entangled field lines of the blob spread out and magically arrange themselves within the pre-injection toroidal plasma. The method saw a brief surge of current after which the plasma cooled having merged with the relatively cooler blob.

1.4 Summary of Experimental and Theoretical Results

Two audio frequency high-power oscillators were designed, built, and integrated into MST's toroidal and poloidal circuits. Each oscillator delivered up to about 2 MVA of reactive power to satisfy the enormous power requirements of OFCD. In an effort to determine the optimum frequency for current drive, experiments have been conducted at 530 and 280 Hz.

The toroidal field oscillator came online before the poloidal field oscillator so the first set of experiments studied the plasma's response to it. Since an oscillating toroidal field induces an oscillating poloidal current these experiments came to be known as OPCD (Oscillating Poloidal Current Drive). Control variables included oscillator amplitude, coupling coefficient between oscillator and MST, and equilibrium plasma current and density. We found that as much as 30 kW of the available power was absorbed by the plasma, presumably to simple resistive dissipation. Interesting effects observed in OPCD experiments include an entrainment of the sawtooth instabilities to the applied oscillation, decoupled entrained bursts of core and edge fluctuations, and a substantial but difficult-to-reproduce oscillation in the ion temperature. We also found that the plasma was far from the relaxed state at 530 Hz. This ultimately led to experiments at the lower frequency.

Once the poloidal field oscillator was brought online we again conducted experiments with just this one oscillator running. Since an oscillating poloidal magnetic field yields an oscillating toroidal current these experiments came to be known as OTCD (Oscillating Toroidal Current Drive.) Since the equilibrium poloidal field in an RFP is substantially larger than the toroidal field our OTCD perturbation was much less significant than OPCD and we saw little discernable effect on the plasma.

With both oscillators running we began OFCD experiments. Control variables included oscillator amplitudes and relative phasing, equilibrium plasma current and density. We found effects on the plasma fluctuations and instabilities were similar to those of OPCD. The most interesting effect was that of the relative phase between the oscillators. According to theory, there is an optimum phase ($90°$) for helicity injection and, presumably, current drive. We measured the mean current at this optimum phase (Drive) and $180°$ from it (Antidrive) and found that the *difference* was very nearly the difference predicted by theory, offering a ray of hope that the plasma was at least to some extent responding as expected. As far as current drive, at 530 Hz we saw no consistent increase in the plasma current even at the optimum phase. In fact, OFCD appeared to actually decrease the mean current from its equilibrium value. We suspect two confounding effects may be at play. First, the $F - \Theta$ trajectory indicates that the oscillation rate is too high for the plasma to remain in its usual nearly-relaxed state. Second, as with ZT-40, we are seeing a slight increase in plasma impurities after the oscillation begins.

In the final set of experiments, in order to allow the plasma to strive to achieve the relaxed minimum-energy state throughout the period of oscillation, the frequency of both oscillators was decreased to 280 Hz. The control variables were the same as at 530 Hz. At the lower frequency we saw oodles[1] of current drive, easily maintaining a steady state RFP with no ohmic drive for hours and hours. Fusion was readily achieved until the vacuum vessel melted. Actually, we saw as much as 20kA of additional current drive on top of the nominal 255 kA. This was about what we expected/hoped-for from theoretical studies.

[1] An industry term.

As for those theoretical studies, two tools were employed not only to predict the plasma's behavior but to optimize the applied oscillation to maximize the current drive without upsetting the plasma too much. One was the nonlinear 3D plasma simulation tool DEBS, an acronym whose meaning no one seems to know. Studies by Ebrahimi[22] showed current drive and a plasma response comparable to experimental results. They showed a phase dependent current drive and a modification of the tearing instabilities. The other tool was a macroscopic relaxed state model that presumed a current profile described by the alpha model (described later,) an energy balance equation derived from Poynting's theorem, and nothing else. The algorithm predicted current drive also comparable to experimental results - remarkable for such a simplified model. The relaxed state model was also employed in an effort to optimize the shape of the applied oscillation to maximize current drive and minimize the modulation of the toroidal field at the wall. This effort met with disappointing results due to the plasma's persistent ability to filter any waveform down to a single low frequency sine-wave.

1.5 Outline

In chapter 2 we briefly review the physics of the RFP that are most relevant to OFCD. We'll introduce the concepts of magnetic helicity and relaxation culminating in Taylor's theorem. In chapter 3 we discuss the physics of OFCD including one and three dimensional numerical studies. In chapter 4 we describe the experimental setup including MST, the oscillators, and diagnostic instruments used to study the plasma. In chapter 5 we discuss the experimental procedures and results for various hardware configurations and plasma control variables. Chapter 6 wraps it up.

Chapter 2

Review of magnetic helicity and relaxation

To understand the physics of OFCD we need to introduce some relevant plasma physics. In section 2.1 we discuss the Reversed Field Pinch, the platform on which we will apply OFCD. This leads to section 2.2 and the concept of magnetic helicity, a key geometric attribute of the magnetic field lines in a toroidal pinch that plays a pivotal role in OFCD. Section 2.3 discusses Taylor's theorem which describes the ideal equilibrium state of toroidal pinches, an equilibrium we hope to sustain (on average) with OFCD. Sections 2.5 through 2.8 describe the dynamics that lead to the Taylor state.

2.1 The Reversed Field Pinch

Most toroidal pinch devices start with the same recipe. 1) Take a large hollow steel or aluminum torus and suck the air out of it. 2) Squirt in a little hydrogen or deuterium gas along with a few loose electrons to start ionizing the gas. 3) Run a large poloidal current around the perimeter of the vessel. In MST the vacuum vessel itself carries the poloidal current. This generates the toroidal magnetic field. 4) Run a large toroidal current through the plasma, induced via transformer action. This toroidal current finishes ionizing the gas, heats the plasma, and generates the poloidal magnetic field. The poloidal and toroidal components of the magnetic field combine to create a corkscrew pattern characteristic of toroidal pinches and linear screw pinches. The field lines arrange themselves on concentric toroidal surfaces called flux surfaces. Those flux surfaces on which the field lines close on themselves are called rational surfaces since the ratio of the poloidal turns/toroidal turns for one field line is a rational number. Rational surfaces are especially important for reasons explained later.

In a tokamak the toroidal field is far stronger than the poloidal field. In the RFP they are comparable, the poloidal field being somewhat stronger over most of the plasma cross-section. This eventually leads to the peculiar magnetic field configuration shown in figure 2.1. At some radius (the reversal surface) the toroidal field spontaneously reverses direction giving the RFP its name.

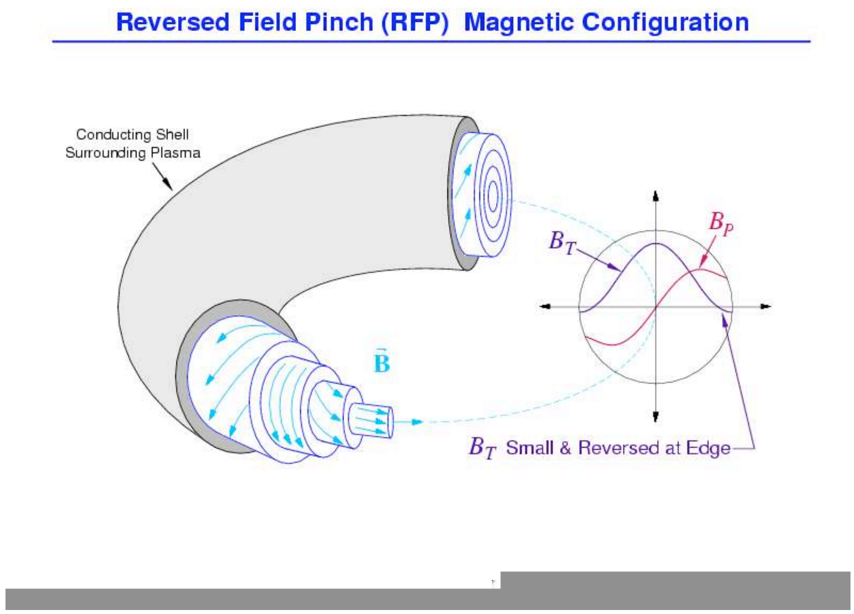

Figure 2.1 Magnetic field lines in an RFP

Taylor[2] explained this unexpected plasma state by starting with the postulate that a magnetically confined plasma left to its own devices while in electrical contact with a perfectly conductive boundary (the vessel) would 'relax' to the state of lowest magnetic energy while conserving total magnetic helicity, a measure of flux linkage. Note that Taylor describes an equilibrium state. Taylor's theorem tells us nothing about how the plasma gets there.

In MHD, the dynamics required to achieve the Taylor state is driven by the MHD dynamo, to be discussed in the section on the MHD Dynamo.

2.2 Magnetic Helicity

Magnetic helicity is a measure of magnetic flux linkage. Imagine two 'tubes' of magnetic flux ϕ_1 & ϕ_2 linked as in figure 2.2. The magnetic helicity of this picture would be $2\phi_1\phi_2$.

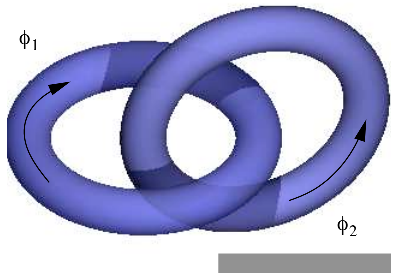

Figure 2.2 Linked tubes of magnetic flux

The formal definition of helicity is

$$\mathbf{K} = \int \mathbf{A} \cdot \mathbf{B} \, dV$$

where **A** is the magnetic vector potential, **B** is the magnetic field, and the integral is taken over the volume of all space. For the example above, consider a section of one tube as in figure 2.3

$$\mathbf{K} = \int \mathbf{A} \cdot \mathbf{B} \, dV = \int \int \mathbf{A} \cdot \mathbf{B} \, d\mathbf{a} \, d\mathbf{l}$$

Since $\mathbf{B} \cdot d\mathbf{a} = d\phi_1$ where $d\mathbf{a}$ is the cross sectional area:

$$\begin{aligned} \mathbf{K} &= \int \int \mathbf{A} \, d\phi_1 \, d\mathbf{l} = \phi_1 \int \mathbf{A} \cdot d\mathbf{l} \\ &= \phi_1 \int \nabla \times \mathbf{A} \cdot d\mathbf{a} \end{aligned}$$

where $\int d\mathbf{a}$ is the area encircled by tube 1 (thus intersected by tube 2)

$$\mathbf{K} = 2\phi_1 \int \mathbf{B} \cdot d\mathbf{a} = 2\phi_1\phi_2$$

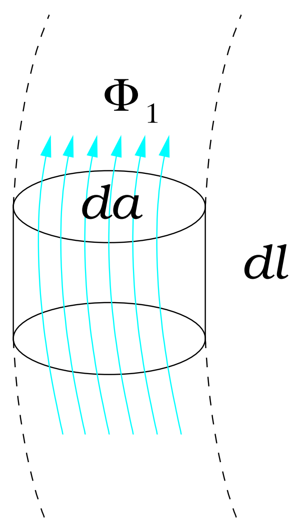

Figure 2.3 Differential element of flux tube 1

The 2 is thrown in to account for the volume integral over the other flux tube.

The toroidal current in a magnetically confined toroidal device is driven by transformer action. A large magnetic flux is ramped up in an iron or air core that threads through the center of the torus inducing a large toroidal electric field which drives a large toroidal current which provides a large poloidal magnetic field. To maintain gauge invariance the linkage of this imposed flux and the net toroidal flux have to be removed from our definition of K.

$$\mathbf{K} = \int \mathbf{A} \cdot \mathbf{B}\, dV - \phi_T \phi_{ext} \tag{2.1}$$

where ϕ_{ext} is the flux that threads the central hole of the torus[6]. For a linear or toroidal pinch the integral is taken over the entire volume of the plasma to yield the *global magnetic helicity*.

2.3 Taylor's theorem and relaxation

For a pressure-free plasma in equilibrium the momentum equation

$$\rho \frac{d\mathbf{v}}{dt} = \mathbf{J} \times \mathbf{B} - \nabla p \tag{2.2}$$

becomes just $\mathbf{J} \times \mathbf{B} = 0$ implying $\mathbf{J}$ is everywhere parallel to $\mathbf{B}$ or, in terms of just $\mathbf{B}$,

$$\nabla \times \mathbf{B} = \Lambda \mathbf{B} \tag{2.3}$$

where Λ is some scalar function of radius.

In 1974 Taylor[2] derived a minimum magnetic energy equilibrium for a pressure free linear screw pinch in contact with a perfectly conducting boundary assuming a conservation of global magnetic helicity, and conservation of toroidal flux. The result was a flat normalized current profile[1] $\Lambda = J(r)/B(r) = constant$ and magnetic field profiles $B_z = B_0 J_0(\mu r)$ and $B_\theta = B_0 J_1(\mu r)$ where J_0 and J_1 are the zeroth and first order Bessel functions of the first kind. With the right values of μ this equilibrium state has a peculiar property; the toroidal field reverses direction near the edge.

[1]Reader beware. J/B is often erroneously referred to as the current profile. We may slip from time to time in this thesis and call it that.

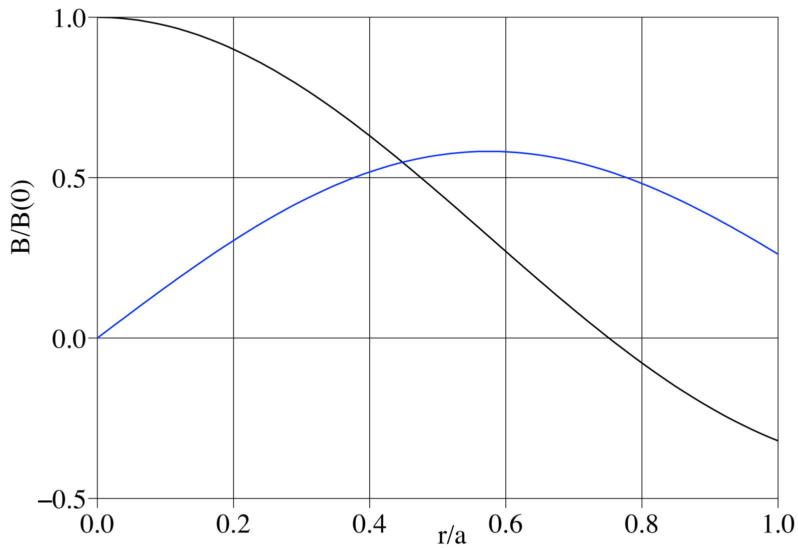

Figure 2.4 The magnetic field profiles according to Taylor.

2.4 Magnetic and Current Profile Models

The magnetic field profile of a plasma in the Taylor state is described by the Bessel Function Model (BFM) (even though it is more a conclusion than a model.) The BFM profile is shown in figure 2.4. The shape of the magnetic field profile in the BFM can be (and usually is) characterized by the pinch parameter $\Theta = B_\theta(r = a)/ < B_z >$.

Taylor's results describe a normalized current profile, J/B, that is flat across the radius. In reality, the current profile cannot be flat. Since the plasma rests against a cool wall the resistivity is so much higher at the edge that J/B at r=a must go to zero. Also, the parallel electric field, $E_\|$, drops below zero at the wall where the toroidal field is reversed. Also the electric field in any torus driven by a central flux trails off with 1/R (or thereabouts) where R is the distance from the center of the donut hole. So, for a variety of reasons the current profile is never flat. To coerce Taylor's results into accommodating reality, various models of either the magnetic field or the current profile have been used in the past to account for this, including the Modified Bessel Function (MBFM)[4] which assumes the current profile J/B is flat out to some point (typically r/a = .7) then drops linearly to zero at the edge. Another is the Polynomial Function Model (PFM)[15] that smoothly drops to zero at the edge and includes the effect of the pressure profile. Like the BFM, the PFM is characterized by Θ (but at r=0.) Another is the less restrictive Modified Polynomial Function Model[19] that does the same but is characterized by both Θ and the reversal parameter $F = B_z(r = a)/ < B_z >$ yielding a more accurate shape. Finally there is the alpha model that is characterized by the value of $\lambda_0 = J/B$ on axis and a shape factor α. Figure 2.5 shows the sundry models using experimental values for the characteristic parameters. The alpha model is the most fashionable model in MST because it comes closest to reality and can be fitted exactly to the edge measured values of F and Θ. It will be used throughout this thesis.

It bears emphasizing that the alpha model and company cannot really be placed on the same plane as the Bessel Function Model. The BFM is a product of Taylor's theory. The others are just parameterizations of reality used for numerical studies and toroidal equilibrium reconstruction.

Whatever model is used, the RFP equilibrium state can be completely characterized by the two dimensionless parameters F and Θ. A curve in figure 3.18 of F vs Θ shows the locus of points available to the RFP. Roughly speaking, F is proportional to the toroidal field, and hence the poloidal current while Θ is proportional to the poloidal field, and hence the toroidal current. So the relation between F and Θ represents a nonlinear coupling between the toroidal and poloidal circuits of the RFP. We exploit this nonlinearity in OFCD.

It bears repeating that the Taylor state is an equilibrium state. The dynamics of getting there is another question entirely.

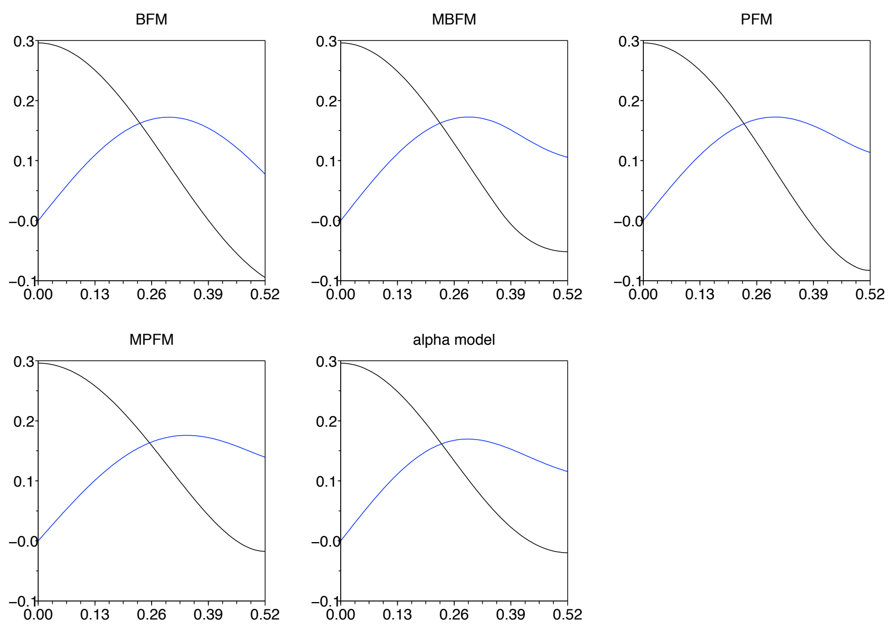

Figure 2.5 The various models of magnetic field profile. The black curves are the toroidal field vs radius. The blue curves are the poloidal field.

2.5 Rational Surfaces, fluctuations, and instabilities

Every gradient in a magnetized plasma is a source of free energy. The gradient in the current profile in the RFP drives waves that fluctuate both the plasma velocity **v** and the magnetic field, distorting the flux surfaces. Because of the periodicity in the poloidal and toroidal directions and the boundaries in the radial direction, waves in any torus are of the form

$$f(\mathbf{r})e^{i(\mathbf{k}\cdot\mathbf{r})}e^{i\omega t} = f(\mathbf{r})e^{i(m\theta+n\phi)}e^{i\omega t} \tag{2.4}$$

where $\mathbf{k}$ is the wave number, m and n are the poloidal and toroidal mode numbers, ω is either their frequency of oscillation ($Im(\omega) = 0$), growth rate $Re(\omega) = 0, Im(\omega) > 0$, or both. At the rational flux surfaces, waves that propagate everywhere perpendicular to the equilibrium magnetic field lines, with

$$\mathbf{k}\cdot\mathbf{B_0} = 0 \rightarrow \frac{rB_\phi}{RB_\theta} = -\frac{m}{n} \tag{2.5}$$

can grow without bound causing all sorts of problems including increased transport. This is because, on a rational surface, there is none of the field line bending that would otherwise stabilize any perturbation. Magnetic field lines have tension like a rubber band. Those modes that require a lot of field line bending are more stable than those that don't. Compounding that, magnetic reconnection (described later) can occur at the rational surfaces. The ratio rB_ϕ/RB_θ is the safety factor $q(r)$. On a rational surface $q(r) = m/n$, hence the name. There are obviously a countably infinite number of rational surfaces each with its own m/n fluctuations but modes beyond $m = 1$ are stable[28] and n values beyond about 32 are of such short wavelengths that they are suppressed by viscous and resistive damping and magnetic field line bending (short wavelengths require more bending.) Figure 2.6 shows a typical q profile for MST. Marked are the m=1 rational surfaces. Take note of the crowding of the m=1 surfaces near the reversal (m=0) surface.

In MST, the first $m = 1$ flux surface is at $n = 5$, at about r=10 cm (though, as the plasma profile evolves with time, $q(0) < 1/5$ more often so the n=6 mode is usually dominant.) In any toroidal magnetized plasma, instabilities occur wherever $q < 1$. Unfortunately $q < 1$ everywhere in the RFP. The *shear* of the plasma, the rate of change of adjacent field lines with r, is the slope dq/dr. The steeper the shear the more difficult it is for instabilities to grow.

The fluctuations have components in all directions, but of particular interest are the radial components

$$\tilde{B}_r, \tilde{v_r} \sim e^{i(m\,\theta+n\,\phi)}e^{i\omega t} \tag{2.6}$$

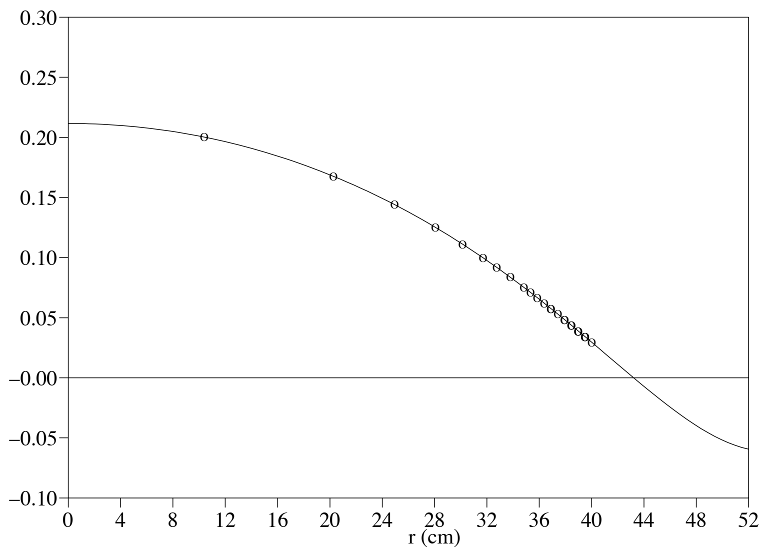

Figure 2.6 A typical q profile in MST

since the radial direction is exactly where we do not want the plasma to go. We will usually approximate the torus as a periodic cylinder so that the toroidal angle $\phi = z/R$.

Of the sundry fluctuations that can occur in an RFP the ones of most interest are the resistive tearing modes. These are long wavelength modes that displace the entire plasma, have frequency content up to tens of kilohertz due to toroidal rotation, and growth periods at a hybrid time scale of $\sqrt{\tau_R \tau_A}$ where τ_R is the resistive diffusion time and τ_A is the Alfvèn time. On a rational surface they are resonant giving these surfaces the synonym, oddly enough, *resonant surfaces*.

2.6 MHD dynamo

Looking at Ohm's law from the MHD equations

$$\mathbf{E} + \mathbf{v} \times \mathbf{B} = \eta \mathbf{J} \tag{2.7}$$

we see there are two terms driving current in the plasma, the applied electric field and the $\mathbf{v} \times \mathbf{B}$ term. Dynamo action is prevalent in the RFP both as a means of approaching the relaxed state and as an irritant driving transport. The dynamo is driven by fluctuations in $\mathbf{v}$ and $\mathbf{B}$ arising from current-driven instabilities within the plasma and flow driven by the applied fields.

We can break $\mathbf{v}$ and $\mathbf{B}$ up into their equilibrium and fluctuating components:

$$\mathbf{v} = \mathbf{V}_0 + \sum_{m,n} \tilde{\mathbf{v}}_{mn} \quad where\ \tilde{\mathbf{v}}_{mn} = |\tilde{\mathbf{v}}_{mn}| e^{i(m\theta + n\phi - w_{mn}t)} \tag{2.8}$$

$$\mathbf{B} = \mathbf{B}_0 + \sum_{m,n} \tilde{\mathbf{b}}_{mn} \quad where\ \tilde{\mathbf{b}}_{mn} = |\tilde{\mathbf{b}}_{mn}| e^{i(m\theta + n\phi - \omega_{mn}t)} \tag{2.9}$$

where $\mathbf{V_0}$ and $\mathbf{B_0}$ are the equilibrium values. The $\mathbf{v} \times \mathbf{B}$ term then becomes

$$\mathbf{v} \times \mathbf{B} = \mathbf{V}_0 \times \mathbf{B}_0 + \sum_{mn} [\mathbf{V}_0 \times \tilde{\mathbf{b}}_{mn} + \tilde{\mathbf{v}}_{mn} \times \mathbf{B}_0] + \sum_{mnm'n'} \tilde{\mathbf{v}}_{mn} \times \tilde{\mathbf{b}}_{m'n'} \tag{2.10}$$

The spatial average of the second term is 0. Most important are the third terms where $m = 1$ ($\tilde{\mathbf{v}}_{1n} \times \tilde{\mathbf{b}}_{1n'}$.) These make up the *MHD dynamo* that is essential to the plasmas effort to achieve a relaxed state. As important as they are, the magnetic fluctuations $\tilde{\mathbf{b}}_{mn}$ are only about 1% of the equilibrium field strength. The need for the dynamo is illustrated in figure 2.7 which shows the parallel (to $\mathbf{B_0}$) time and magnetic surface averaged(¡¿) component of Ohm's law

$$\mathbf{E}_{\|} + \left\langle \tilde{\mathbf{v}}_{\mathbf{mn}} \times \tilde{\mathbf{b}}_{\mathbf{mn}} \right\rangle_{\|} = \eta \mathbf{J}_{\|} \tag{2.11}$$

$\mathbf{E}_{\|}$ is the applied parallel electric field, and $\mathbf{J}_{\|}$ is the net current driven. Note that they are not equal. A third term is required to balance them. The balance is supplied by the MHD dynamo $\tilde{\mathbf{v}} \times \tilde{\mathbf{b}}$.

2.7 Reconnection

In an ideal resistance-free plasma the magnetic field lines are frozen in the fluid. Any displacement of the plasma carries the field lines with it. In this idealism there exists a singularity at a resonant surface that can only be resolved by introducing at least a small resistivity to the plasma.

Picking a rational surface where the fluctuations are resonant and hence unstable, we look at the effect of the growing radial component $\tilde{\mathbf{b}_\mathbf{r}}$ on the equilibrium field. Looking down at a horizontal cut we first subtract the equilibrium helical field strength at the surface as shown in figure 2.8(a). figure 2.8 (b) shows the beginning of the instability. In (c) the field lines on opposite sides of the surface touch. Because of the resistivity in the plasma the field lines lose their identity and can break. Because $\nabla \cdot \mathbf{B} = 0$ dictates that no field line can have a loose end flopping about, the lines have to either break away and return to their original geometry or reconnect and form islands as in (d). They form islands because that geometry has a lower magnetic field energy than the original state. As a cheap analogy, imagine the field lines were stretched rubber bands. When they meet at the separatrix, with a little glue, they lose their identity. Cutting them so that they can relax into smaller circles would obviously reduce the net tension in the system compared to cutting them so they end up as they were before they met.

Reconnection in the RFP is driven by the aforementioned tearing modes (hence the name.) In MHD the modes are stationary (0 frequency). In the two-fluid model of plasma physics and in the experiments, the modes are travelling waves and carry the islands with them. As the m=1 islands grow and begin to interact their coupling 'locks' them together so they all move at about the same velocity; so the above picture works. This interaction is a major source of momentum transport.

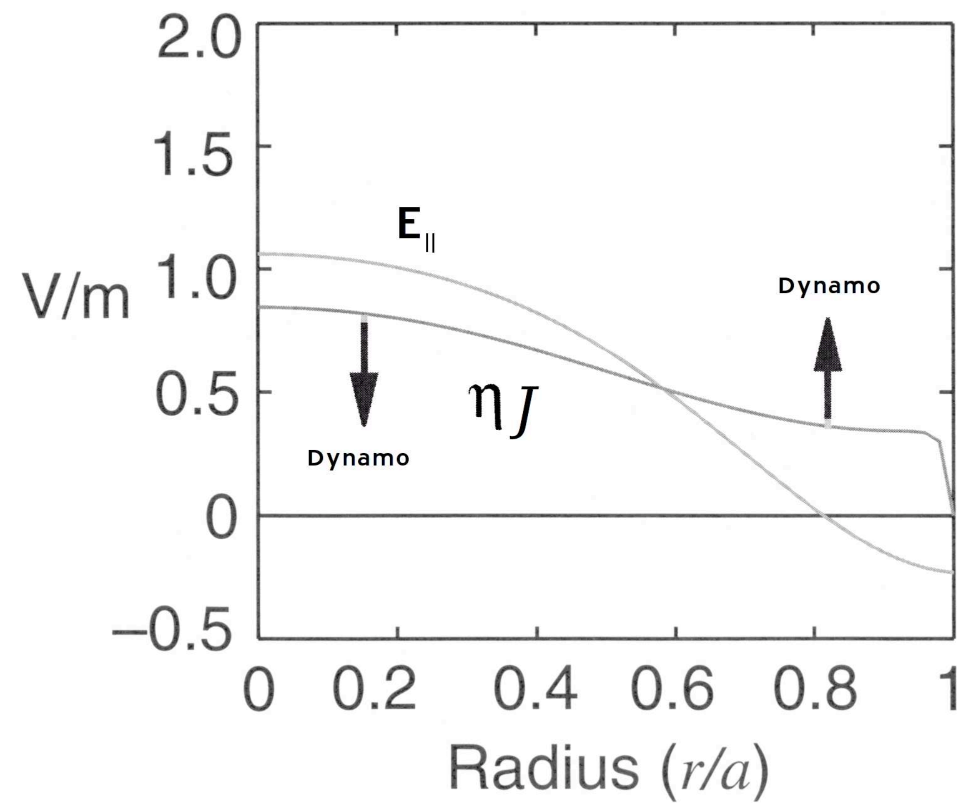

Figure 2.7 The MHD dynamo balances the difference in Ohms law by driving current in the edge

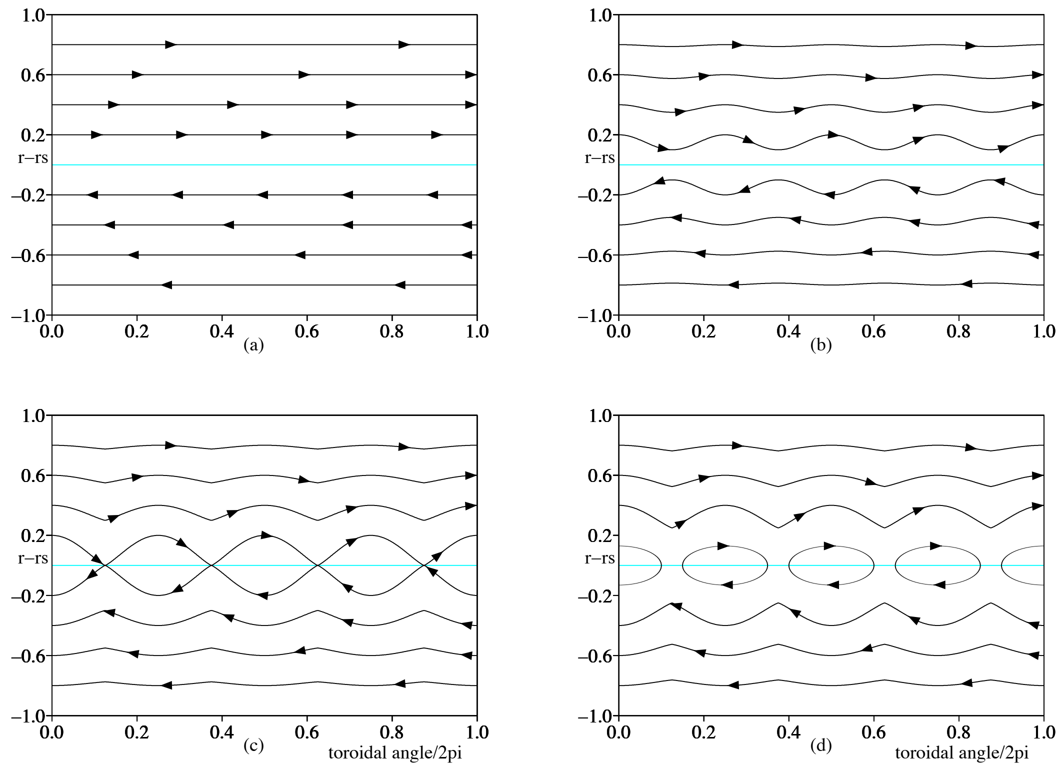

Figure 2.8 Evolution of magnetic reconnection at a resonant surface.

As the islands grow they eventually overlap. The island widths are

$$W_{m,n} = \sqrt{\frac{16\tilde{B}_{rm,n} r_s}{nB_\theta(r_s)} \frac{1}{\|dq/dr\|}} \tag{2.12}$$

where $\tilde{B}_{rm,n}$ is the (m,n) component of the radial magnetic fluctuation amplitude, r_s is the radius of the rational surface, and n is the toroidal mode number. The islands are shown superimposed in the q profile in figure 2.9. Note that the island widths are smaller at higher n where they are almost stabilized by the higher shear.

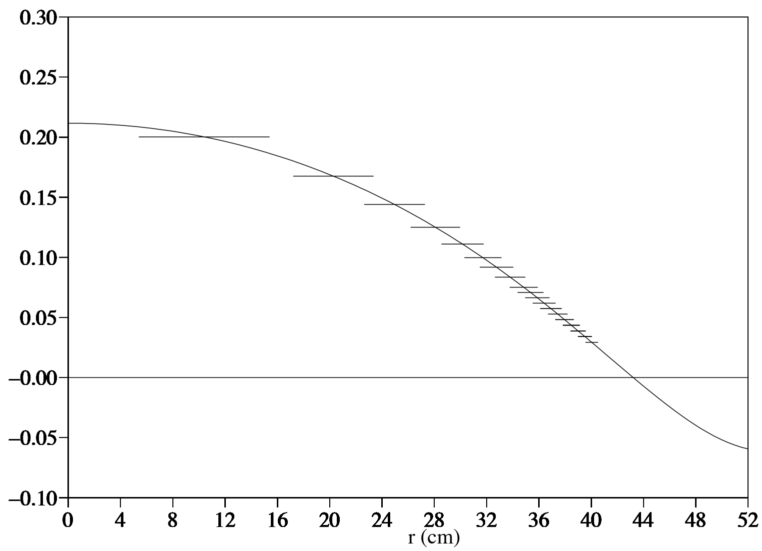

Figure 2.9 The q profile with island widths at the resonant surfaces

2.8 Dynamics of RFP relaxation

When the islands overlap, the nice orderly flux surfaces between them are destroyed and the magnetic field becomes stochastic as shown in figure 2.10. Note that while the higher shear might render them more stable, overlap of the modes at higher values of the toroidal mode number n is nevertheless unavoidable since the islands are packed so much closer together. In a typical plasma the mid-region of MST is always stochastic.

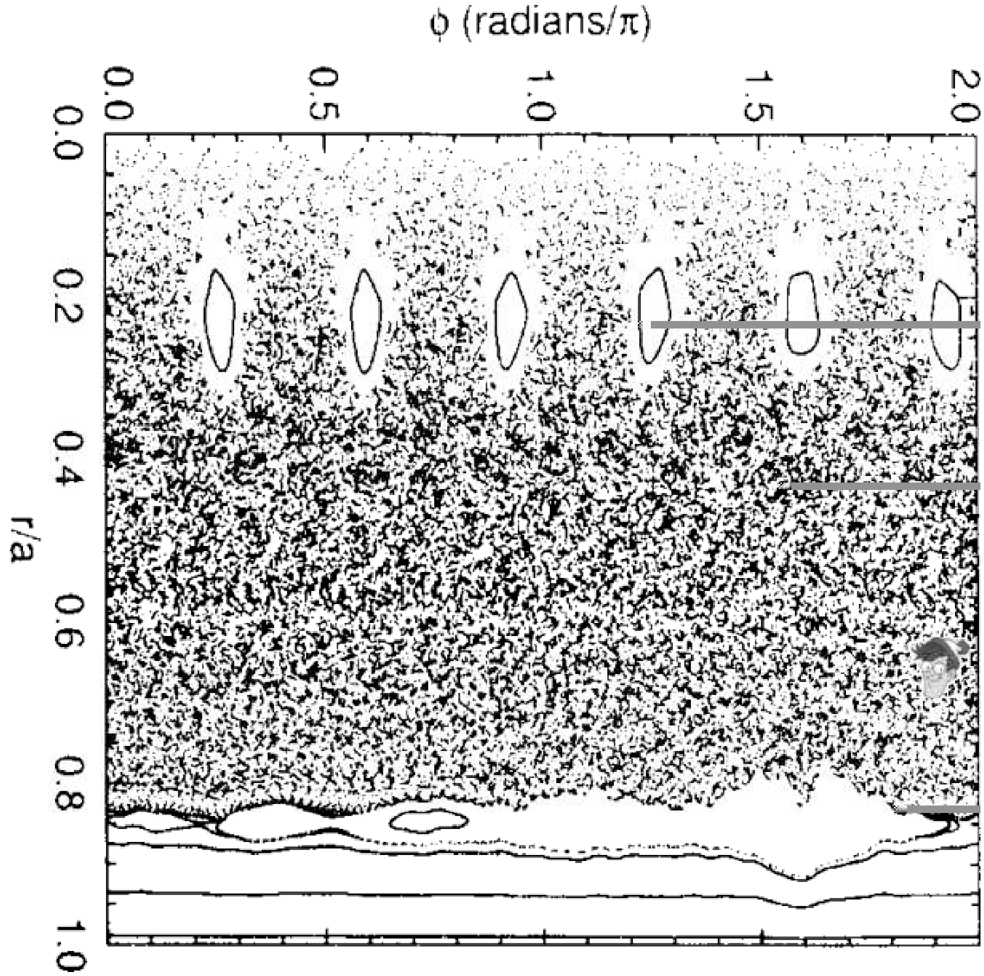

Figure 2.10 Puncture plot from DEBS simulation showing stochastic field after m=1 islands overlap

In MST, the overlap of the modes is accompanied by a violent reorganization. As they approach each other the islands start to interact. The nonlinear coupling between the m=1 modes causes them to combine creating new modes. For instance, an $m = 1$ $n = 6$ mode may beat against an $m = 1$ $n = 7$ mode to create $m = 0$ $n = 1$, $m = 0$ $n = 13$, $m = 2$ $n = 1$, and $m = 2$ $n = 13$ modes. The $m \geq 2$ modes and high values of n are small (at least they appear small at the edge) leaving $m = 0$ $n = 1$ the dominant mode. A cascade of such interactions drives a burst of dynamo activity in the $m = 1$ modes that in turn drives a burst of the normally stable(ish) $m = 0$ modes at the $m = 0$ reversal surface. The result is an effort by the plasma (via the MHD dynamo) to flatten the current profile to eliminate the free energy in the gradient that is driving instabilities and to inject toroidal flux lost to resistive decay. The slow growth and violent decay of the mode amplitudes is called a sawtooth. Figure 2.11 shows the evolution of a sawtooth as measured at the edge.

Note the sudden increase in toroidal flux at the expense of poloidal flux. Figure 2.12 shows a shot that is less common but more descriptive of the process.

To sum up, and because I have ink to kill: The RFP starts with well defined flux surfaces and a current profile flat enough to stabilize the tearing modes (or at least it could if it just sprang into existence at $t = 0$.) Due to resistive dissipation near the wall and a gradient in the driving electric field, the current profile starts to peak with time, exciting the $m = 1$ tearing modes on the resonant surfaces in the plasma. The toroidal flux also suffers resistive decay. The modes grow until they overlap, at which point the flux surfaces are destroyed and the field lines become stochastic. Current is driven via dynamo action in the edge by strong nonlinear interactions between the $m = 1$ modes exciting a burst of $m = 0$ modes and an injection of toroidal flux. As the current profile flattens, the instabilities decay away and field lines fall into a more orderly arrangement. The process repeats.

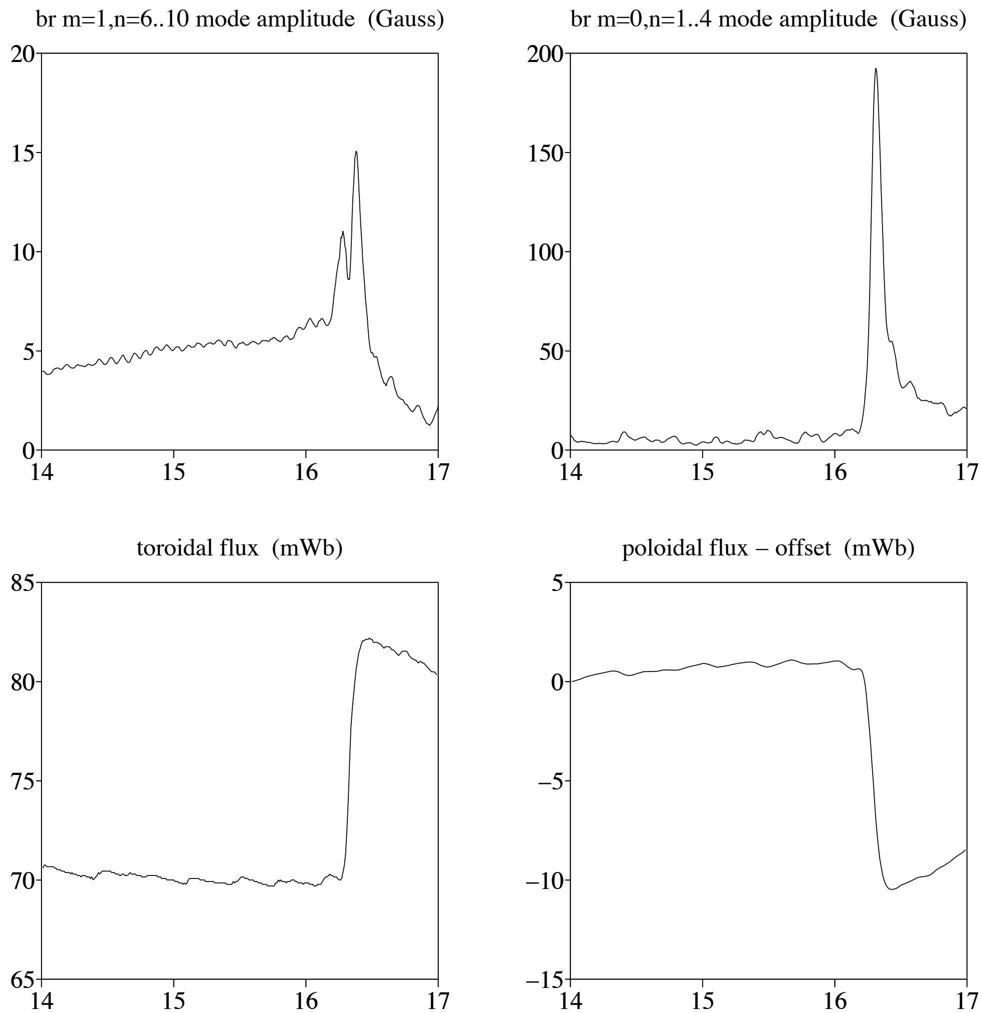

Figure 2.11 Evolution of a sawtooth crash using measured data from MST. Top left:$m = 1$ mode slowly grows before sawtooth. Top right:$m = 0$ mode is stable before sawtooth and gets kicked by nonlinear interaction of $m = 1$ modes. Bottom left:toroidal flux decays before sawtooth restores it. Bottom right:poloidal flux is sacrificed to feed toroidal flux restoration.

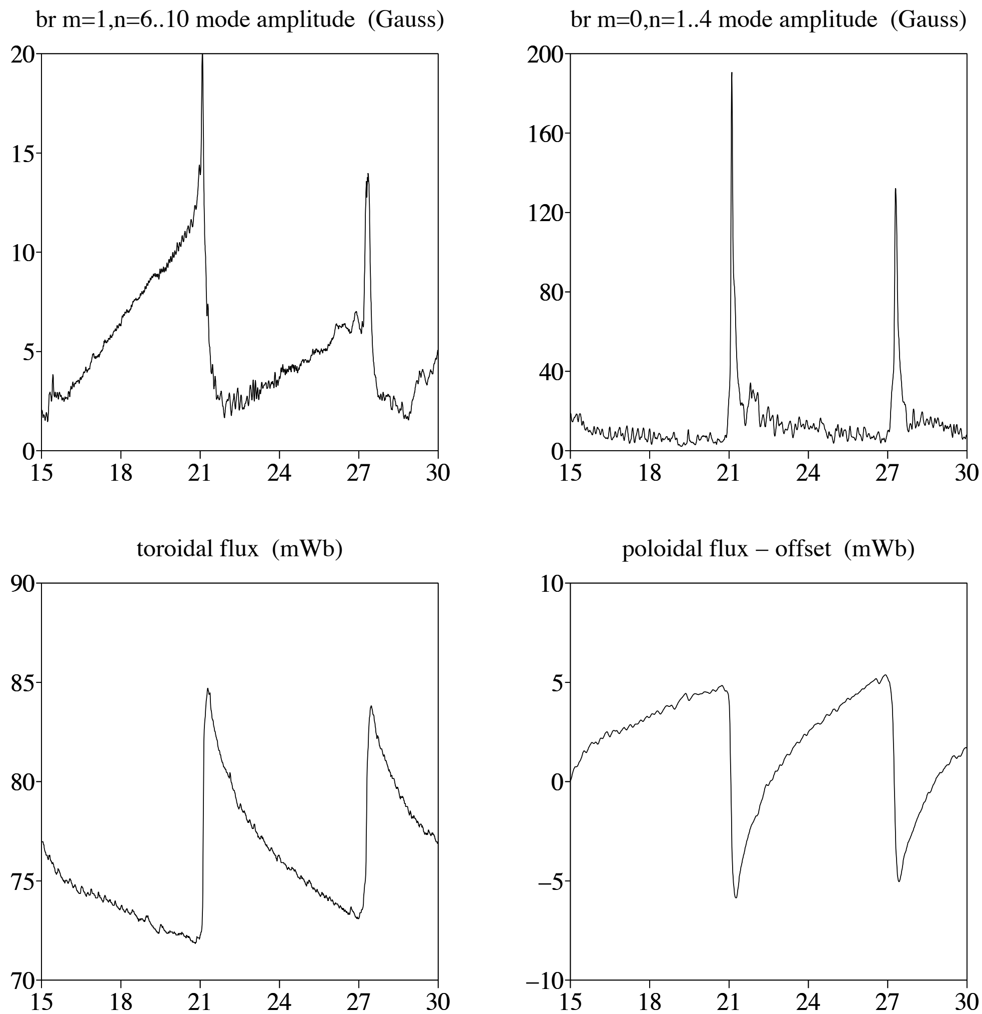

Figure 2.12 Less common but more illustrative version of figure 2.11

Chapter 3

The Physics and Modelling of OFCD

To gain some insight into the physics of OFCD and optimize the applied oscillations we explored the plasma's response to OFCD with two models. The first is a simple 1D model that assumes only energy balance and that a particular shape of the normalized current profile, J/B, is maintained throughout each cycle of the applied oscillations. The assumed shape is described by the α model mentioned in the previous chapter. The other was a more comprehensive model that self-consistently solves the full 3D MHD equations in a cylinder. Both predicted about the same amount of current drive so the emphasis here is on the simpler, faster 1D model. This model was used to optimize the frequencies, amplitudes, phase difference, and waveform shapes of the applied oscillations.

3.1 Helicity Injection

As mentioned in chapter 1, total global magnetic helicity plays a key role in the RFP and hence in OFCD. Like anything else, magnetic helicity is subject to resistive decay. To sustain the RFP is to sustain magnetic helicity (subject to the minimization of magnetic energy.) Reiterating:

$$\mathbf{K} = \int \mathbf{A} \cdot \mathbf{B} \, dV - \Phi_\phi \Phi_\theta \tag{3.1}$$

where Φ_ϕ is the toroidal magnetic flux inside the plasma and Φ_θ is the poloidal magnetic flux that threads through the center of the torus. To sustain an RFP requires some mechanism to overcome the resistive dissipation of K. If K is conserved dK/dt = 0.

$$\frac{\partial K}{\partial t} = \int \underbrace{\frac{\partial \mathbf{A}}{\partial t}}_{-\mathbf{E}} \cdot \mathbf{B}\, dV + \int \mathbf{A} \cdot \underbrace{\frac{\partial \mathbf{B}}{\partial t}}_{-\nabla\times\mathbf{E}} dV - \Phi_\phi \underbrace{\frac{\partial \Phi_\theta}{\partial t}}_{-v_\phi} - \Phi_\theta \underbrace{\frac{\partial \Phi_\phi}{\partial t}}_{-v_\theta}$$

where we have applied the Coulomb gauge $\nabla \cdot \mathbf{A} = 0$ and Faraday's law. v_ϕ and v_θ are the toroidal and poloidal loop voltages respectively. Rearranging,

$$\frac{\partial K}{\partial t} = \Phi_\phi v_\phi + \Phi_\theta v_\theta - \int \mathbf{E} \cdot \mathbf{B}\, dV - \int \mathbf{A} \cdot \nabla \times \mathbf{E}\, dV$$

Using the vector identity $\nabla \cdot \mathbf{A} \times \mathbf{B} = \mathbf{B} \cdot \nabla \times \mathbf{A} - \mathbf{A} \cdot \nabla \times \mathbf{B}$

$$\mathbf{A} \cdot \nabla \times \mathbf{E} = \mathbf{E} \cdot \nabla \times \mathbf{A} - \nabla \cdot (\mathbf{A} \times \mathbf{E}) = \mathbf{E} \cdot \mathbf{B} - \nabla \cdot (\mathbf{A} \times \mathbf{E})$$

leaving

$$\frac{\partial K}{\partial t} = \Phi_\phi v_\phi + \Phi_\theta v_\theta - 2\int \mathbf{E} \cdot \mathbf{B}\, dV - \underbrace{\int \nabla \cdot (\mathbf{A} \times \mathbf{E})\, dV}_{\int (\mathbf{A}\times\mathbf{E})\cdot \mathbf{dS}}$$

where we have used Stoke's theorem to convert the volume integral into a surface integral. We'll now switch to a cylindrical approximation of the torus so the surface is that of the cylinder (not including the caps) of radius a. The toroidal direction of the torus becomes the longitudinal direction of the cylinder $z = R_0\phi$, where R_0 is the major radius of the torus. At the edge of the cylinder (r=a) the area element $d\mathbf{S} = a\, d\theta\, dz\, \hat{r}$. So $(\mathbf{A} \times \mathbf{E}) \cdot \hat{\mathbf{r}} = A_\theta E_z - A_z E_\theta$. By symmetry, nothing varies with z or θ so we can safely rearrange the surface integral into,

$$\int\int (\mathbf{A} \times \mathbf{E}) \cdot \hat{\mathbf{r}}\, a\, d_\theta\, dz = \underbrace{\int A_\theta\, a\, d\theta}_{\Phi_z} \underbrace{\int E_z\, dz}_{v_z} - \underbrace{\int A_z\, dz}_{\Phi_\theta} \underbrace{\int E_\theta\, a\, d\theta}_{v_\theta}$$

Where we have used magnetic flux $\Phi = \int \mathbf{B} \cdot d\mathbf{S} = \int \nabla \times \mathbf{A} \cdot d\mathbf{S} = \oint \mathbf{A} \cdot d\mathbf{l}$ and loop voltage $v = \int \mathbf{E} \cdot d\mathbf{l}$. Bringing it all together

$$\frac{\partial K}{\partial t} = 2v_z\Phi_z - 2\int \mathbf{E} \cdot \mathbf{B} dV \tag{3.2}$$

From the MHD Ohm's law, $\mathbf{E} \cdot \mathbf{B} = \eta \mathbf{J} \cdot \mathbf{B}$, where η is the plasma resistivity.

$$\frac{\partial K}{\partial t} = 2v_z\Phi_z - 2\int \eta \mathbf{J} \cdot \mathbf{B} dV \tag{3.3}$$

So, when in equilibrium $\frac{\partial K}{\partial t} = 0$ and,

$$\underbrace{v_z\Phi_z}_{Helicity\ injection} = \underbrace{\int \eta \mathbf{J}\cdot\mathbf{B}dV}_{Resistive\,decay} \tag{3.4}$$

3.2 Oscillating Field Current Drive

In normal operation, the toroidal loop voltage, v_z, and flux, Φ_z, have static values until the driving power supply saturates. But if each was a sinusoidal voltage (or any cyclic voltage) their product would yield a time averaged constant value. The poloidal loop voltage is the time derivative of the toroidal flux (a $90°$ phase shift). So two sinusoidal loop voltages $90°$ out of phase applied to the plasma could offset the helicity lost to resistive decay, and, presumably, the parallel current that goes with it. Consider,

$$v_z = V_1 sin(\omega t) \quad v_\theta = V_2 sin(\omega t + \delta) \tag{3.5}$$

$$\Phi_z = \int v_\theta dt = \frac{V_2}{\omega} cos(\omega t + \delta) \tag{3.6}$$

yielding a time average helicity injection rate of

$$\left\langle \frac{\partial K_{inj}}{\partial t} \right\rangle = \frac{V_1 V_2}{\omega} sin(\delta) \tag{3.7}$$

So maximum helicity injection occurs if the phase between the oscillators is $+90°$. Note also that if the phase difference between the oscillators is $-90°$ helicity will be *subtracted* from the plasma. We'd expect the toroidal current will also be reduced.

Note that for fixed loop voltage amplitudes, the lower the frequency the more helicity we can inject. Intuitively we expect there to be some frequency below which OFCD will work poorly or stop working altogether. It will obviously stop working at DC because there'd be no "O" in OFCD. Very low frequencies would be no different than dialing the usual loop voltages up and down as in normal operation, causing wide swings in the macroscopic parameters like F, Θ, and the toroidal plasma current. So the period of oscillation τ_ω should be shorter than the resistive diffusion time τ_R or the L/R time constant of the entire plasma. These are the longest timescales governing the settling time of the RFP. Likewise, if the frequency is too high we'd expect the plasma would not have time to respond (by respond I mean relax to a minimum energy state) and the currents would remain within the skin depth at the edge. Compounding this would be the natural inductance of the plasma suppressing any response at high frequencies. So the period of oscillation should be longer than the relaxation time $\tau_H = \sqrt{\tau_R \tau_A}$ of the plasma (where τ_A is the Alfvèn time.) In the numerical studies section, we'll see that these and other effects imply some optimum frequency of operation.

We have only considered the time average values of the plasma response. There is also a sizable modulation on top of each plasma attribute, e.g. the toroidal current. We will go into the consequences of that modulation later.

So far all we've shown is that helicity decay can be balanced to achieve what appears to be a quasi-equilibrium state. It is presumed that injecting helicity will inject current. But all this says nothing about the dynamics of OFCD and how we achieve this quasi-equilibrium state.

Figure 3.1 shows the bare essentials of OFCD. We can't actually drive the loop voltages throughout the plasma (especially the toroidal loop voltage) so we drive them at the edge, at the gaps of the vacuum vessel. The applied electric fields in turn modulate the bulk flow, $V_{m=0,n=0} = E_{00} \times B_{00}$ of the plasma and the equilibrium magnetic field $B_{m=0,n=0}$. This drives a large scale *breathing dynamo* $V_{00} \times B_{00}$ at the edge of the plasma, driving an edge current. The edge current could soak into the plasma by resistive diffusion, but given the conductivity of the plasma that process is too slow. Another mechanism will be required to get current into the core.

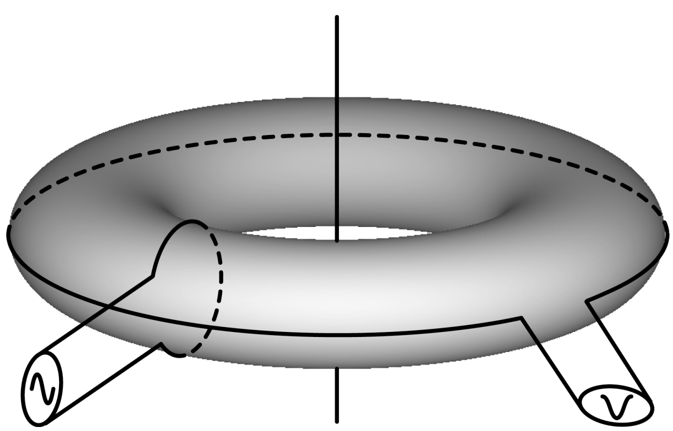

Figure 3.1 OFCD applies voltages at the edge of the plasma

Recall figure 2.7 that showed the MHD dynamo balancing $\mathbf{E}$ and $\eta\mathbf{J}$ in Ohm's law by driving current in the edge. OFCD relies on a similar effect to get current *into* the core. The large current in the edge peaks the current profile there (rather than at the core) flipping the current profile that upsets normal RFP operation. Now the dynamo that once drove current in the edge at the expense of the core is doing just the opposite. Figure 3.2 shows the expected current profile and dynamo contribution during OFCD as predicted by 1D modeling.

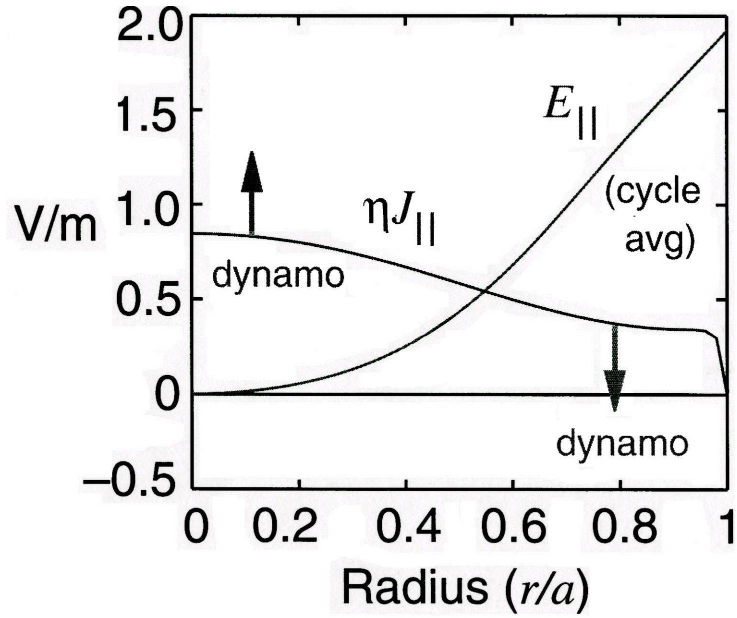

Figure 3.2 Parallel Ohm's law during OFCD sustainment. Dynamo drives current into core

3.3 Numerical Studies

Numerical models were employed to predict what to expect and to optimize the operating parameters for OFCD. A simple 1D relaxed state model provided an expectation of time-averaged current drive and incidental modulation of macroscopic parameters like the reversal parameter. It also provided a platform for studying non-sinusoidal waveforms for OFCD. Results from a prior study [23] using a fully nonlinear 3D model offered the same plus a more detailed look at the dynamics of OFCD, including an expectation of the behavior of the $m = 1$ and $m = 0$ modes and their efficacy in driving current in the core.

3.3.1 The 1D model

MST can be viewed as a black box that takes power from the toroidal and poloidal field circuits (applied at the gap), stores some of that energy, and dissipates the rest.

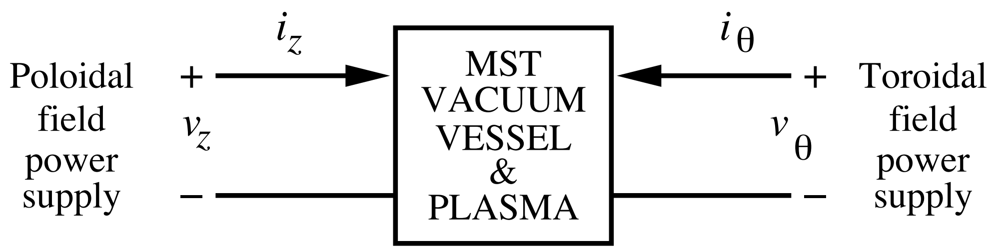

Figure 3.3 A macroscopic 'black box' view of MST

Energy balance dictates:

$$\underbrace{\frac{\partial W}{\partial t}}_{stored} = \underbrace{v_z i_z + v_\theta i_\theta}_{injected} - \underbrace{P_\Omega}_{dissipated} \tag{3.8}$$

where W is the magnetic energy stored in the plasma (the thermal energy in MST is typically about one tenth the magnetic energy, so we ignore it), $v_z(t)$ and $v_\theta(t)$ are the voltages applied at the insulated gaps in the conducting shell, i_z and i_θ are the currents that result, and P_Ω is the power dissipated in the plasma. It's not obvious from figure 3.3 but i_z is the toroidal plasma current. The ohmic power loss is

$$P_\Omega = \int \eta J_\parallel^2 dV \tag{3.9}$$

where η is the resistivity of the plasma and the integral is taken over the volume of the plasma. The same equation can be derived by a laborious calculation using Poynting's theorem. v_ϕ is a little hard to visualize as a gap voltage given it's applied by induction. When we stretch the toroid out into a cylinder the toroidal loop voltage $v_\phi = v_z$ can be thought of as being applied to caps at either end of the cylinder. Lest we forget, the toroidal current i_z is our desired response. We need the time-averaged value $\langle i_z \rangle > 0$.

In the energy balance equation, the voltages are given but the remaining four quanitities come from the plasma response. So a model of the plasma must be assumed. The α model described in chapter 2 will be used in a periodic cylinder. Added to that is a fixed parabolic pressure gradient. From chapter 2 the magnetic field profile (+ the pressure term) is the solution to

$$\nabla \times \mathbf{B} = \lambda \mathbf{B} + \mathbf{B} \times \nabla p / B^2 \tag{3.10}$$

Due to symmetry $\frac{\partial}{\partial z} = \frac{\partial}{\partial \theta} = 0$. So $\mathbf{B} = B_\theta(r)\hat{\theta} + B_z(r)\hat{z}$. The α model describes the current profile $J/B = \lambda(r) = \lambda_0(1 - (r/a)^\alpha)$. From experiments it's known that α is usually around 4 and λ_0 hovers around 6 m. We can either fix α and let λ_0 roam free or vice versa or even let both α and λ_0 vary in time. We'll do each. Writing everything out in cylindrical coordinates, including some needed auxiliary equations:

$$\frac{\partial W}{\partial t} = v_z i_z + v_\theta i_\theta - P_\Omega \tag{3.11}$$

$$\frac{\partial B_z}{\partial r} = -\lambda(r,t) B_\theta - \frac{B_z}{B^2}\frac{\partial p}{\partial r} \tag{3.12}$$

$$\frac{\partial B_\theta}{\partial r} = \lambda B_z - \frac{B_\theta}{r} - \frac{B_\theta}{B^2}\frac{\partial p}{\partial r} \tag{3.13}$$

$$i_z = \frac{2\pi a B_\theta(a)}{\mu_0} \tag{3.14}$$

$$i_\theta = \frac{2\pi R_0 B_z(a)}{\mu_0} \tag{3.15}$$

$$P_\Omega = \int \eta(r) J_\parallel^2 dV \tag{3.16}$$

$$J_\parallel = \frac{\lambda B}{\mu_0} \tag{3.17}$$

$$\frac{\partial \Phi_z}{\partial t} = -v_\theta \tag{3.18}$$

$$W = \int \frac{B^2}{2\mu_0} dV \tag{3.19}$$

The inputs to our model are α for the fixed α model or λ_0 for the fixed λ_0 model, the imposed edge voltages v_θ and v_z, and the initial conditions taken from real data. The outputs include the 'toroidal' and poloidal currents i_z and i_θ, the magnetic energy W and the ohmic dissipated power P. To solve for B_z and B_θ requires two boundary conditions. Ideally we'd have the core value of both but we don't know $B_z(r=0)$. What we do have is $B_\theta(r=0)=0$, the toroidal flux Φ_z, and, from the energy equation, W (after each time step.) The resistivity profile $\eta(r)$ is taken from real data and assumed fixed in time. It's worth noting that the only assumptions in the 1D model are energy balance and the α model profile. There is no mention of flow velocities or temperatures or such.

So, starting with initial values taken from real data just before the real oscillators turn on, the recipe for solving the fixed α model is

1. Advance W and Φ_z.

2. Using W and Φ_z find the field profile. For this an optimization routine was used to find the best value of $B_z(0)$ and λ_0 (α for the fixed λ_0 model) that yields W and Φ_z.

3. From the new field profile get new values of i_z , i_θ , and P_Ω.

4. Repeat.

The differential equation solver was the improved Euler method[1]. It's robust, easy to code, and almost as fast as Runge-Kutta. For the fixed α and fixed λ_0 versions, most of the calculations in step 3 were bundled into a lookup table for speed.

The fixed α/variable λ_0 is probably the most accurate approximation of Taylor-like relaxation since the shape of the J/B profile stays constant, as it would in the true Taylor state. The variable α/fixed λ_0 is a better model of the effects of shallow current penetration since oscillations in the shape factor α are most visible near the edge. Finally, we expect the variable α/variable λ_0 to enjoy the benefits of both effects and provide the most accurate depiction of real MST behavior. We'll examine each model and later compare the results with experimental findings.

3.3.1.1 Fixed α

We use our model by driving it with realistic parameters from current MST experiments where OFCD is applied in addition to the normal loop voltages. This is *partial sustainment*. This allows

[1] also known as the predictor-corrector method

a direct comparison with existing results before we start making predictions of *full sustainment* where the background DC loop voltage is shut off and OFCD carries the day.

NOFCD Our standard case is a flattop (oscillators off) toroidal current of 255kA and DC toroidal loop voltage of 26V. For brevity (and levity) we'll call this the NOFCD mode. The α value used was the average taken from real data over the duration of flat-top operation tweaked to ensure the NOFCD simulation matched the real data. The resistivity was calculated from electron temperature profiles measured by Thomson scattering experiments [24]. It too had to be tweaked to get the right current but the result was still within the error bars on the original resistivity measurements (so who's to say we're not right?) Table 3.3.1.1 shows the results of the NOFCD simulation and experimental values for comparison.

Take note that in this discussion we're treating the relaxed state model as a predictor of what to expect and a tool for optimizing the experimental setup and to gain some insight into the plasma behavior. We're pretending the hardware has not been built yet and the tense taken here reflects that. This is cheating somewhat because we know from experience the maximum voltages the oscillators can apply to the gaps without blowing up any more frequently than they normally do. Comparisons to experimental data will be made in chapter 5.

Partial sustainment Our reference firmly established, the virtual oscillators were turned on. Past studies by Sprott [15] have predicted optimum current drive occurs when the ratio of the applied gap voltages was between 8 and 10. Knowing in advance what our hardware can deliver we set the voltages of the toroidal and poloidal oscillators to 98 and 13 volts respectively. The frequency was set to 280Hz for starters (clairvoyance.) This yields a cycle average helicity injection rate $\langle V_\theta V_\Phi/\omega\rangle$ of $.72\,V\,Wb$, which is about 28% of the DC injection rate. The increase in current is less than the increase in $\dot{K}$ because of the nonlinear relationship between K and I_z. The duration of the simulation is longer than a real discharge to make sure the L/R time constant of the plasma has been overcome.

Value	Model	Actual
Toroidal current I_z	255 kA	250 kA
Magnetic energy W	80 kJ	73 kJ
Reversal parameter F	-.33	-.37
Pinch parameter	1.67	1.76
Ohmic power P_Ω	6.7 MW	-
Toroidal flux	0.05 Wb	0.05 Wb
Toroidal field at wall	-196 G	-204 G
Shape factor α	3.65	-
J/B on axis λ_0	6.4 A/Wb	-
Helicity injection rate	1.3 V Wb	-

Table 3.1 Results of NOFCD simulation with relaxed state model. Second column shows experimental values.

Figure 3.4 shows the results of two phase shifts of the oscillating gap voltages ($\pm 90°$), the so-called drive and anti-drive phases. The dark lines are the cycle average values. The faint oscillations superimposed on the cycle averages are the modulations that are an unavoidable byproduct of OFCD. We usually emphasize the cycle average values because that's what we care most about and the relaxed state model is a pseudo-equilibrium model, so we have more faith in long term averages than short time scale behavior. The graph shows current drive of 13 kA (+5.1%) and antidrive of 14 kA (-5.5%). At the drive phase the modulation of the current is about 8%. Note that the L/R time appears to be about 30 msec. This is important because we expect our real oscillators will only run about 25 msec. So the values we see in the experiment may be smaller than their potential values.

Theory (eqn 3.1) says the cycle average helicity injection goes with the sine of the phase difference between the oscillators. Presumably the current does the same. Figure 3.5 shows the expected sinusoidal dependence. Drive and antidrive occur $180°$ out of phase as expected. The slight distortion is probably an artifact of the optimizer or the coarseness of the lookup table used.

Figure 3.6 shows the normalized parallel current density ($J_{\|}/B$) scale factor λ_0 vs time. It's no surprise that the curve follows the toroidal current I_z so we are injecting parallel current.

Key parameters describing the RFP plasma are the reversal parameter,F, and pinch parameter, Θ. Figure 3.7 shows both vs time for the maximum drive phase. Θ exhibits about a 13% modulation while F has a 68% modulation. The plasma very nearly comes out of reversal even with such a small perturbation. This bodes not well for higher power solutions in MST. It means our pinch might oscillate between being a very deep RFP and a crummy tokamak. 3D simulations say otherwise. As the electron temperature of the plasma goes up, these modulations are lessened for the full sustainment case. According to Taylor, being in the relaxed state, the $F - \Theta$ trajectory should follow a nearly straight line during a cycle. Figure 3.8 shows that indeed it does.

Figure 3.9 shows the magnetic energy, W, stored in the plasma. About 11 kJ of additional energy is injected by OFCD accompanied by a 17% modulation. Figure 3.10 shows the ohmic power dissipated by the plasma. About 1.1MW (16%) of additional power is dissipated accompanied by a 21% modulation.

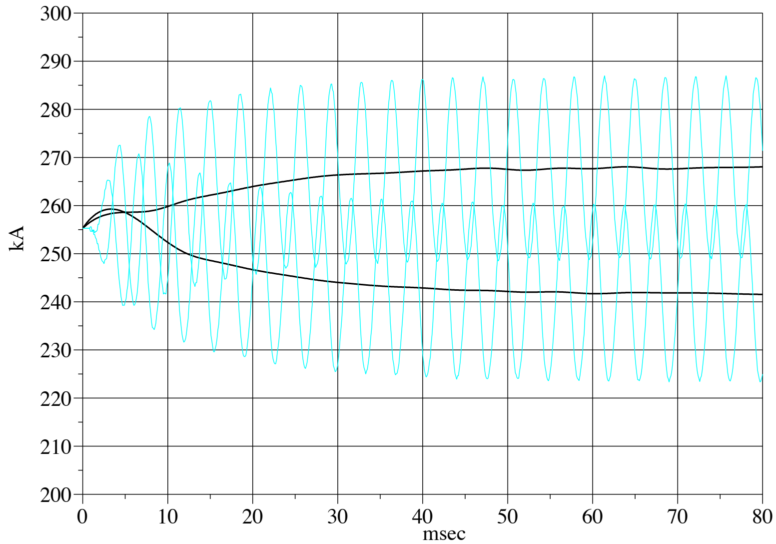

Figure 3.4 The toroidal current for the drive and antidrive phases during 280 Hz partial sustainment using the fixed α model. The upper curve is the drive phase and the lower the antidrive phase.

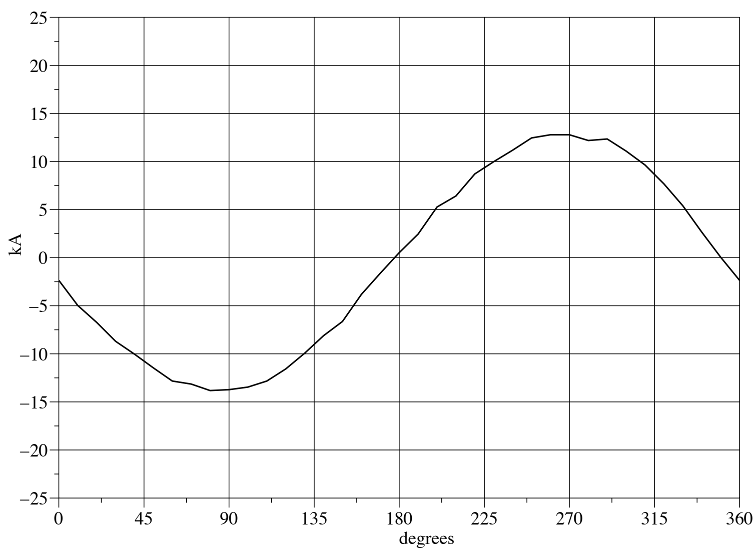

Figure 3.5 Current drive vs the phase difference between the oscillating voltages for 280 Hz partial sustainment using the fixed α model.

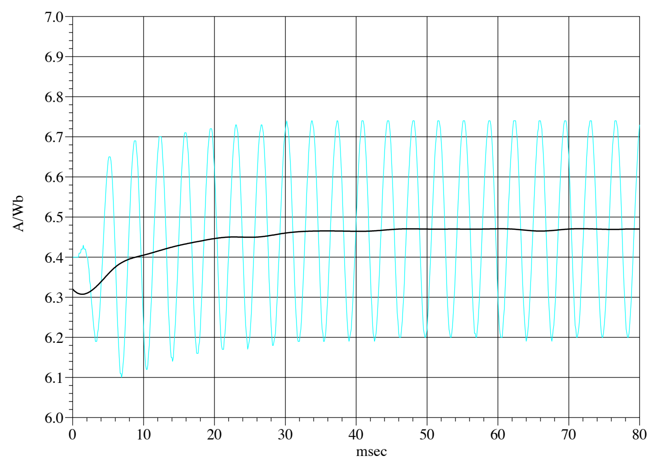

Figure 3.6 Normalized parallel current density λ_0 during 280 Hz partial sustainment using the fixed α model.

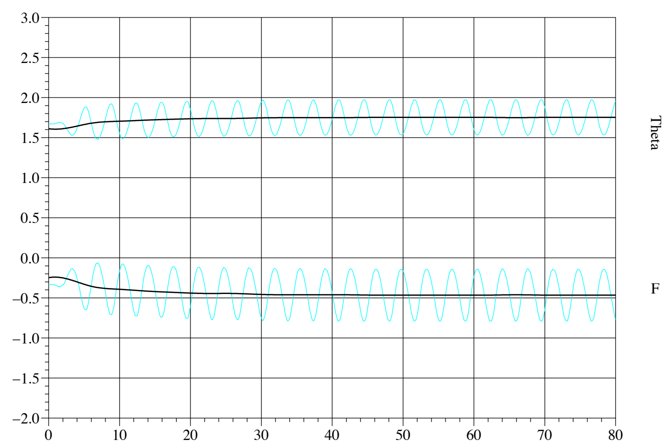

Figure 3.7 The reversal and pinch parameters for the maximum drive phase during 280 Hz partial sustainment using the fixed α-model.

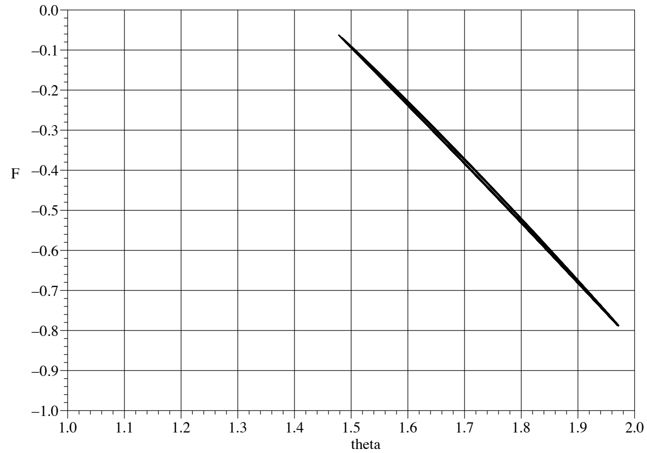

Figure 3.8 The $F - \Theta$ trajectory for maximum current drive phase during 280 Hz partial sustainment using the fixed α-model.

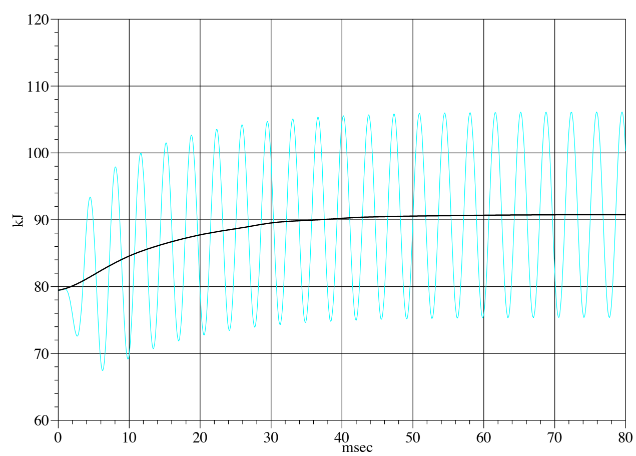

Figure 3.9 Magnetic energy W during 280 Hz partial sustainment using the fixed α -model.

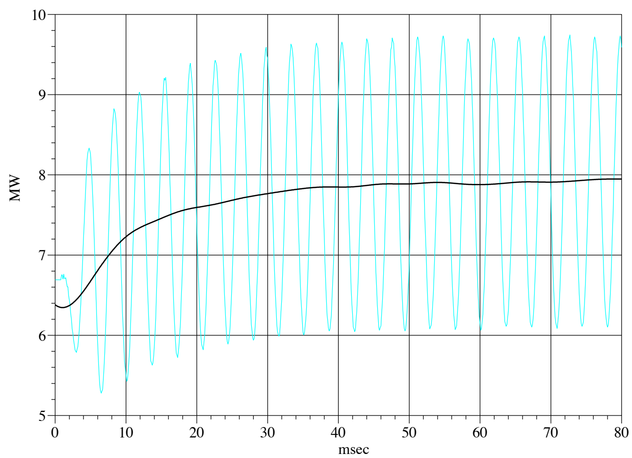

Figure 3.10 Ohmic power dissipation during 280 Hz partial sustainment using the fixed α -model.

With newfound confidence in our model we start applying it to the task of optimizing the applied oscillations. We start first with the frequency, holding the oscillating voltage amplitudes constant. Figure 3.11 shows the current drive vs frequency referenced to the nominal 255 kA. The curve has a bandpass filter like shape. This is to be expected. The inductance of the relaxed plasma is evident in the R/L rise times of time domain curves like figure 3.9. At high frequencies this inductance combined with the 1/f dependence of the injection rate (eqn 3.7) suppresses everything, and at DC there can be no induction so there must be a maximum somewhere in between. Also plotted is the 1/f dependence of the helicity injection rate from chapter 2 (normalized to match at 280 Hz.) At higher frequencies they almost exactly match. Maximum current drive of 38 kA occurs at about 115 Hz. That's nearly four times the current we expect at our test frequency of 280Hz. There is, however, a price to pay at that lower frequency. The modulation of both the current and the reversal parameter rise rapidly below 250Hz. Figure 3.12 shows the modulation of F vs frequency. A respectable mean value of F is about -0.3, so, to avoid coming out of reversal, the lowest frequency we can use for partial sustainment at these voltages is about 280 Hz. We might have to go to higher frequencies for full sustainment to avoid losing reversal. This will decrease the efficiency of OFCD if not hinder it's application altogether. In the experimental results we'll discuss experiments in partial sustainment OFCD where the plasma was intentionally allowed to come out of reversal during part of the cycle.

Figure 3.13 shows the added (beyond the NOFCD value) ohmic power dissipated in the plasma for these voltages vs frequency. It too rises rapidly below 250 Hz. The rise is likely due to the increase in I^2R_p loss (where R_p is the equivalent plasma resistance.) What's peculiar about the plot is that P_Ω appears to rise without bound as the frequency approaches 0. We'd expect it to drop to zero as I_z did. This inexplicable rise casts some doubt on the model.

So, for the voltages we expect our oscillators to apply to the edge of the plasma, it looks like 280 Hz is the best compromise between current drive, modulation of the reversal parameter, and ohmic power dissipation.

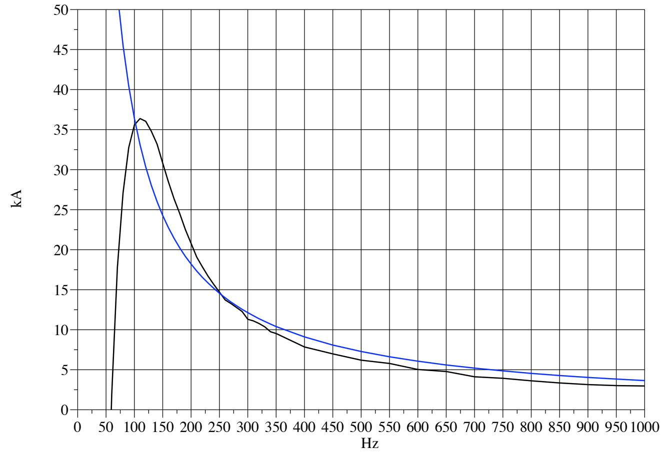

Figure 3.11 Current drive vs frequency for partial sustainment using the fixed α model.

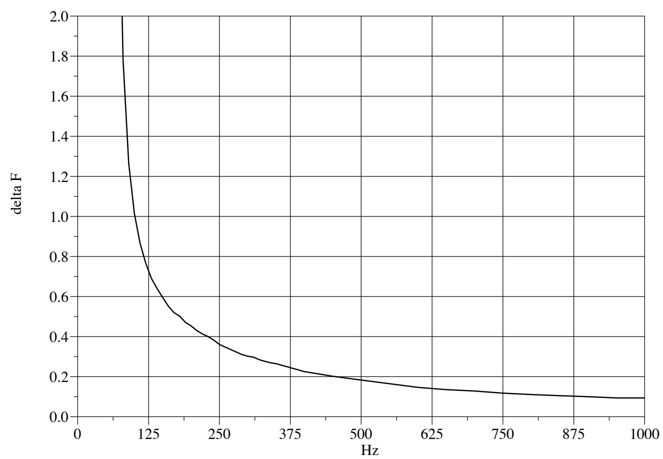

Figure 3.12 Modulation of reversal parameter vs frequency for partial sustainment using the fixed α model.

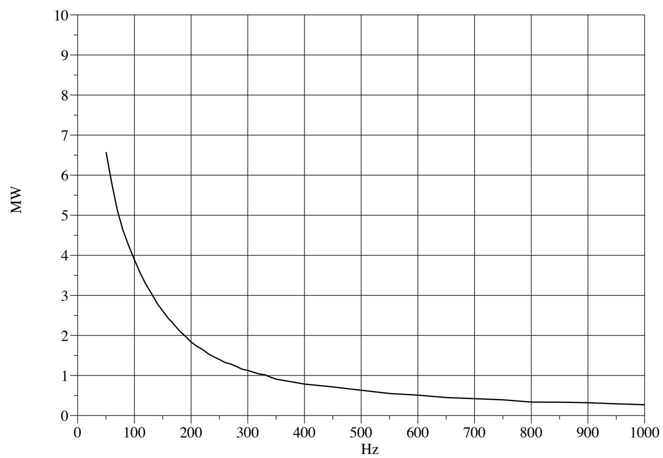

Figure 3.13 Ohmic power dissipation vs frequency for partial sustainment using the fixed α model.

We now look at the voltage amplitude ratio v_z/v_θ to see if lowering one of the voltages can lower the modulation of F without compromising too much current. Figure 3.14 shows the modulation of the reversal parameter vs the ratio while holding the current to within 5% of our 13kA maximum drive. Since the current was held constant, v_θ had to be increased at lower ratios to compensate for lower v_z. Since v_θ is the dominant contributor to the toroidal field at the edge, the modulation rises rapidly at low ratios. It looks like anything above 7 will keep the plasma from coming out of reversal.

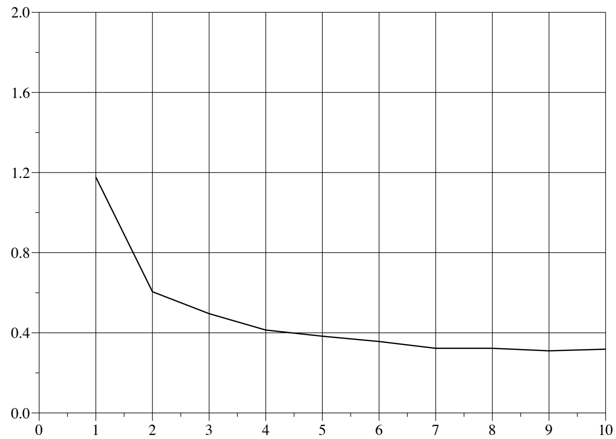

Figure 3.14 Modulation on F vs v_z/v_θ during 280 Hz partial sustainment in the fixed α model.

Now we consider the waveform itself. A sinusoid is the first waveform to come to mind when talking about oscillations but with modern high power solid-state technology we can generate almost any waveform we can get through the MST power supply circuits.

A Fourier series spread from 250 to 1000Hz was fed to an optimizer that adjusted the coefficients for maximum current drive balanced equally with minimum modulation of the reversal parameter F. A variety of waveforms was used as the starting point: sawteeth, exponentials, rectified sinusoids, ... The complete bestiary is shown in figure 3.15. But no matter what the starting point was, the optimizer always whittled the Fourier series down to the lowest harmonic unless the modulation of F was grossly overweighted. The reason is seen in figure 3.11. The frequency response of the plasma is so steep that anything above a few hundred Hz is filtered out. Even bunching frequency components within the range 115 to 250 Hz resulted in one harmonic: at the peak of the curve. So, after months of trying to find some excuse to justify dumping our current oscillator design in favor of a programmable supply it looks like we're stuck with sinusoids, at least according to the 1D model. There are still good reasons to switch. The 1D model doesn't cover short timescale events so high frequency terms might have some favorable effect at least in the edge. It also might be easier to build a nonsinusoidal high power source. Finally, the frequency and phase can be much more easily changed with a programmable supply. They can even be modulated within a discharge.

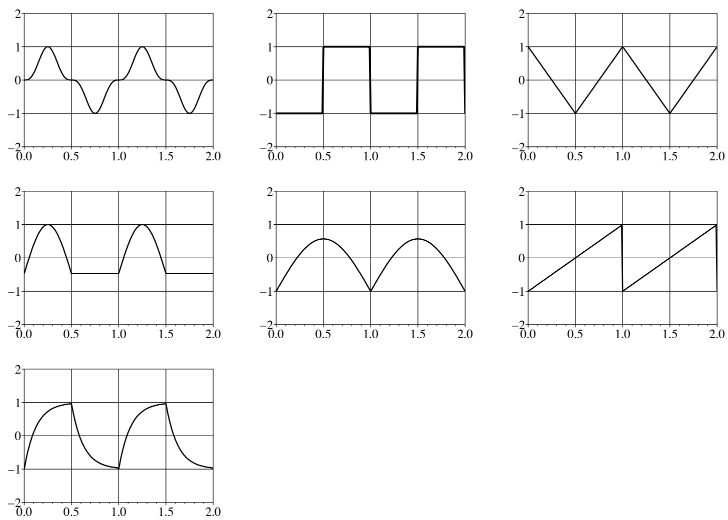

Figure 3.15 Various waveforms used as the starting point in waveform optimization for 280 Hz partial sustainment with the fixed α model.

So, for partial sustainment, the optimal parameters according to our relaxed state model are 280Hz sine waves with a $+90°$ phase difference and ratio v_z/v_θ greater than 7.

3.3.1.2 Full sustainment

We now shut off the DC toroidal sustainment voltage, dial up our oscillator voltages, and see if OFCD can sustain the toroidal current. Once again our control variables include the applied oscillations amplitudes and frequencies and the shape factor α. The desired quantities are plasma current, ohmic power dissapation, F, and Θ. We need to know the voltages required and just how much these larger voltages will upset the plasma. Of particular concern is whether the modulation will push the plasma out of reversal.

Figure 3.16 shows the toroidal current for full sustainment. The DC toroidal loop voltage cuts off at 15 msec leaving OFCD to sustain I_z. The initial ramp up is due to the presence of both. By trial and error the oscillator voltages were scaled up until the time averaged current was held at our NOFCD current, 255kA. Both voltages had to be scaled up by only a factor of 2.85 (16 MVA reactive power) from their partial sustainment values to 280V on the poloidal gap and 37 V on the toroidal gap. Three times the voltages means only nine times the helicity injection rate but yields 19 times the current drive. This is surprising and speaks to the nonlinearity of the plasma response to OFCD. It's also encouraging since the hardware for full sustainment shouldn't be much more difficult than our low power solution. The resulting current has a sizable 21% modulation. Note that the L/R time of the plasma is vividly illustrated after the DC loop voltage cuts off.

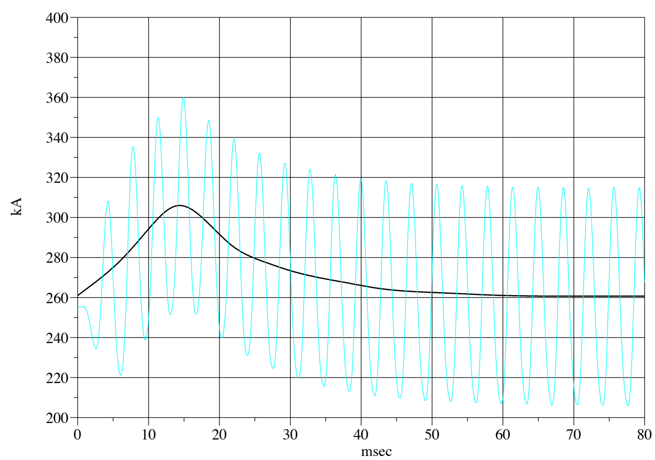

Figure 3.16 Fully sustained current drive during 280 Hz full sustainment using the fixed α model. DC loop voltage cuts off at 15 msec.

Figure 3.17 shows the reversal and pinch parameters vs time. Unfortunately the plasma does come out of reversal but only for about 20% of the cycle. It remains to be seen what effect this will have on the plasma. In figure 3.8 the $F-\Theta$ trajectory still follows the requisite straight(ish) curve during the oscillation.

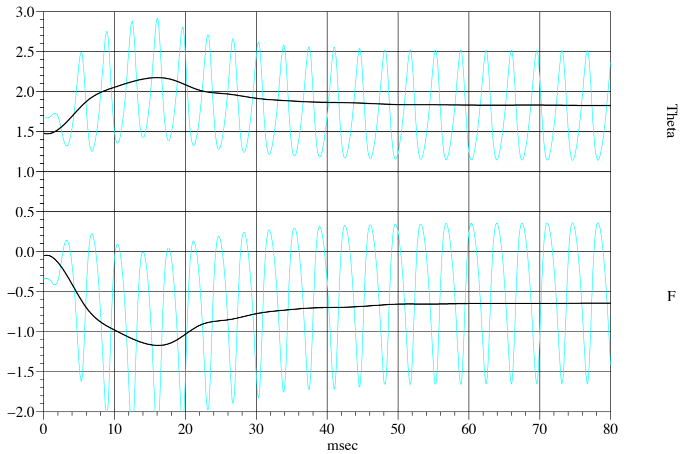

Figure 3.17 Reversal and pinch parameters during 280 Hz full sustainment using the fixed α model.

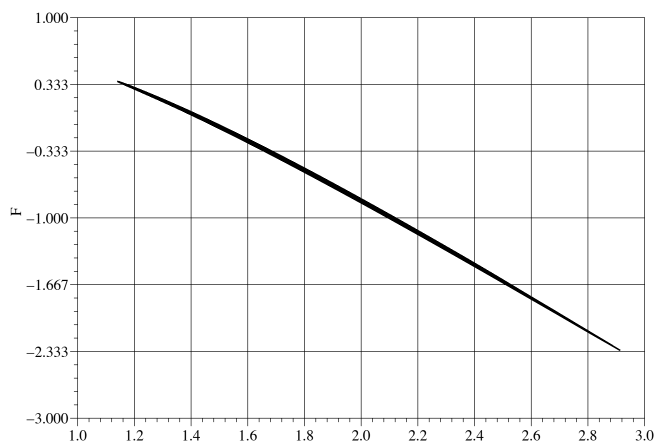

Figure 3.18 The $F - \Theta$ trajectory for during 280 Hz full sustainment using the fixed α model.

Figures 3.19 and 3.20 show that the normalized current and magnetic energy also settle to their NOFCD values. In Figure 3.21 the ohmic power settles to 400 kW more (1.5 MW) than its NOFCD value.

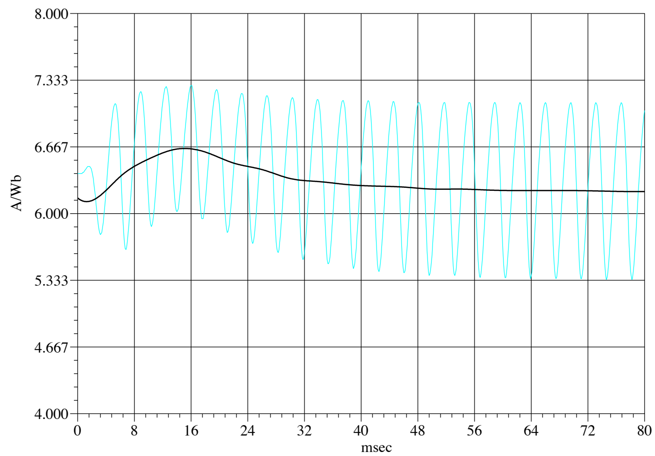

Figure 3.19 Normalized parallel current density λ_0 predicted by the fixed α model during 280 Hz full sustainment.

Our results are encouraging. According to the one-dimensional relaxed-state fixed-alpha model full sustainment is possible for MST and requires only about 280 Volts on the poloidal gap and 37 Volts on the toroidal gap. If they'll just stop blowing up, the ignitron based oscillators now in use could be scaled up to these voltages.

3.3.1.3 Fixed λ_0, variable α

We now fix the scale factor λ_0 and let α roam free. As the two gap voltages oscillate in the real plasma we expect intuitively that the plasma will 'breathe' in and out so that the reversal surface oscillates back and forth about it's nominal position. We might also expect the core value of J/B to not respond instantaneously to the applied voltages as they do in the fixed α model. In the fixed α model the entire J/B profile oscillates because, after all, λ_0 is a scale factor. So it's worth considering the case where λ_0 is fixed and the shape factor α is allowed to oscillate. The same algorithm was used for the fixed λ_0 model as in the fixed α case. A lookup table was employed

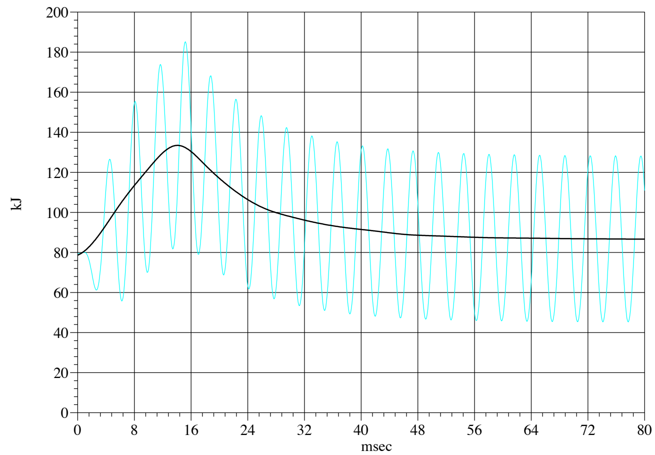

Figure 3.20 Magnetic energy W predicted by the fixed α model for 280 Hz full sustainment.

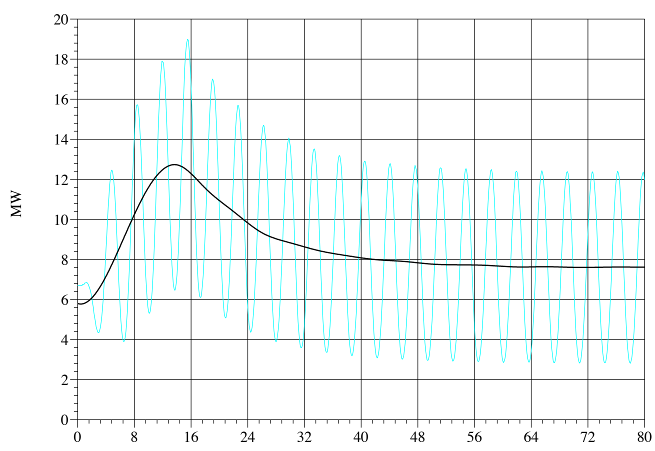

Figure 3.21 Ohmic power dissipation predicted by the fixed α model for 280 Hz full sustainment .

again to speed things up. The fixed value of λ_0 was 6.4, the same as the initial value used in the fixed α model.

Figure 3.22 shows the partial sustainment toroidal current vs time for the two different phases, drive and antidrive. The results are nearly identical to the fixed α model. Figure 3.23 shows a full phase scan which again is nearly identical to the phase scan of the fixed α model. There is one small difference: the anti-drive phase subtracts a few kA more current from the nominal value.

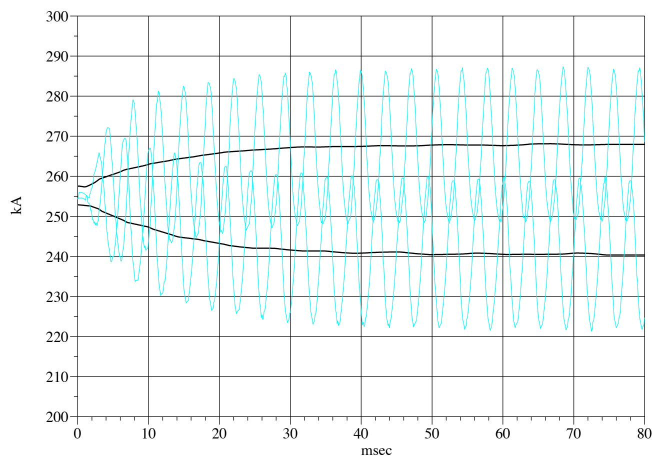

Figure 3.22 Toroidal current for drive and antidrive phasing predicted by the constant λ_0 model for 280 Hz partial sustainment

Figure 3.24 shows the α shape parameter oscillating in time for the drive phase during partial sustainment. The cycle average value rises to about 4.2 with the same time constant of everything else. The peak-to-peak excursion is about 2 which is comparable to the variation of α measured in experiments (away from the sawteeth) though the α measured in experiments does not oscillate so nicely, as seen in the ensemble averages in figure 3.25. The initial values for the fixed λ_0 model were the same as for the fixed α model. The initial value of α was 3.65 (estimated just before the oscillators kick on.) It is interesting that the cycle-average value of α should rise to 4.1 rather than just oscillate about its initial value. To add current is to flatten the current profile (since λ_0 is fixed) so α should increase. It's always encouraging to see a simulation agree with intuition.

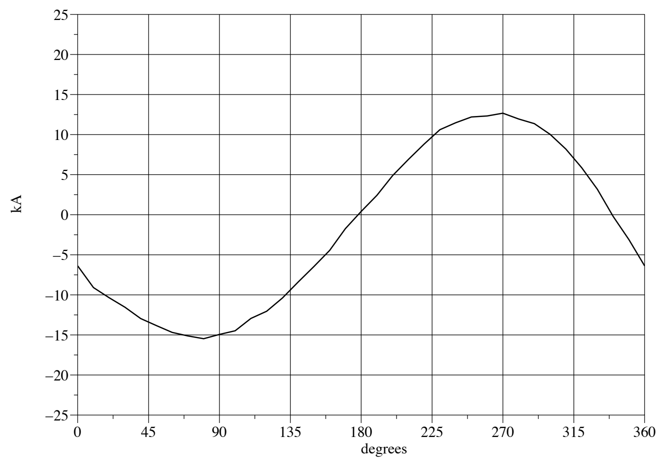

Figure 3.23 Current drive vs phase for fixed λ_0 model during 280 Hz partial sustainment

Unfortunately, the fixed λ_0 model failed miserably for full sustainment. The current dropped like a stone after the DC voltage switched off. Many of the variables went off into the weeds and eventually crashed the simulation. The reason is probably due to the sensitivity of the current to α and λ_0. The total current I_z very roughly goes with the area under the $\lambda = J/B$ curve. With a little calculus and using the average values for α and λ_0 we see that the area is 3 times more sensitive to λ_0 than to α. This sensitivity was not a problem for the slight perturbations of partial sustainment, but a more aggressive impact is necessary to drive full sustainment. What we learn from this is that OFCD must do more than just modulate the flatness of the current profile.

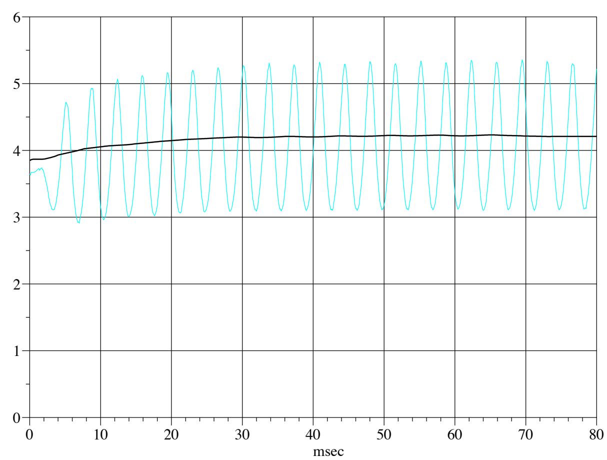

Figure 3.24 The α shape parameter vs time during 280 Hz partial sustainment using the fixed λ_0 model. Rising α means a flattening J/B profile.

Figures 3.26 through 3.29 show the reversal and pinch parameters, magnetic energy, and power lost to ohmic dissipation. They are each nearly identical to the results for the fixed α model. The $F - \Theta$ trajectory in figure 3.27 shows a somewhat wider excursion than what we saw in figure 3.8.

Since the fixed λ_0 model failed in full sustainment, we'll eventualy concentrate on the fixed α relaxed state model.

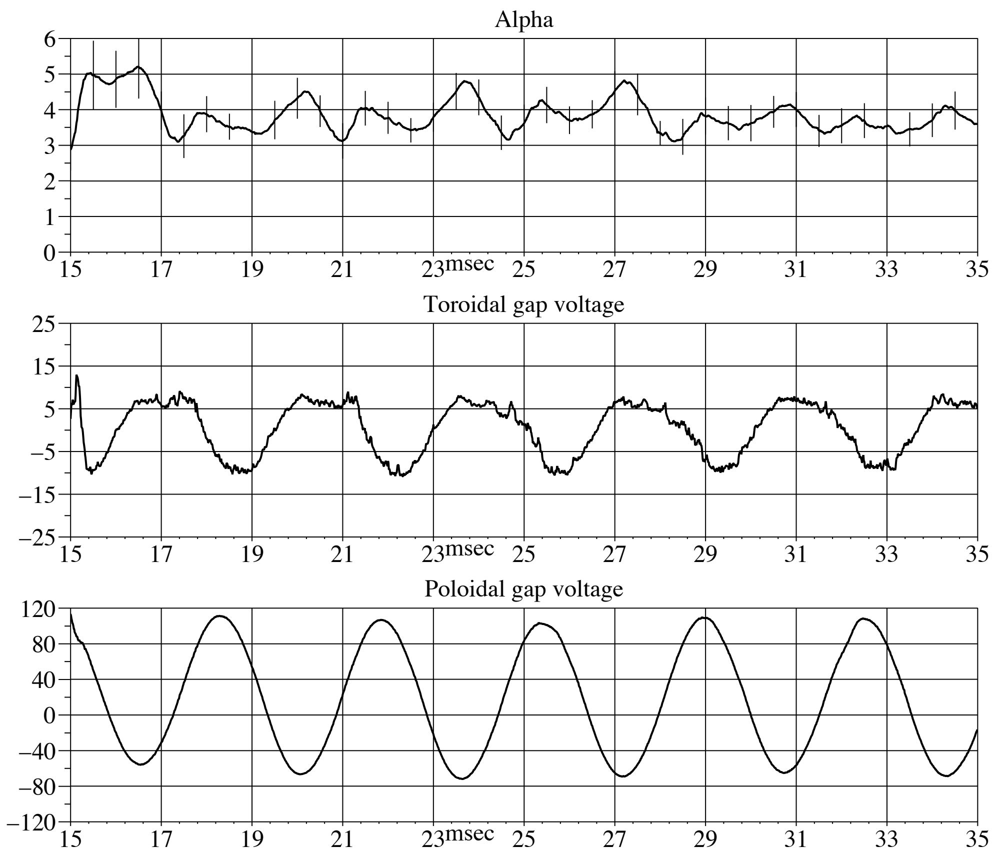

Figure 3.25 Measured value of the α shape factor along with the toroidal and poloidal gap voltages for 280 Hz OFCD.

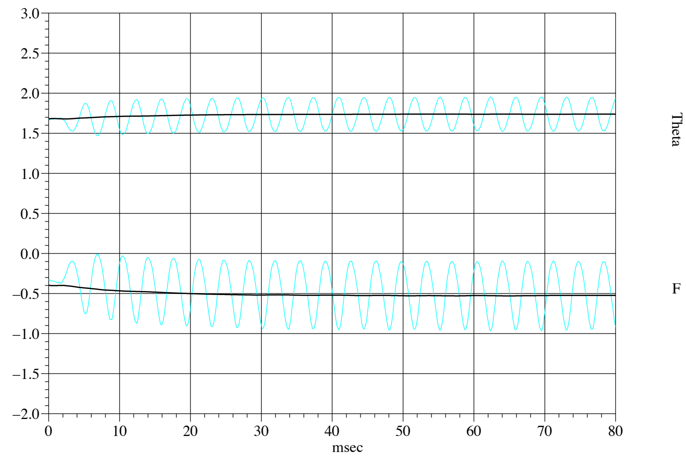

Figure 3.26 The reversal and pinch parameters predicted by the fixed λ_0 model for 280 Hz partial sustainment

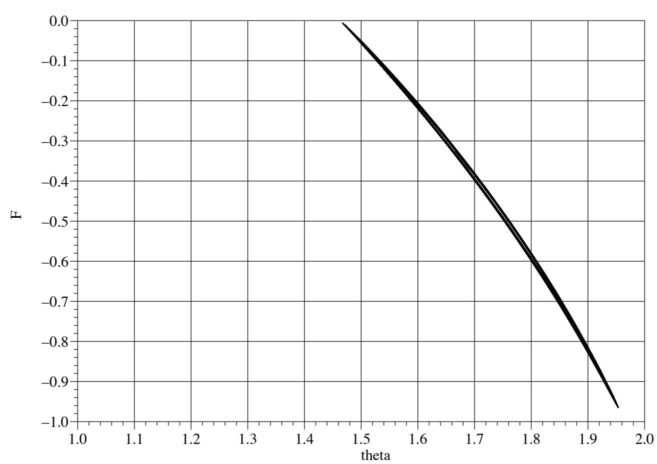

Figure 3.27 The $F - \Theta$ trajectory predicted by the fixed $lambda_0$ model for 280 Hz partial sustainment

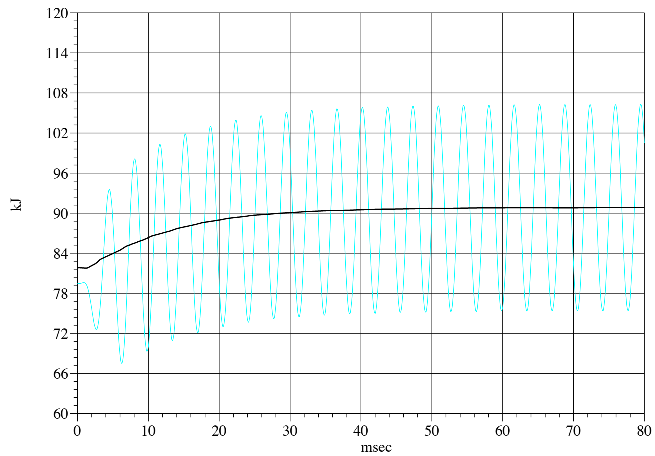

Figure 3.28 Magnetic energy vs time predicted by the fixed λ_0 model for 280 Hz partial sustainment

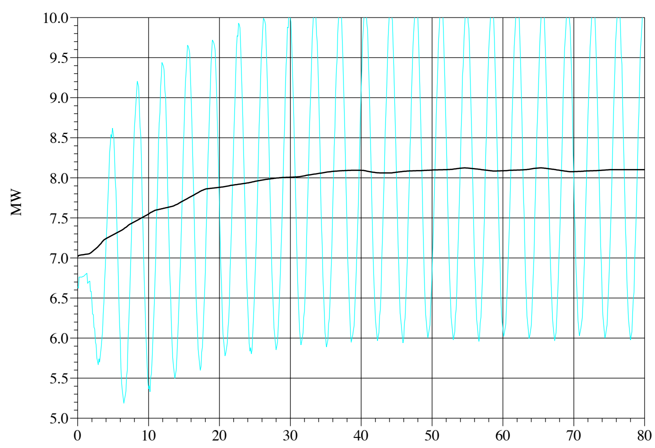

Figure 3.29 Ohmic power dissipation predicted by the fixed λ_0 model for 280 Hz partial sustainment

3.3.1.4 Variable α and λ_0

Having seen somewhat similar behavior in both the fixed α and fixed λ_0 models we are encouraged to let both λ_0 and α roam free. The algorithm is pretty much the same as with the fixed α and λ_0 cases, but the optimizer that determines the best fit magnetic field profile now controls α as well as λ_0 and $B_z(0)$, the toroidal field on axis. Since we have three unknowns now we need one more constraint, namely the poloidal flux (from the time integral of the toroidal loop voltage.) For the fixed α or fixed λ_0 models we used a large lookup table rather than calculate everything on the fly to speed things up. We could use another lookup table for this model but with 3 dimensions the table would be huge and require a month to generate. So we calculate the magnetic field profiles on the fly, and the model doesn't run as fast. The model was not explored as extensively as the fixed α model because of time constraints.

Partial sustainment: We start, as we did for the fixed α model, with partial sustainment. Figure 3.30 predicts a current drive of about 10 kA, less than predicted by the fixed α model and not as steady. Narrowing the optimization criteria might smooth the curve out, but it would lengthen the simulation time unacceptably.

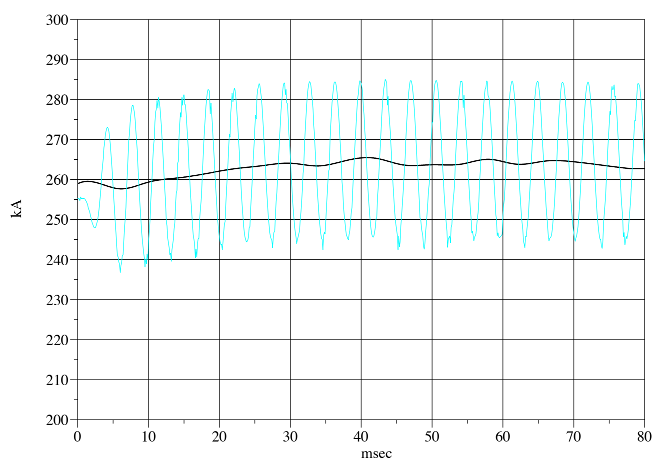

Figure 3.30 Toroidal current predicted by the free α and λ_0 model for 280 Hz partial sustainment .

Figure 3.31 shows the scale factor of the alpha model $\lambda_0 = J_\parallel/B$ vs time. It unexpectedly drops with time. But the toroidal current I_z in figure 3.30 is increased by OFCD so the shape factor α must change with time to compensate. Figure 3.32 shows that α increases with time, broadening the current profile. It is disturbing that these two quantities don't settle down within the L/R time scale of the plasma as everything did in the fixed α and fixed λ_0 models. This casts doubt on the validity of the model. It may be that the optimizer is just not fast enough. Further studies are needed.

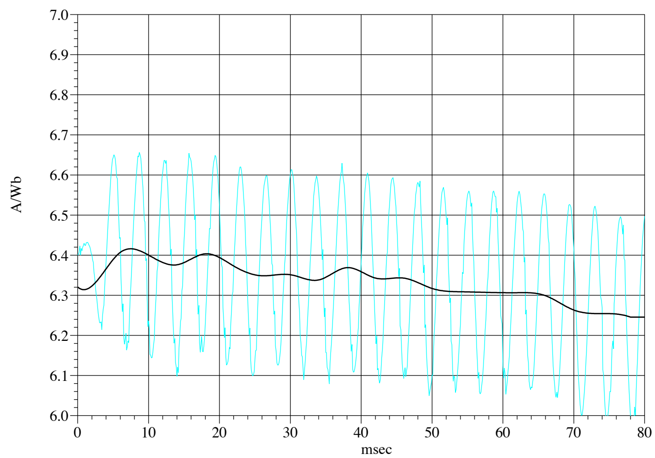

Figure 3.31 Normalized parallel current density λ_0 predicted by the free α and λ_0 model for 280 Hz partial sustainment.

Figures 3.33 and 3.34 show that the evolution of the reversal and pinch parameter differ little from the fixed α model.

Finally, the magnetic energy in figure 3.35 and ohmic power dissipation in 3.36 are comparable, on average, to the fixed α model, if a bit bumpier. They are slightly smaller reflecting the lower current drive in figure 3.30.

Full sustainment: Figures 3.37 through 3.43 show the results for full sustainment simulations. Again the dc toroidal loop voltage cuts off at 15msec. The voltage amplitudes are the same as for the fixed α full-sustainment case. The results are pretty much same as for the fixed α except

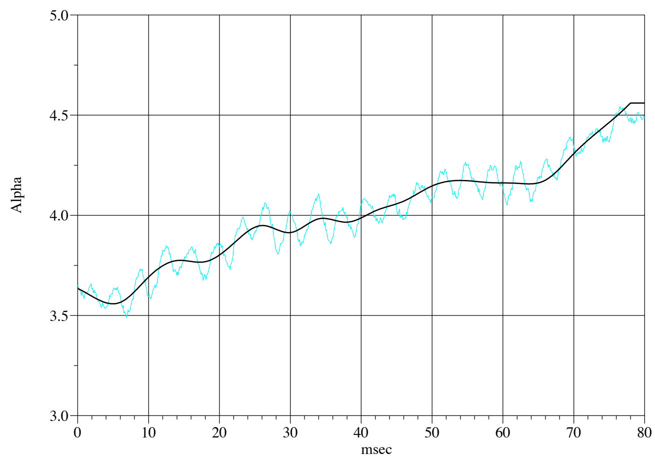

Figure 3.32 Shape factor α predicted by the free α and λ_0 model for 280 Hz partial sustainment .

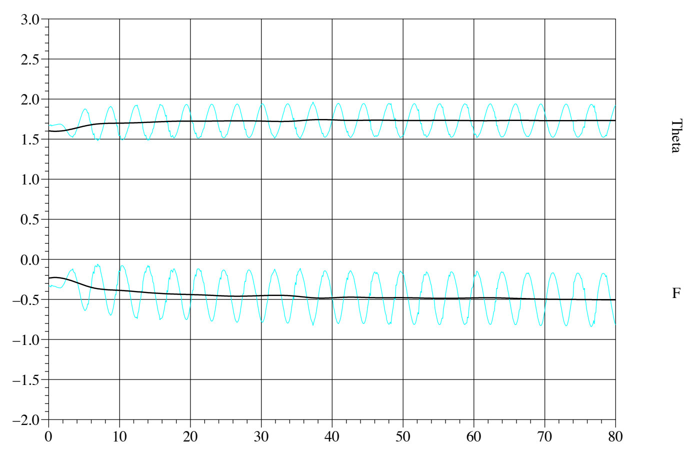

Figure 3.33 Reversal and pinch parameters predicted by the free α and λ_0 model for 280 Hz partial sustainment .

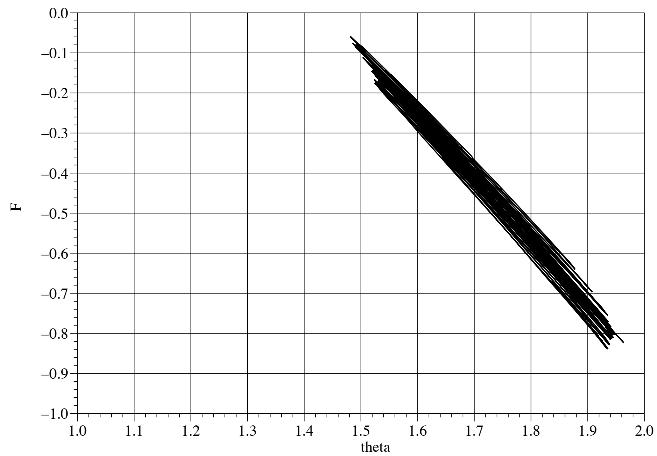

Figure 3.34 The $F - \Theta$ trajectory predicted by the free α and λ_0 model for 280 Hz partial sustainment .

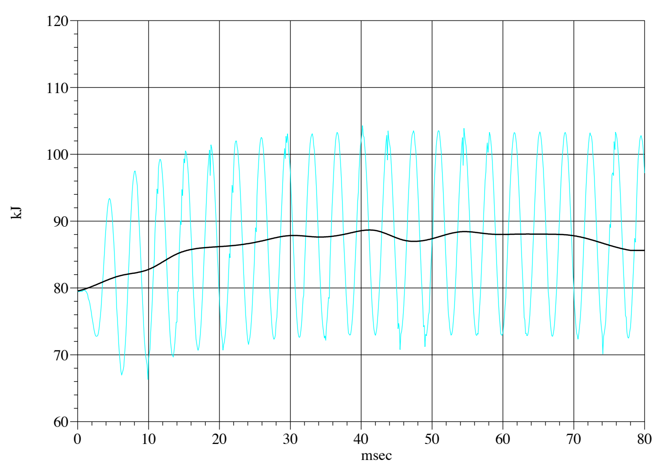

Figure 3.35 Magnetic energy W predicted by the free α and λ_0 model for 280 Hz partial sustainment.

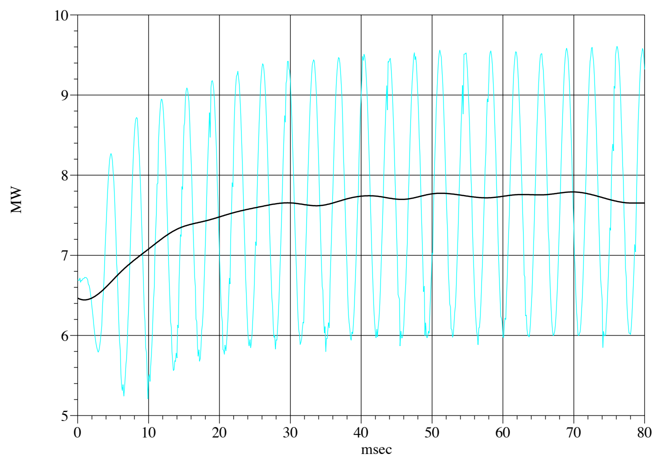

Figure 3.36 Ohmic power dissipation predicted by the free α and λ_0 model for 280 Hz partial sustainment .

for the scale factor λ_0 in figure 3.38 and the shape factor in figure 3.39. λ_0 settles to a lower value (6) compared to the fixed α case (6.3). The difference is not insignificant since the model is particularly sensitive to λ_0. Figure 3.39 shows that α appears to compensate for the lower value of λ_0 by settling to a higher value (4.6) compared to the fixed α value of 3.77. Higher values of α mean a flatter current profile. All the other results (magnetic energy, F-Θ trajectory, etc) are very nearly the same as for the fixed α model. Admittedly, the peculiar shape of the α vs time is suspicious and calls into question the variable α , λ_0 model, or at least the way I'm solving it.

Since the results of the fixed and variable α models are very nearly the same and because the variable α model is so much more computationally expensive (4 hours vs 30 sec) any further studies will be performed using the fixed α model.

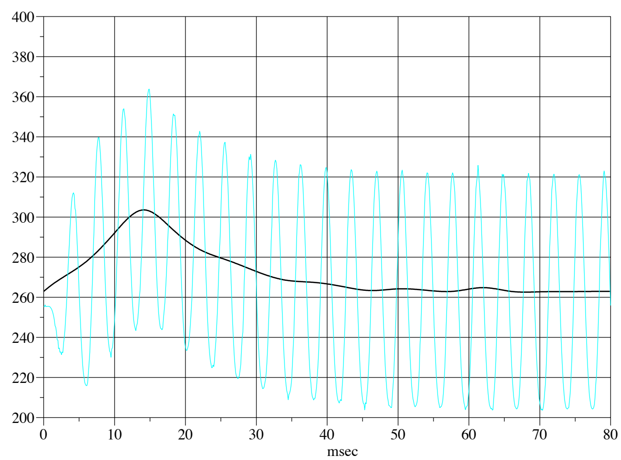

Figure 3.37 Fully sustained current drive as predicted by the free α and λ_0 model. DC loop voltage cuts off at 15 msec.

3.4 Summary

We discussed the physics and optimization of OFCD. With a little math we examine OFCD from a helicity injection standpoint. From the math we find that, on average, helicity decay can be overcome by oscillating the toroidal and poloidal loop voltages at the same frequency and the right phase difference. We saw that the helicity injection rate has a sinusoidal dependence on the phase

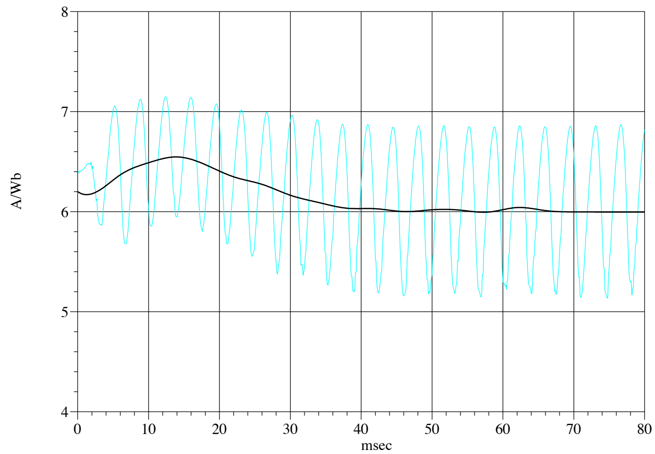

Figure 3.38 Normalized parallel current density λ_0 predicted by the free α and λ_0 model for 280 Hz full sustainment.

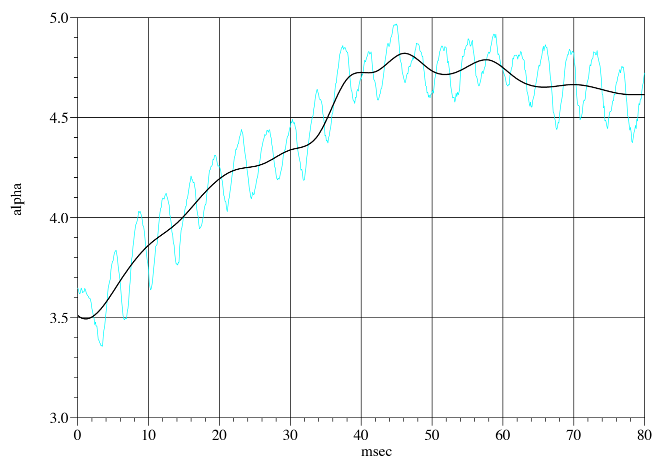

Figure 3.39 Shape factor α predicted by the free α and λ_0 model for 280 Hz full sustainment.

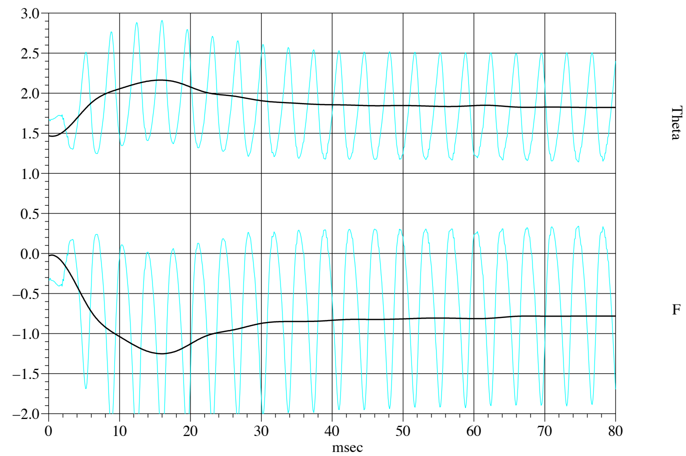

Figure 3.40 Reversal and pinch parameters predicted by the free α and λ_0 model for 280 Hz full sustainment.

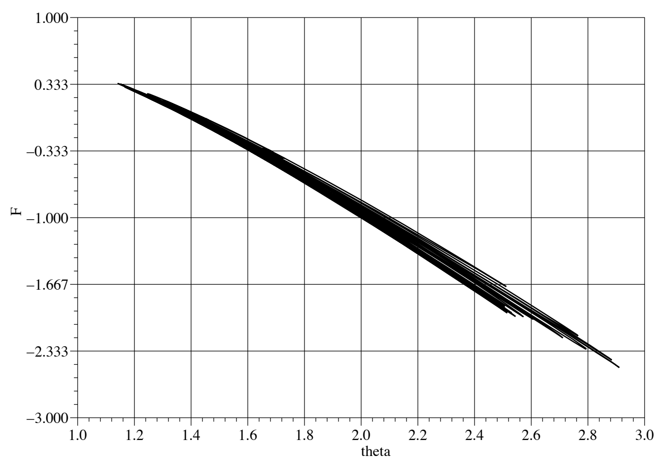

Figure 3.41 The $F - \Theta$ trajectory predicted by the free α and λ_0 model for 280 Hz full sustainment.

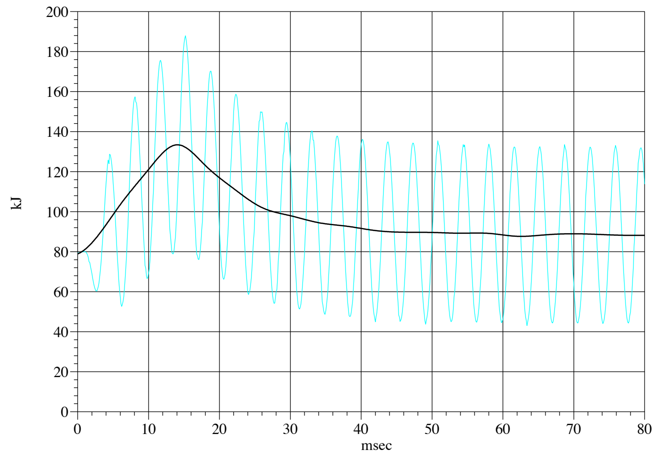

Figure 3.42 Magnetic energy W predicted by the free α and λ_0 model for 280 Hz full sustainment

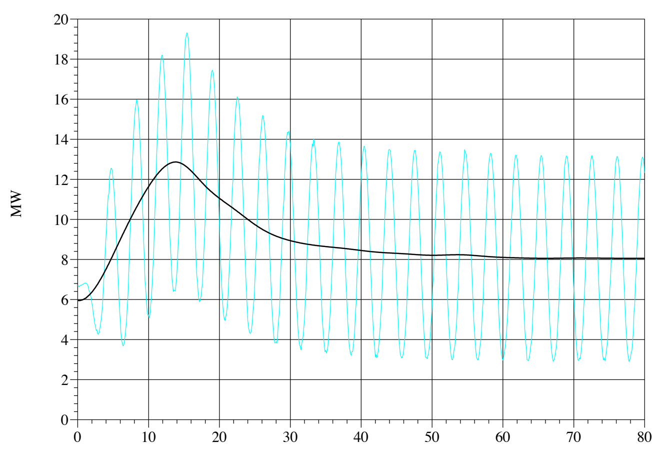

Figure 3.43 Ohmic power dissipation predicted by the free α and λ_0 model for 280 Hz full sustainment.

difference between the oscillating volages. We presume this will translate into current drive since you can't have one without the other.

With a 1D numerical model we make some assumptions about the current profile (namely, the α model) and otherwise treat the whole problem as a big black box to which we apply two voltages and examine the currents that result. We consider three dynamic versions of the α model. The first is a relaxed state model where the shape parameter α is held constant and the scale factor λ_0 is allowed to vary in time. We examined current drive, effects on the reversal and pinch parameters, ohmic power dissipation, and magnetic energy. For the case where the usual DC loop voltages are present and OFCD is only a small perturbation (partial sustainment), this model predicted additional current drive of about 5% for the hardware we have. The current drive exhibited the sinusoidal dependence predicted by the math. Using this model we found that the optimum parameters for partial sustainment were a frequency of 280 Hz, an amplitude ratio of about 7 (measured at the gaps), and a phase difference of $90°$. For full sustainment, the optimum values were the same but the applied voltages were 3 times larger. One disconcerting feature of the full sustainment results is the prediction that the plasma will be driven out of reversal for part of the oscillation. The effects of this can't be predicted by our simple model.

The second dynamic version of the α model holds the scale factor λ_0 constant and allows α to vary, emulating the effect of an edge current. The results for partial sustainment were nearly identical to the relaxed state model.

The third version allowed both α and λ_0 to vary. The results were again nearly the same as the relaxed state model for both partial and full sustainment, though some observed behavior of the simulations were unsettling. The results from this third version are suspicious and worthy of further study (by somebody else.)

Chapter 4

Experimental Setup

The platform for our OFCD experiments is the Madison Symmetric Torus described briefly in section 4.1. The two oscillators that provide the oscillating toroidal and poloidal loop voltages are described in section 4.2. Section 4.3 describes the diagnostics native to MST that were used to characterize OFCD's performance and effects on the plasma. Due to power limitations of the oscillator we were unable to try for full sustainment. The specifications of the oscillator reflect that limit.

4.1 The Madison Symmetric Torus

MST is an unusual reversed field pinch because the toroidal winding is the vacuum vessel itself, yielding very little magnetic field error. The vessel is made of 5cm thick aluminum and serves as the conducting wall required by Taylor's boundary conditions and to stabilize the ideal kink. The poloidal loop voltage that creates the initial toroidal field is applied to a toroidal gap on the inside perimeter of the vessel. The toroidal loop voltage is provided by induction from a large 2 volt-second iron core threading the machine, giving it its transient nature. The vessel has a poloidal gap allowing the toroidal electric field into the plasma. Both loop voltages are driven by pulse transformers fed by a 4 story 5kV capacitor bank. A pulse length is typically about 60 msec and the flattop lasts for about half that. The vacuum vessel has a soak in time of about 1 sec, so the vessel confines the magnetic flux throughout the flattop portion of the shot. A crowbar power supply is switched on after reversal to overcome the resistive loss of the toroidal field circuit.

The important parameters for MST are listed below.

major radius R_0	1.5 m
minor radius a	.52 m
peak plasma current Ip	600kA
density	$0.5 - 3\ 10^{13}/cm^3$
β	.1

4.2 The Ignitron Oscillator

For a first stab at OFCD we decided to try a low power partial sustainment system that would add about 10kA to (or subtract from) the flattop current. This is obviously not nearly enough for full sustainment but it would give us the opportunity to study the physics of OFCD and see if the concept would work at all before committing to a high power solution.

So a simple cheap low power (if a million watts is your idea of low power) oscillator was proposed using ordinary household ingredients. Two would be built, one for the poloidal and one for the toroidal circuit. They were expected to produce about 1 MVA of power and could be slapped together in maybe a year. Seven years later they still do not work consistently and have been an endless source of irritation to the author. An idealized schematic of the oscillator is shown in fig 4.2. For the familiar reader, it looks kind of like a bistable multivibrator. The frequency is set by the LC tank. Current is fed into a center tap of the inductor from a Pulse Forming Network (PFN.) The switches commutate back and forth pulling the input current back and forth sustaining the oscillation in the LC tank. Energy is coupled off the inductor and routed to MST. Each oscillator is in series with some part of the MST power supplies.

A more realistic schematic of the circuit is shown in figure 4.3. The commutating switches are ignitrons, a mercury-based switch that prefers to work at DC. The LC tank is broken by an ignitron/diode combination so that the tank can be precharged to ensure the first cycle is at the full voltage. Since the timing of the commutation is critical, a sample of the tank current is coupled off with a Rogowski coil and used as feedback to the ignitron triggers.

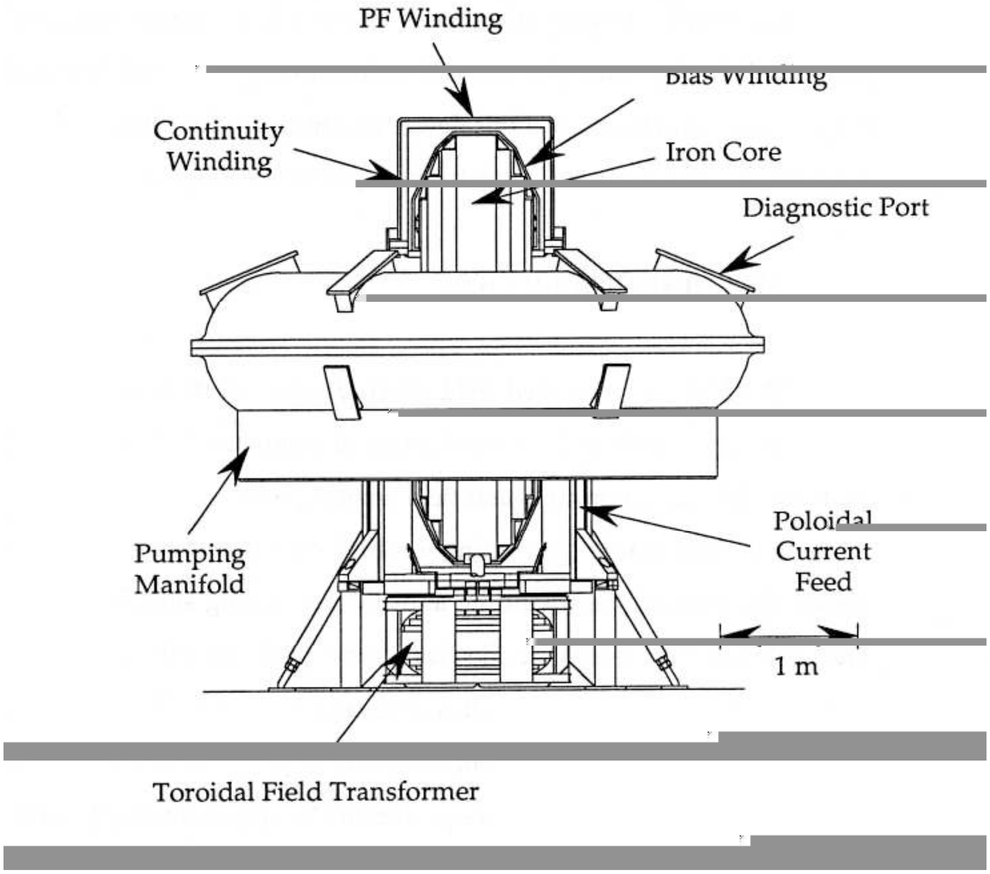

Figure 4.1 The Madison Symmetric Torus

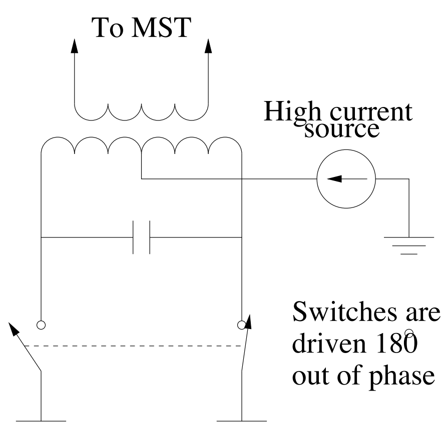

Figure 4.2 Idealized schematic of the ignitron oscillator

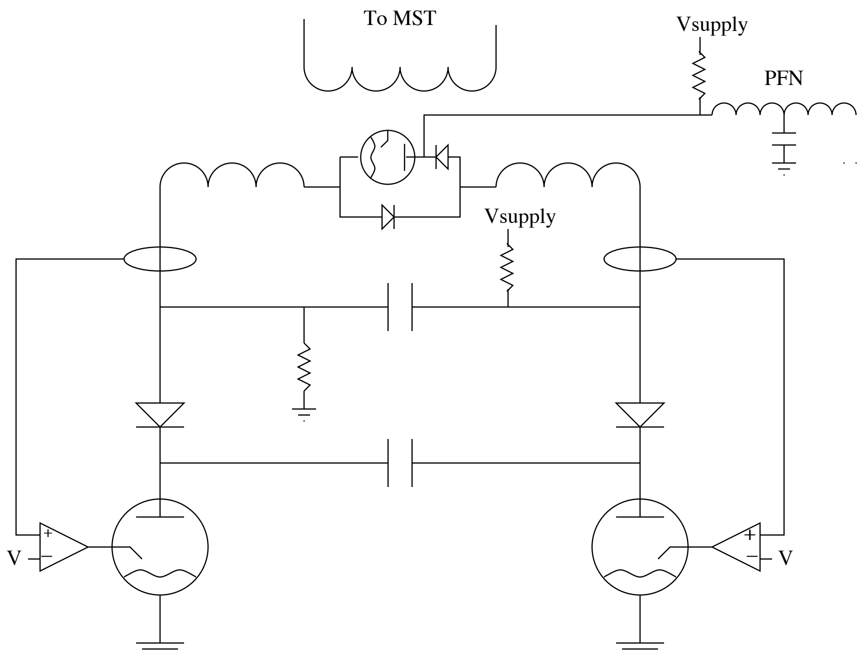

Figure 4.3 Schematic of the ignitron oscillator version 12.something

Given that one oscillator drives a poloidal current and the other drives the toroidal current they are referred to as the Oscillating Poloidal Current Drive (OPCD) oscillator and the Oscillating Toroidal Current Drive (OTCD) oscillator.

Figure 4.4 shows the OPCD oscillator. It is connected to the Bt circuit through the crowbar supply. The LC tank is made up of the suitcase sized capacitors in the foreground and a transformer made of garden hose sized cables wound on a wooden form in the background. The ignitron that breaks the tank circuit (the *connect ignitron*) is mounted on a shelf above the transformer. Figure 4.5 shows the connect ignitron assembly. The D-size ignitron is accompanied by stacks of the white hockey puck-size diodes seen in figure 4.5. The arrangement of diodes attempts to maintain positive current flowing through the connect ignitron to keep it turned on. The diodes are connected in series to reduce the voltage across each of them. Nevertheless we frequently kill these diodes even though together they are rated for much higher voltages than we've measured at that point in the oscillator. Their demise remains an unwelcome mystery.

Figure 4.6 shows the commutating ignitron assembly. The assembly now holds two A size ignitrons but may be upgraded to larger devices if this design is scaled up for the next step in the OFCD program. The stack of white hockeypucks next to each ignitron are the diodes in series with each anode. The glass mica capacitors strung across the anodes of the ignitrons help snuff out one ignitron when the other fires. Looking at figure 4.3 we see that when one oscillator turns on the anode is suddenly pulled to ground (minus the voltage drop across the ignitron, which is small.) The glass mica capacitors carry the jump to the other ignitron pulling the anode negative (it was already near zero) thereby reverse biasing the device. Since ignitrons only conduct in one direction (supposedly) the reverse bias snuffs that ignitron out. Half a cycle later the process is mirrored to the other ignitron. So the commutating ignitrons not only pull the current from the supply into the tank but in doing so they aid each others efforts to switch off when doing so. From bitter experience we've found that they often conspire against each other to stay on.

Figure 4.7 shows the anode voltages of the two commutating ignitrons and the tank current of the OPCD oscillator on a good day. The current plot is uncalibrated, so ignore the scale. The actual amplitude is about 8 kA. Also ignore the start up transients at the beginning. Start at 19.3 msec.

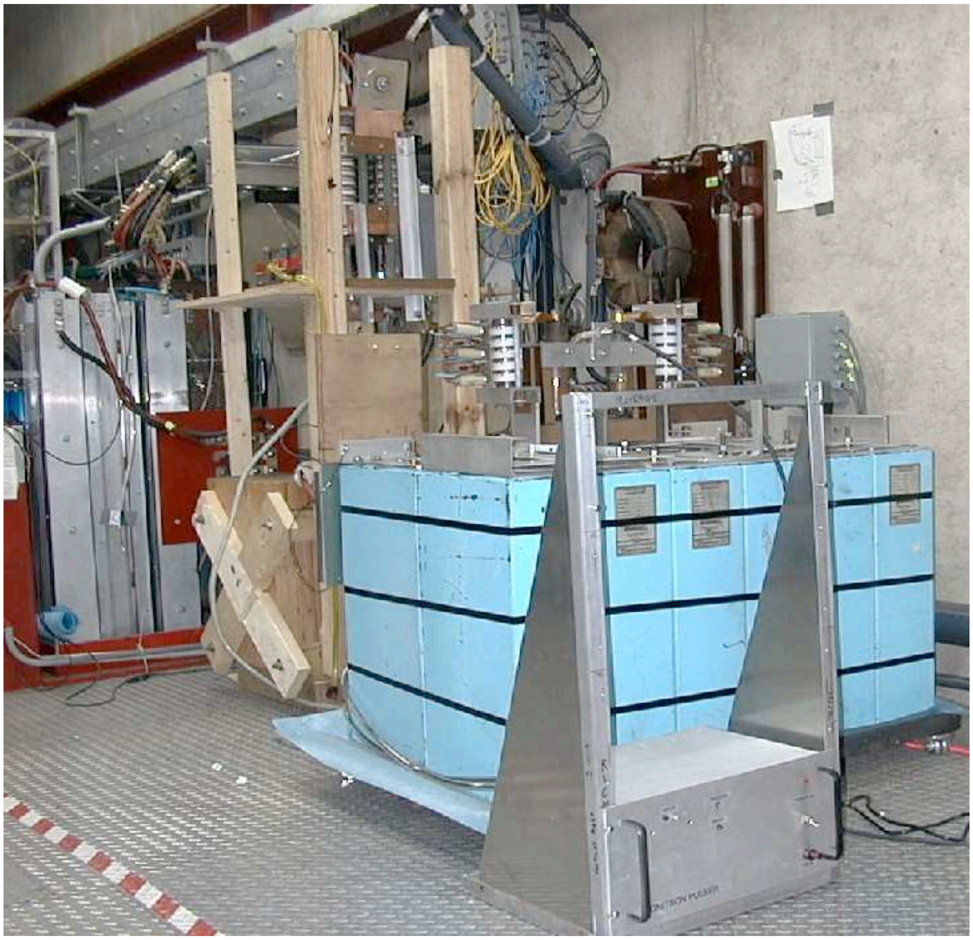

Figure 4.4 An actual photograph of an actual ignitron oscillator

Figure 4.5 The connecting ignitron assembly.

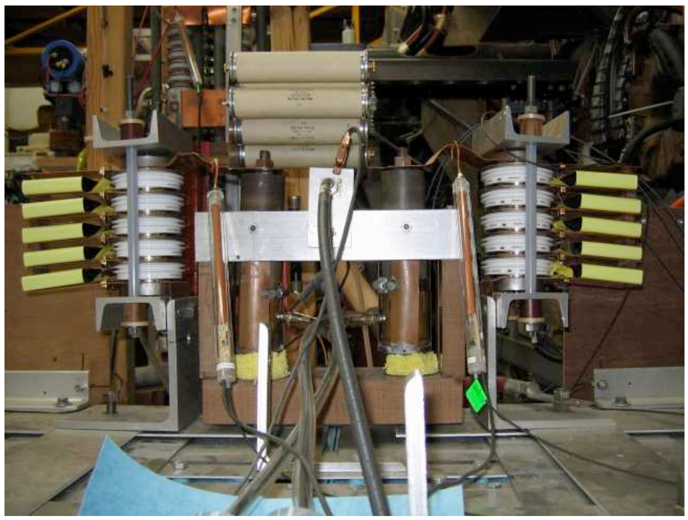

Figure 4.6 The commutating ignitron assembly.

Ignitron 1 has just turned on so the anode voltage holds at zero. Ignitron 2 just turned off so it starts to fall. As the anode voltage of ignitron 2 nears completion of its half cycle a threshold detector senses that the voltage is about to cross zero and fires a trigger into that ignitron, turning it on and clamping the anode to zero. This sends a pulse (visible at 21 msec) through the mica capacitors to ignitron1 reverse biasing it momentarily and turning it off. The situation is then mirrored for the other half of the cycle. The result is the clean sinusoidal tank current shown in the bottom plot. Note that the threshold detector in this plot is firing a bit early in each half cycle.

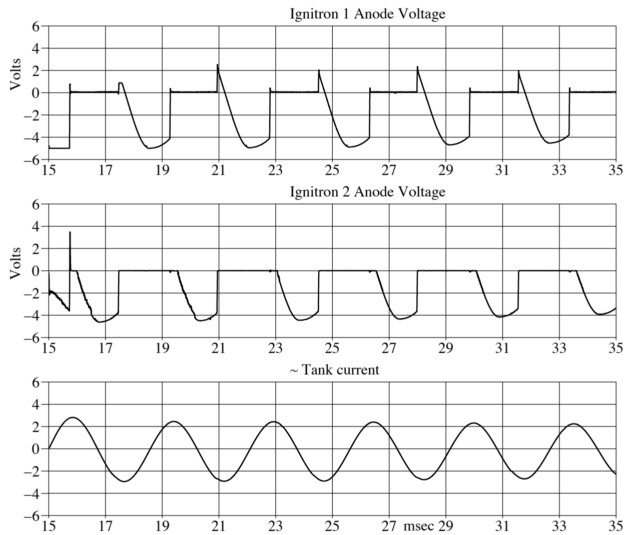

Figure 4.7 Anode voltages of the commutating ignitrons and the tank current.

In reality either ignitron is often happy to conduct current in the wrong direction. The result, at best, is a commutation failure as seen in figure 4.8. The plot shows the anode voltages for the two commutating ignitrons in the OPCD oscillator. There are two commutation failures, one at 25.5 and one at 32.5 msec. To see what's happening, start at 24.5 msec. Ignitron 1 has just turned off and ignitron 2 has just turned on. The anode voltage on ignitron 1 starts to fall, but halfway through its half cycle ignitron 1 breaks down and turns on, clamping the anode to zero. The mica capacitors connecting the anodes thus carry a large pulse across to ignitron 2, turning it off. The cycle has been disrupted. In the next cycle the oscillator recovers until another failure at 32.5 msec. Each time a cycle is disrupted the current dips and the phase of the whole waveform is shifted. Sometimes an ignitron will just stay on and drain the PFN while the tank rings down.

Why the commutation failures occur has not been concretely determined. One possibility is mercury collecting on the anodes. Heating the anodes helped, but not much. We've seen more improvement by cooling the cathodes, which are usually encased in ice. The biggest improvement in avoiding reversed current came by putting diodes in series with the ignitrons. This helped a great deal but we frequently kill the diodes (which fail shorted,) nullifying the improvement. Why the diodes die is a mystery. It takes a large voltage spike to kill one of these diodes and we can find no voltages in our system that come close to what it takes to kill an entire stack. Heftier diodes are now in place and are dying less frequently.

Another source of aggravation has been the connect ignitron. It is supposed to stay on once the oscillation begins, but will sometimes switch off and stay off, bringing the oscillation to a grinding halt. Or it will switch on and off intermittently either distorting the waveform with sharp transients or triggering a commutation failure.

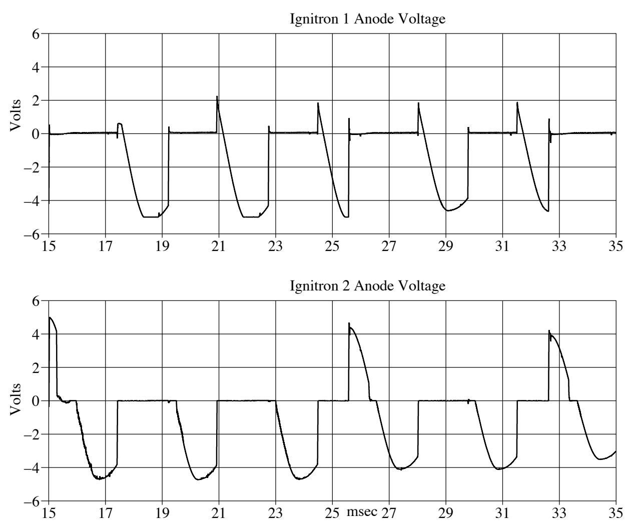

Figure 4.8 The anode voltages of the commutating ignitrons during a failure

Ignitrons are mercury based thyristors that were never meant to be switched on and off while current is still flowing through them. But they are cheap and can move an enormous amount of current with very little loss. They work great as long as you trigger them only once, run a unidirectional current through them, and wait till the current runs out. A schematic of an ignitron is shown in fig 4.9a. The cathode is a pool of mercury. A voltage is applied to the anode and a pulse is fired into the ignitor. The ignitor causes a small arc that establishes a cathode spot on the mercury. Electrons are boiled off the mercury and hit the anode as with any vacuum tube.

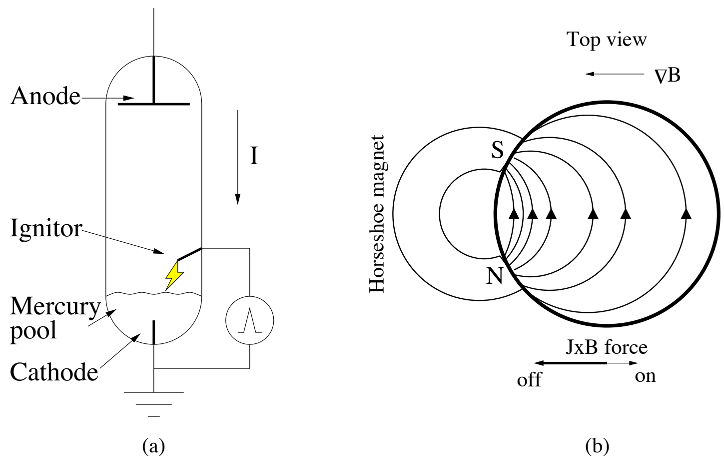

Figure 4.9 (a) The ignitron switch. (b) one of many tricks employed to make them behave.

Like any thyristor the ignitron is supposed to conduct current in only one direction. But with enough reversed voltage they can, unfortunately, be pursuaded to carry reverse current. Shown in fig 4.9b is one of the more clever tricks devised by Paul Nonn to coax the commutating ignitrons to switch off when the current is reversed. Small horseshoe magnets create a large magnetic gradient across a cross section of the ignitron. The electron beam is deflected by the $\mathbf{J} \times \mathbf{B}$ force one way or the other depending on the direction of current flow. When current is flowing in the right direction it is deflected into the region of weaker magnetic field so the path is only slightly diverted. But when current is flowing in the wrong direction the beam is deflected into the region of stronger field where it will eventually hit the wall and be quenched. It helped. But the biggest improvement in the reliability of the oscillators was still the diodes in series with the commutating ignitron anodes and the diode arrangement at the feedpoint that almost ensured positive current was always flowing through the connect ignitron.

After 7 years and all this, one of our not-so-cheap and not-so-quick oscillators works very consistently and delivers twice as much power as expected for about 30 msec. The other still has a failure rate of about 50%, primarily due to the connect ignitron switching off in mid-cycle.

Another problem is the frequency and relative phase of the two oscillators. 1D modeling says they should be $90°$ out of phase for maximum current drive. We set the phase difference by firing one oscillator before the other. Unfortunately the resonant frequency of each LC tank changes as the load on the secondary changes as a function of time. So the frequencies and/or relative phases of the oscillators can drift a lot during the shot as shown in figure 4.10. Tuning the oscillator frequency is laborious. The only practical way is to change the inductance in the LC tank by adding windings or adjusting the spacing between the windings. Either can take hours but it only has to be done once (hopefully.) There is little that can be done about the phase drift without sacrificing power coupling. The drift is not consistent so we rely on statistics to give us enough good shots to do ensemble averaging.

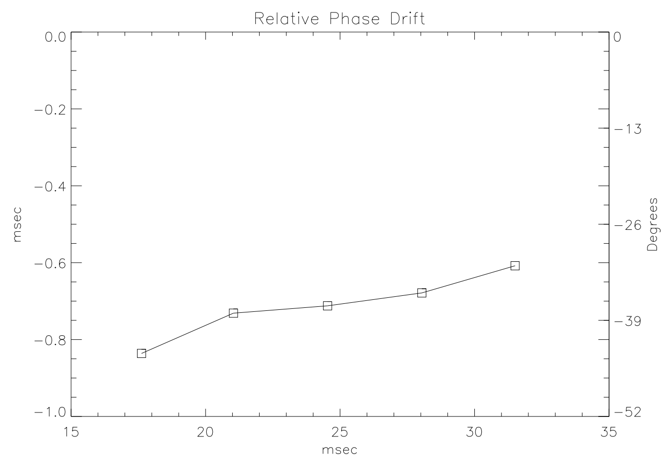

Figure 4.10 Drift in the relative phase of the oscillators

One of those rare occasions where both oscillators are working is shown in 4.11 at the gaps.

Other designs The ignitron oscillator has been a long time coming and is still not quite working properly. One of the two oscillators still has a failure rate of nearly 50%. It may be that ignitrons were the wrong device for this application. Or it may be that ”OFCD” is a satanic incantation in some dead language or we built the damn things over an ancient indian burial ground. For future experiments it is worth knowing that other designs do exist. The HIT-SI[26] device at University of Washington uses an H-Bridge programmable power supply as shown in figure 4.12 to power their

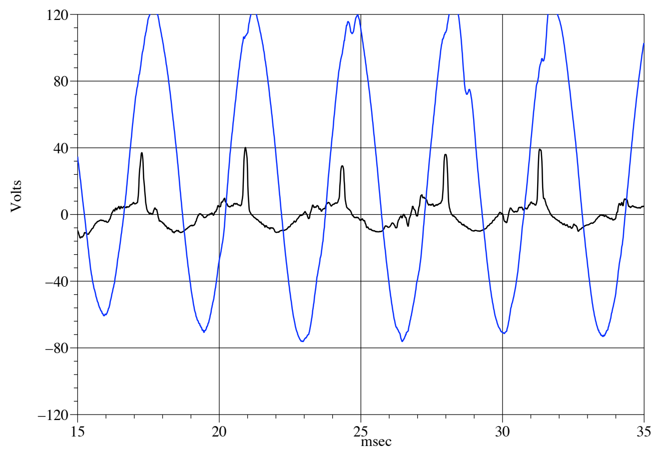

Figure 4.11 The toroidal and poloidal gap voltages during a good OFCD shot

device. The device uses Insulated Gate Bipolar Transistors as switches and pulse width modulation to make a 500kW arbitrary waveform generator with a bandwidth of about 1kHz. The design is so robust the HIT crowd simply bolts the outputs together to run them in parallel for higher power. A lower power version of this supply is already in use in the field error correction system of MST[27]. The H-Bridge can produce a waveform of any shape that will fit within its bandwidth (about 1 kHz). If OFCD is condemned to sinusoids the H-Bridge would at least allow the frequency to be easily adjusted and even chirped during the discharge to accommodate slowly changing plasma conditions. There are plans in place to replace the Bt power supply with a programmable supply perhaps using a collection of H-bridges. The design may accomodate sinusoidal perturbations at OFCD frequencies. Someday the Bp power supply might be replaced as well, but that is a much more expensive and long term venture.

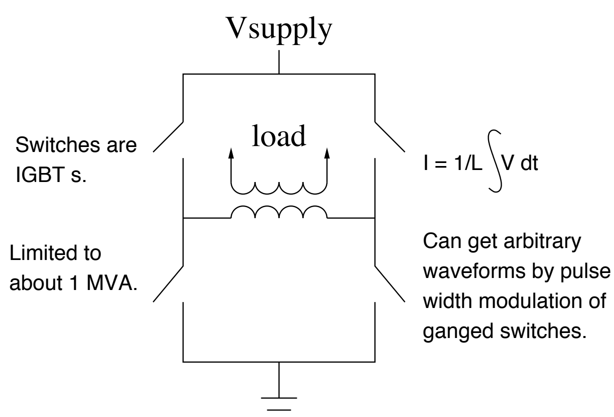

Figure 4.12 H Bridge programmable power supply

4.3 Diagnostics

We here briefly review the diagnostic tools used to gather the data seen in chapter 5.

4.3.1 Edge magnetic probes

To measure the magnetic fluctuations in the plasma, small coils are arrayed around the toroidal and poloidal direction inside the vacuum vessel as shown in figure 4.13. The diagnostic relies on the fact that the radial fluctuations in $\mathbf{B}$ are global, so they can be measured at the edge of the plasma. Each package contains 3 coils, one each for the toroidal, poloidal, and radial directions. Since a coil only measures $\dot{B}$, each is fed to an integrator. Sampling the fluctuations in the toroidal (or poloidal) direction is like sampling a waveform in time. You need more than 2 points per cycle (wavelength) to reconstruct the waveform. There are 32 coils that sample the poloidal component of the fluctuation. There are 64 that sample the toroidal component. So we can examine the spectra of the m=0 and m=1 fluctuations up to n=32 with a discrete Fourier transform (DFT.)

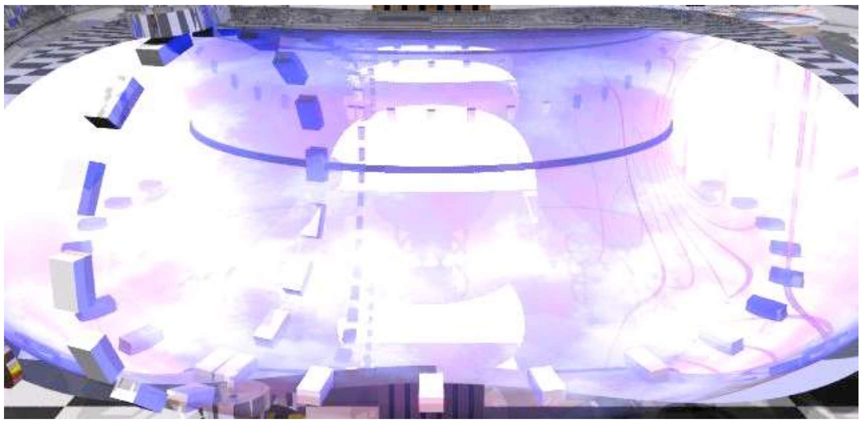

Figure 4.13 Artistic cutaway section of MST shows $\dot{B}$ coils arrayed in toroidal and poloidal directions

4.3.2 Rutherford Scattering

In days of yore, Rutherford scattering was used to measure properties of the nucleus by firing light ions, usually α particles, at a thin foil and measuring the distribution of scattered particles. The scattering was caused by simple Coulomb repulsion between the two ions. In plasma experiments like MST, Rutherford scattering measures the deuterium ion temperatures by firing a monoenergetic beam of neutral helium atoms into the plasma and measuring the broadening of the energy spectrum of particles scattered only a few degrees from the beam.[20] The signals are noisy and require large ensemble averages to shrink the error bars.

4.3.3 FarInfraRed interferometer

FIR, or Far Infrared, refers to light with wavelengths between 1 and 10 mm. The FIR system provides a radial profile of the electron density, plasma current density, and magnetic field. The FIR system has 2 modes of operation: interferometry and polarimetry.

A plasma has a refractive index that depends on the electron density. The FIR system sends one laser beam through the plasma (the probe beam), one through the air (the reference beam), and measures the phase difference between them. The measured phase difference is proportional to the average plasma electron density along the beam path. In MST, the FIR folks send multiple probe beams through the plasma at different radii. They then apply an inversion technique to obtain a profile of the plasma electron density.

When a linearly polarized electromagnetic wave is propagating parallel (or anti-parallel) to the magnetic field in a plasma, the polarization of the wave exiting the plasma will rotate by a small angle called the Faraday rotation angle. The FIR system measures the Faraday rotation, which is proportional to the line average of the electron density times the magnetic field component parallel to the beam path. The combined interferometer phases and Faraday rotation angles can then be combined to determine the poloidal magnetic field distribution. Using Ampere's law, the toroidal plasma current can be determined as well.

4.3.4 Thomson scattering

Thomson scattering is the result of a collision between a photon and a charged particle, such as an electron in the plasma. When an electron and photon collide the electron feels a Lorentz force from the oscillating electric and magnetic fields of the photon and is accelerated. This acceleration causes the electron to emit a different photon in a different direction. This emitted photon has a wavelength shifted from that of the incident photon by an amount dependent on the electron energy. This scattering of a photon by an electron is called Thomson scattering. Since the wavelength of the scattered photon depends on the energy of the scattering electron, Thomson scattering is good way to measure the energy of an electron. This is done by creating a photon of known wavelength and measuring the wavelength of the scattered photon. The wavelength distribution of the scattered photons tells us the energy distribution of the electrons in the plasma, giving us a direct unobtrusive way of getting the temperature of the electrons. The amount of photons we actually collect can also tell us something about the electron density of the plasma.

4.3.5 CHERS/IDS

Ion Doppler Spectroscopy (IDS) measures emissions from impurity ions. Emissions from electron-impurity ion recombination are Doppler broadened by the thermal motion of the ion. Measuring that broadening and relying on fast equilibration between the impurity and deuterium ions yields a rough measure of the bulk ion temperature. In Charge Exchange Emission Recombinations Spectroscopy (CHERS) the effect is enhanced by injection of energetic hydrogen neutrals.

4.3.6 Edge probe

A triple-tip Langmuir probe was employed to measure the stability of the m=0 mode. To understand what the probe measurement mean, we first need to do a little math. Take the curl of Ohms law (assuming constant resistivity),

$$\nabla \times \mathbf{E} + \nabla \times \mathbf{v} \times \mathbf{B} = \eta \nabla \times \mathbf{J} \tag{4.1}$$

Apply Faradays law on the first term, Amperes law on the third term, and rearrange:

$$\frac{\partial \mathbf{B}}{\partial t} = \nabla \times \mathbf{v} \times \mathbf{B} - \frac{1}{\mu_0} \eta \nabla \times \nabla \times \mathbf{B} \tag{4.2}$$

using the vector identity $\nabla \times \nabla \times \mathbf{B} = \nabla(\nabla \cdot \mathbf{B}) - \nabla^2 \mathbf{B}$ and the fact that $\nabla \cdot \mathbf{B} = 0$

$$\frac{\partial \mathbf{B}}{\partial t} = \nabla \times \mathbf{v} \times \mathbf{B} - \frac{1}{\mu_0} \eta \nabla^2 \mathbf{B} \tag{4.3}$$

dot the whole thing with $\mathbf{B}$, use a little calculus:

$$\mathbf{B} \cdot \frac{\partial \mathbf{B}}{\partial t} = \frac{1}{2} \frac{\partial B^2}{\partial t} \tag{4.4}$$

Recall the magnetic energy density is $W = \frac{B^2}{2\mu_0}$. So we have an equation for the rate of change of magnetic energy density

$$\frac{\partial W}{\partial t} = \frac{1}{\mu_0}\nabla \times \mathbf{v} \times \mathbf{B} \cdot \mathbf{B} + \frac{\eta}{\mu_o^2}\nabla^2 \mathbf{B} \cdot \mathbf{B} \tag{4.5}$$

The last term is negligible so we'll drop it. Linearizing the rest, dropping high order terms we are left with an equation for the rate of change of energy in the m=0,n=1 mode.

$$\frac{\partial W_{01}}{\partial t} = \mu_0 \nabla \times \mathbf{v_{01}} \times \mathbf{B_{00}} \cdot \mathbf{B_{00}} \tag{4.6}$$

The tips of the probe measure the velocity, and a small Bdot coil on the probe measures the local magnetic field. By measuring the rate of change of the magnetic energy we can determine if the m=0 mode is linearly stable[25]. The signal from the probe is noisy so *a lot* of shots are required to complete a decent ensemble averaged waveform.

Chapter 5

The Experiments

The effect of each oscillator was studied seperately before applying both. So there are three sets of experiments described herein. In Oscillating Poloidal Current Drive (OPCD), only the oscillator that drives the poloidal edge voltage was turned on. The ensuing poloidal current creates an oscillating axisymmetric toroidal magnetic field at the edge B_{z00}. Also, the poloidal electric field is nearly parallel to the magnetic field at the edge so we expect to have a significant impact on the parallel current in the plasma, at least at the edge. But since only one oscillator is running, we expect it (at least on an intuitive level) to have little or no net additional current drive.

In Oscillating Toroidal Current Drive (OTCD), only the oscillator that drives the toroidal edge voltage was turned on. The combination of this oscillating toroidal electric field and the equilibrium poloidal magnetic field should yield an oscillating radial velocity $V_{00} = E_{z00} \times B_\theta / B_\theta^2$, pinching the plasma in and out. The toroidal electric field is nearly perpendicular to the edge magnetic field so we expect little contribution to the parallel current when acting alone. As with OPCD, since only one oscillator is on we expect to have no net effect on anything.

Finally, in OFCD, both oscillators were turned on. The combination of the two effects above $V_{r00} \times B_{\theta 00}$ should drive a current in the edge of the plasma. The dynamics of relaxation should transfer this edge current into the core. Results for each case will be compared to the values when the oscillators are off (NOFCD.)

We found a lot of unexpected behavior for each, including synchronization of the sawteeth, decoupling of $m = 0$ and $m = 1$ modes, an enormous but fickle modulation of the core ion temperature, a slow periodic modulation of the $m = 0$ modes, and significant current drive, some aspects of which did not conform to expectations.

The experiments started out at 530 Hz and about 10 V peak-to-peak toroidal loop voltage and 64 V peak-to-peak poloidal loop voltage. As described in the following sections, we found that 530 Hz was too fast for OFCD and the frequency was lowered to 280 Hz and the oscillator amplitudes increased to about 20 and 200 V at the gaps. We'll discuss results for both frequencies but the emphasis will be on the 280 Hz case since it yielded better results and we have studied it more closely.

5.1 OPCD

In Oscillating Poloidal Current Drive (OPCD) only the poloidal edge voltage oscillator is turned on. Figure 5.1 shows the gap voltages for 280 Hz OPCD. The peak-to-peak amplitude on the toroidal gap is about 20 V. Most noticeable in this plot is the entrainment of the sawteeth to our applied oscillation. More on this later.

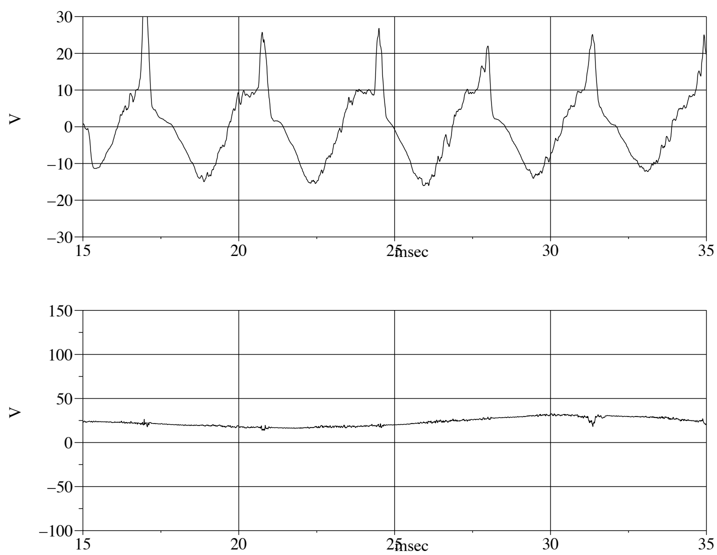

Figure 5.1 The gap voltages measured at the toroidal (top) and poloidal (bottom) gaps during 280 Hz OPCD.

Figure 5.2 shows $B_z(r = a)$, the toroidal magnetic field at the wall (Btw). Since OPCD drives a poloidal current at the edge it's no surprise that, at least at the edge, it has a greater effect on the toroidal field than on the poloidal component. Even at these relatively small amplitudes, Btw is modulated nearly 100%. The plasma is very nearly brought out of reversal. Figure 5.3 shows F, the reversal parameter ($F = B_z(wall)/ < B_z >$), and Θ, the pinch parameter ($\Theta = B_\theta(wall)/ < B_z >$.) Again we see F nearly crosses zero into unwanted territory for an RFP. The pinch parameter is less affected since the poloidal component of $\mathbf{B}$ is less affected. This could be a problem in higher power experiments. When the plasma comes out of reversal it looks more like a weak tokamak than an RFP. Later we'll see how this brief 'unreversal' will affect the stability and current drive in MST.

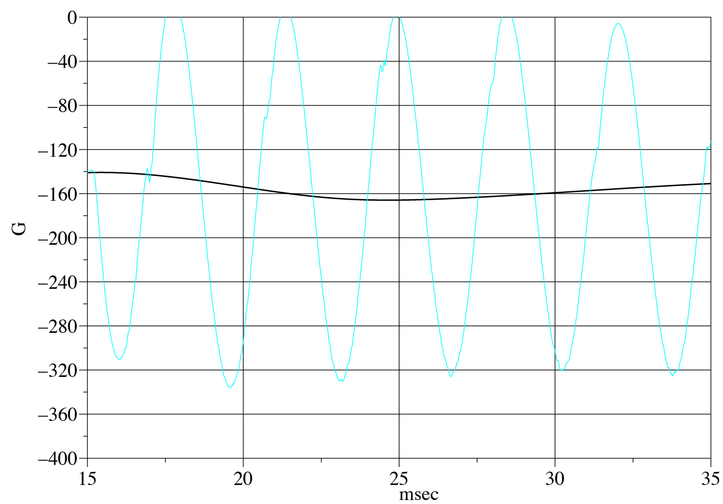

Figure 5.2 The toroidal field at the wall during 280 Hz OPCD. Thick curve is cycle average.

Figure 5.4 shows the $F - \Theta$ trajectory over several cycles. Also plotted is the theoretical curve from the α-model (the thick black line that's barely visible.) We can see that the measured trajectory pretty closely follows theory. The major excursions are caused by sawteeth. This is good news since it means we're not perturbing the plasma so much that it cannot remain in it's usual pseudo-relaxed(ish) state. For comparison look at the $F - \Theta$ trajectory for 530 Hz OPCD in figure 5.5. The blobbish trajectory was a good indication that the frequency was too high for the plasma to remain in a relaxed(ish) state throughout a cycle.

Contrary to our intuition and 1D modeling, 3D numerical studies [23] say OPCD should drive a slight increase in the cycle averaged axial current due to a reduction of helicity dissipation. Figure

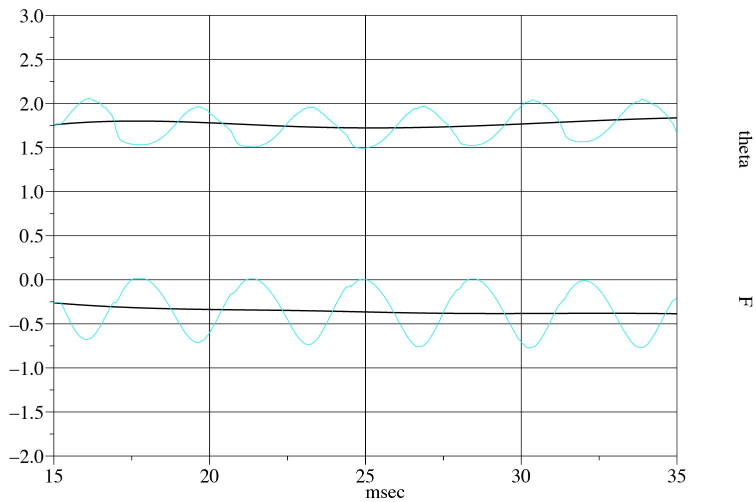

Figure 5.3 The reversal and pinch parameters during 280 Hz OPCD.

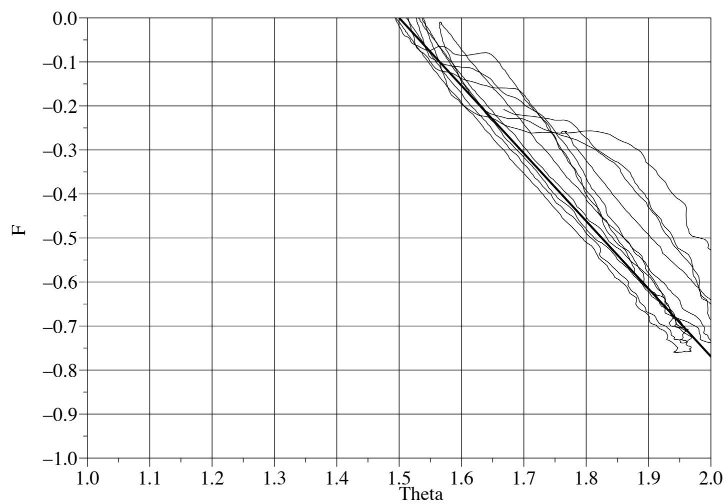

Figure 5.4 The $F - \Theta$ trajectory during 280 Hz OPCD. Dark line is ideal trajectory from the α model with $\alpha = 4$.

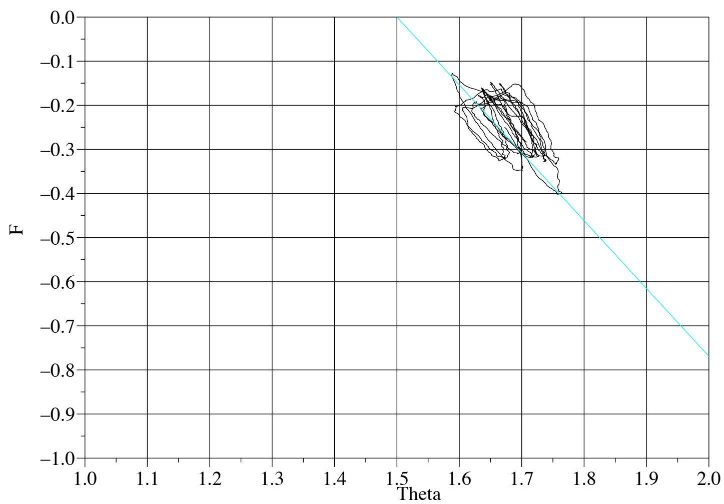

Figure 5.5 The $F - \Theta$ trajectory during 530 Hz OPCD. Dark line is ideal trajectory from the α model with $\alpha = 4$.

5.6 shows the cycle averaged plasma current for a large ensemble of OPCD shots. Also shown is the current for NOFCD with the same plasma conditions. No such increase is observed. On the contrary, the current is actually decreased. This might be due to increased wall interactions dumping impurities into the plasma driving up the resistivity. Figure 5.7 shows the six impurities measured by MST's monochromater array. They show an increase of the mean value of between 14% (Carbon V) to 100% (Boron IV). Several show the distinct signature of our applied oscillation. Increased wall interactions might prove to be a problem for full sustainment. It is one of the problems that hindered the ZT-40 OFCD experiment. If the impurities are at fault, then it's impossible to say for sure whether OPCD would drive a current in the plasma.

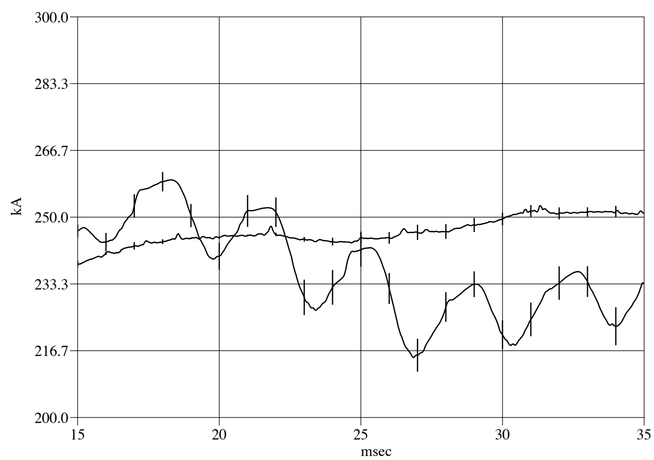

Figure 5.6 Plasma current during and without 280 Hz OPCD.

5.1.1 Sawtooth Entrainment

We start by looking at the most obvious effect OPCD has on the plasma. Recall that a sawtooth event is accompanied by a jump in the toroidal flux and hence, thanks to Faraday, a jump in the poloidal loop voltage at the edge. So the voltage across the toroidal gap (which breaks the poloidal loop) is a good place to watch for sawteeth. Figure 5.8 shows Vtg during a single NOFCD shot. The sawteeth are placed semi-randomly. There is, on average, a natural sawtooth period that scales with the resistivity of the plasma. For 250 kA (our usual nominal plasma current) discharges this

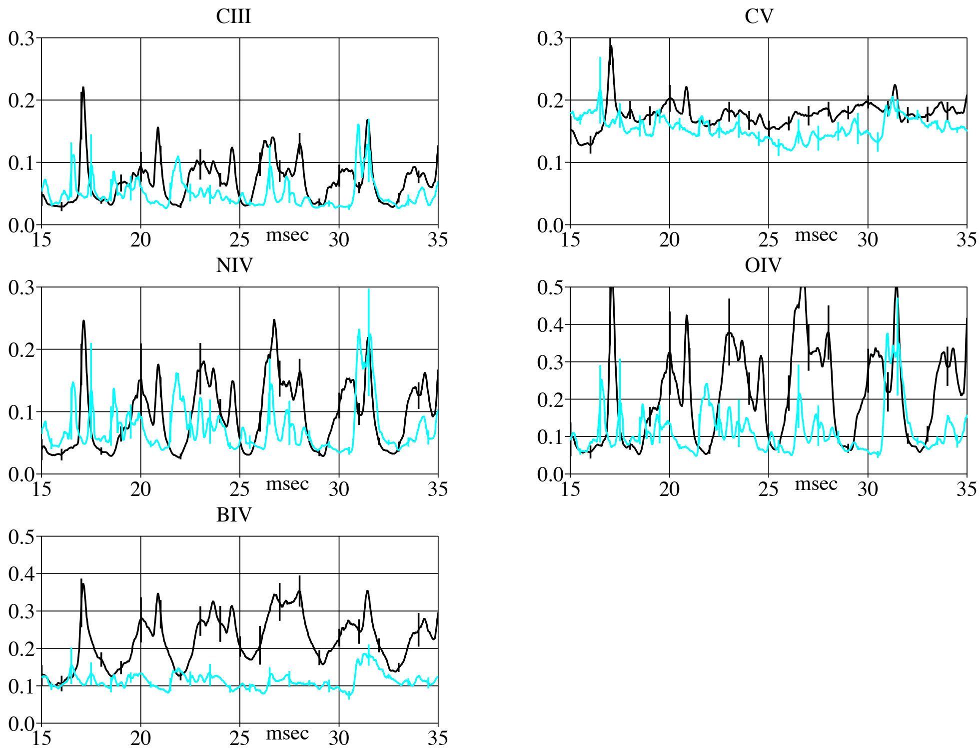

Figure 5.7 Impurity measurements from monochromater array. Black lines are with 280 Hz OPCD oscillator on. Blue lines are with oscillator off.

period is a few msec. Whatever the semiperiodic nature of the spacing between them, a sawtooth can occur anywhere.

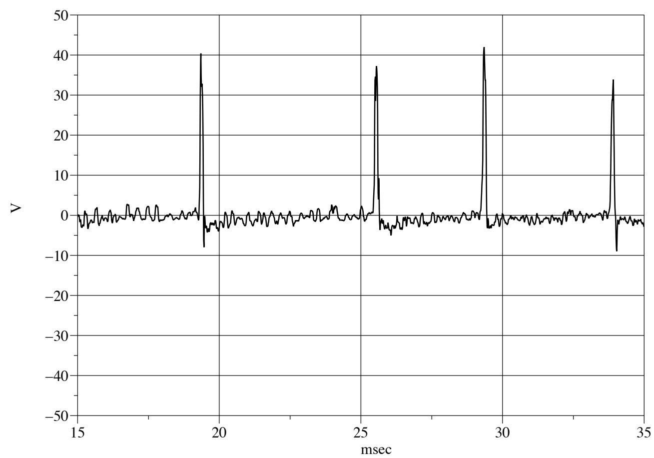

Figure 5.8 The toroidal gap voltage without any applied oscillation.

Now we turn on the OPCD oscillator. Figure 5.9 shows Vtg during 280 Hz OPCD where the nominal current is about 250 kA. We can clearly see that the sawteeth are entrained in lock step with our applied oscillation. The reason for the entrainment is simple. Recall that the tearing instabilities behind sawteeth are driven by the current gradient/q-profile. A steep profile excites the plasma while a flat profile calms it. Consider the upper and lower halves of one cycle of OPCD. During the lower half of the cycle, current is being injected into the edge flattening the current profile just as the Pulsed Poloidal Current Drive (PPCD) experiment does. Flattening the current profile (and hence the q profile) calms the plasma by separating the resonant surfaces. We call this the PPCD half of the cycle. During the other half cycle we are driving negative current into the plasma edge, decreasing it there and hence peaking the profile. Doing so excites a sawtooth event. We call this the anti-PPCD phase for obvious reasons.

By dialing up the nominal current to 475 kA we increase ohmic heating of the plasma which increases the temperature which decreases the plasma resistance which increases the natural sawtooth period. Figure 5.10 shows Vtg for this high current case. We can see that the sawteeth are entrained to about every other cycle. So it looks like the plasma is trying to maintain it's natural sawtooth period subject to the phase of the applied oscillation.

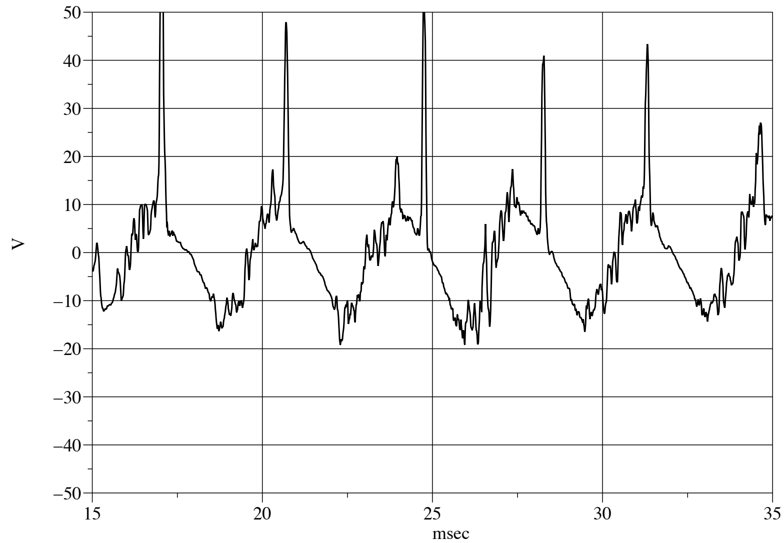

Figure 5.9 Toroidal gap voltage during 280 Hz OPCD. Iz = 250 kA

The picture is the same at 530 Hz. In figure 5.13 we see Vtg during 530 Hz OPCD with a nominal current of 350 kA. The natural sawtooth frequency at this current is about 4 msec. The period of our oscillator is 2 msec. As expected the sawteeth occur at about every other cycle. So again the sawteeth more or less maintain their natural period but are regulated by the phase of the oscillator.

As our edge current injection oscillates between the PPCD and anti-PPCD phases we believe the current profile should be flattening and peaking. Recall that a sawtooth marks a violent flattening of the current profile. The shape factor α from the α-model is a good 'measure' of the flatness of the current profile. Large α means a flatter profile. Small α means the profile is peaked. We 'measure' α by fitting the α-model to edge measurements. Figure 5.11 shows a typical evolution of the α parameter during a standard (NOFCD) 250 kA discharge. We see that the profile slowly and smoothly becomes peaked until it hits some threshold (around 2) and a sawtooth is born, flattening the profile and calming the plasma. Now look at figure 5.12. This is the α parameter during

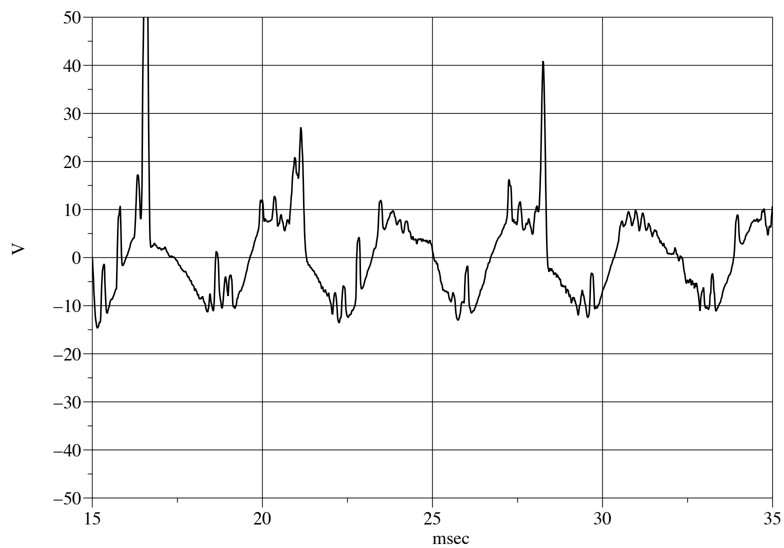

Figure 5.10 Toroidal gap voltage during 280 Hz OPCD. Iz = 475 kA

OPCD. An enormous modulation of α is evident. The sawteeth are the narrow spikes between the large lumps (we'll discuss those lumps later.) We can see that when α drops below about 3, a sawtooth is triggered, although the threshold is harder to spot since shot averaging smears things out. Smeared or not, we can still see that a sawtooth is triggered when the profile becomes too peaked, with or without OPCD. Also shown in that plot is the scale factor, λ_0. Recall from the discussion of the α model that λ_0 is the normalized current density J/B at the core. Since OPCD drives poloidal current and the core field is toroidal OPCD has little effect on λ_0. We'll compare this later to OTCD. For now, we take comfort in knowing at least some things behave as expected during OPCD.

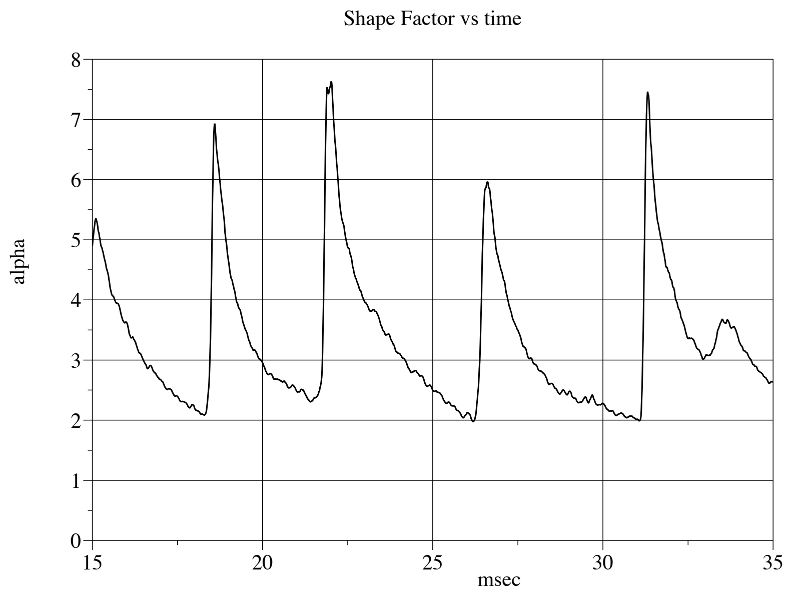

Figure 5.11 The shape factor α vs time during a standard 250 kA discharge.

5.1.2 Mode Spectra

We now examine the peculiar effects OPCD has on the mode spectra. For comparison, the modulation of the mode spectra predicted by the 3D model is shown in figure 5.14. The dominant core mode in MST is $m = 1$,$n = 5$. Out of necessity, the 3D model assumed a larger aspect ratio so the dominant toroidal mode is $m = 1$,$n = 4$. The damn curves are plotted on a log scale

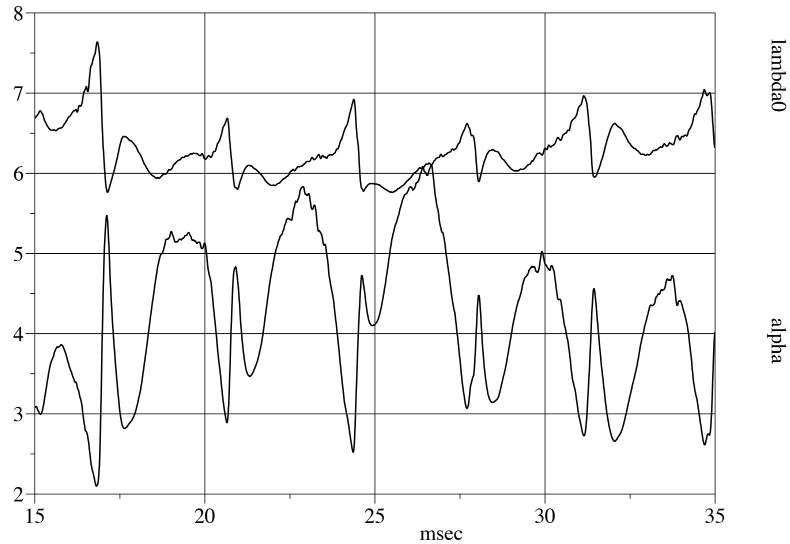

Figure 5.12 The scale factor λ_0 and shape factor α vs time during 280 Hz 250 kA OPCD

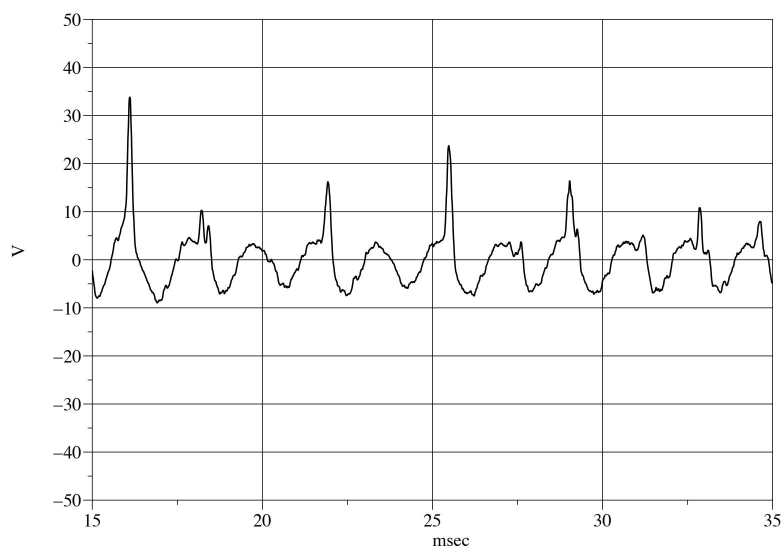

Figure 5.13 Toroidal gap voltage during 530 Hz OPCD. Iz = 350 kA

using normalized variables that were hard to cast into reality but they clearly show a sinusoidal modulation on, for instance, the $m = 0$,$n = 1$ mode, of 2 orders of magnitude synchronized with the applied oscillation. The mean level of the $m = 0$ mode also appears to drop about one order of magnitude when the oscillator kicks on. One disturbing feature of this plot is that, prior to the oscillation (the 'NOFCD' region), the average value of the $m = 1$ modes are about ten times larger than the $m = 0$ modes. In MST, the $m = 1$ modes are typically four times smaller than the $m = 0$ modes.

5.1.2.1 280 Hz

We start our study of the mode spectra at 280 Hz, our preferred frequency. Figure 5.15 shows ensemble averages of the m=0 and m=1 modes vs time. There is a visible modulation of the m=1 modes and an enormous modulation of the m=0 modes. Of particular interest are the normally quiet regions between sawteeth. In NOFCD discharges this region is quiet because the relaxation event of the previous sawtooth has flattened the current profile and calmed the plasma. With OPCD there is this enormous bubble of m=0 activity accompanied by a lesser degree of m=1 activity. The figure is a large ensemble average. Many shots showed immeasurable m=1 activity during the bubble. This was unexpected because it is normally the m=1 modes beating together that drives the m=0 mode. The bubbles are usually larger than the sawteeth. We are somehow exciting m=0 modes, possibly by creating a larger current gradient in the edge than expected. We have no current profile measurements during OPCD to confirm this.

Figures 5.16 and 5.17 show the n (the toroidal mode number) spectra for the m=0 and m=1 modes. The m=1 spectral distribution is not unlike the NOFCD spectra. The modulation is most prominent at lower n. The m=0 spectral distribution appears to be pretty flat (across n, not time), implying the mode is localized toroidally. The vertical spikes are error bars, not noise.

5.1.2.2 m=0 bubbles

To better understand what's happening to the m=0 mode during OPCD a high-frequency triple-tip Langmuir probe was inserted a few centimeters into the plasma to see if the $m = 0$ mode is

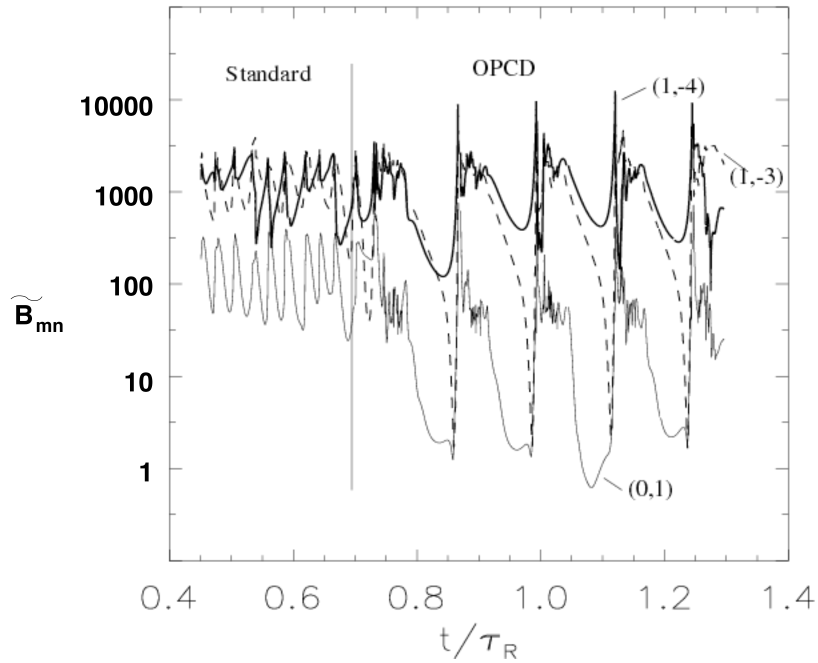

Figure 5.14 Mode amplitudes for m,n = (1,3), (1,4), (0,1) during and without OPCD as predicted by the 3D model.

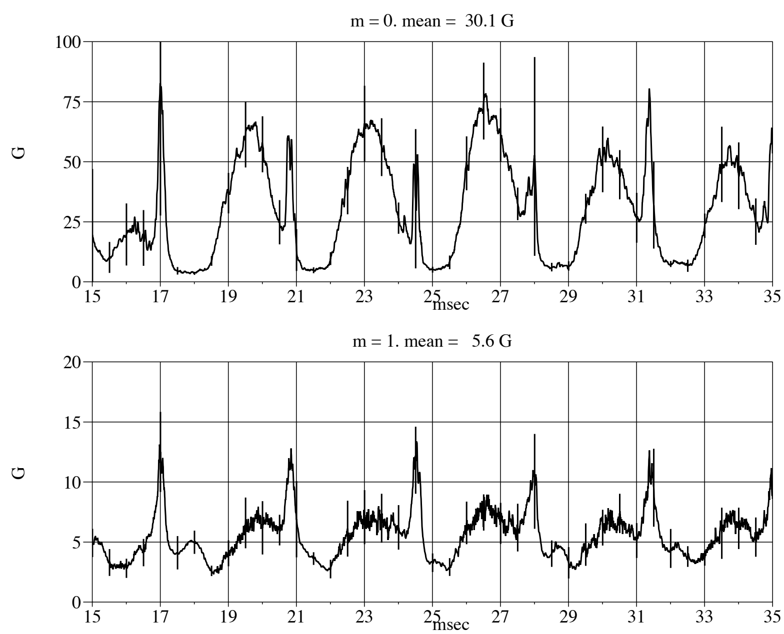

Figure 5.15 The m=0 and m=1 mode amplitudes during 280 Hz OPCD. The plots are ensemble averages. The vertical spikes are error bars.

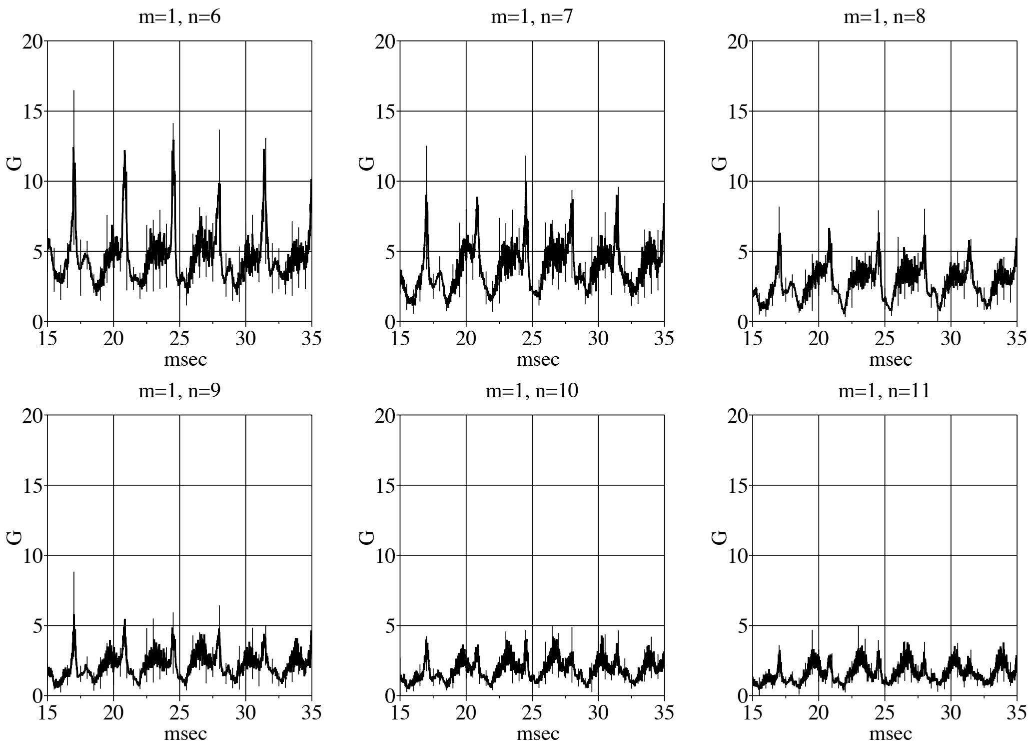

Figure 5.16 The m=1 mode n-spectra during 280 Hz OPCD.

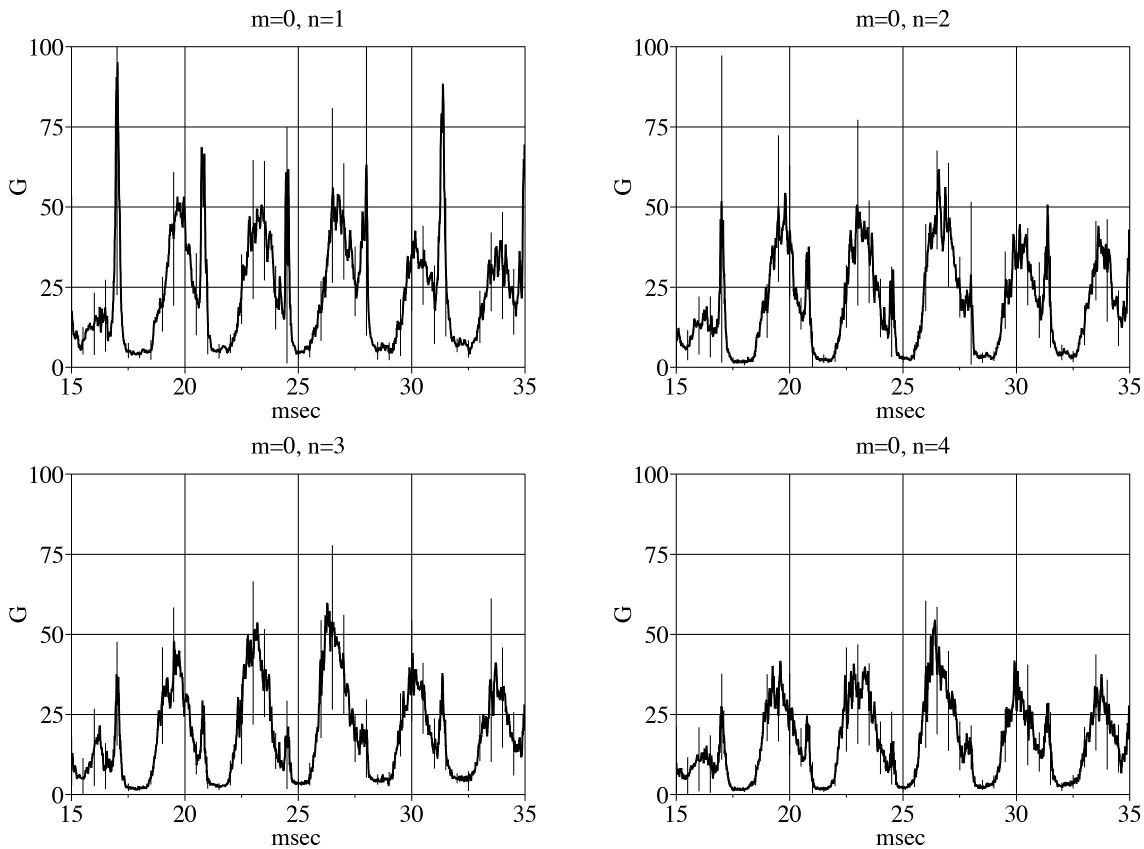

Figure 5.17 The m=0 mode n-spectra during 280 Hz OPCD.

linearly unstable during the bubbles. Repeatability is easy since the sawteeth always occur at the same time due to entrainment. Figure 5.18 shows the ensemble averaged result during one cycle of 280 Hz OPCD ending in a sawtooth. The top plot clearly shows the $m = 0$ bubble unaccompanied by $m = 1$ activity. The lower plot shows our $\frac{\partial W_{01}}{\partial t}$ term. The data is still noisy so the error bars are large, but it appears that $\frac{\partial W_{01}}{\partial t} > 0$ during the bubble so the $m = 0$ mode is growing and hence linearly unstable. Nipple. The results are remarkable. In usual operation the $m = 0$ mode is linearly stable. Even during a sawtooth, when the $m = 0$ mode is created by the interaction of m=1,n=whatever modes, $m = 0$ is still linearly stable and dies off as the $m = 1$ modes calm down. It appears that the poloidal current we drive in the edge has become the source for the $m = 0$ mode energy. It may be that we are driving so much current in the edge that the gradient has reversed and is strong enough across the $m = 0$ resonant surface to drive it unstable. It's easy to make this claim because it's hard to verify. The FIR data we have near the edge is inadequate to make any definitive claim about the current gradient.

As we'll see later the m=0 bubbles occur in both OTCD and OFCD but are not nearly as strong as in OPCD. Figure 5.19 shows a single 280 Hz OFCD shot. Both oscillators are on, but the OTCD oscillator suffers a failure early in the shot and rings down with a time constant of a few msec while the OPCD oscillator continues unabated. As the OTCD oscillator decays we see the $m = 0$ bubbles growing with each cycle. The presence of the OTCD oscillator seems to spoil the effect by stabilizing the mode.

5.1.2.3 530 Hz

At 530 Hz something peculiar occurs; between sawteeth, the patterns of m=1 and m=0 modes nearly reverse. Figure 5.20 shows a large ensemble average of the m=0 and m=1 mode amplitudes during 350 kA 530 Hz OPCD. The shots were chosen so that the entrained sawteeth fall on the same cycle in each shot. The first 3 sawteeth are at 16.2, 20.1, and 25 msec. In between we see bubbles of m=1 activity largely unaccompanied by m=0 activity. This is an even more bizarre result than the mode behavior at 280 Hz. Intuitively we expect 530 Hz to have even less effect than the lower 280 Hz since the skin depth is less and the plasma has less time to respond to the

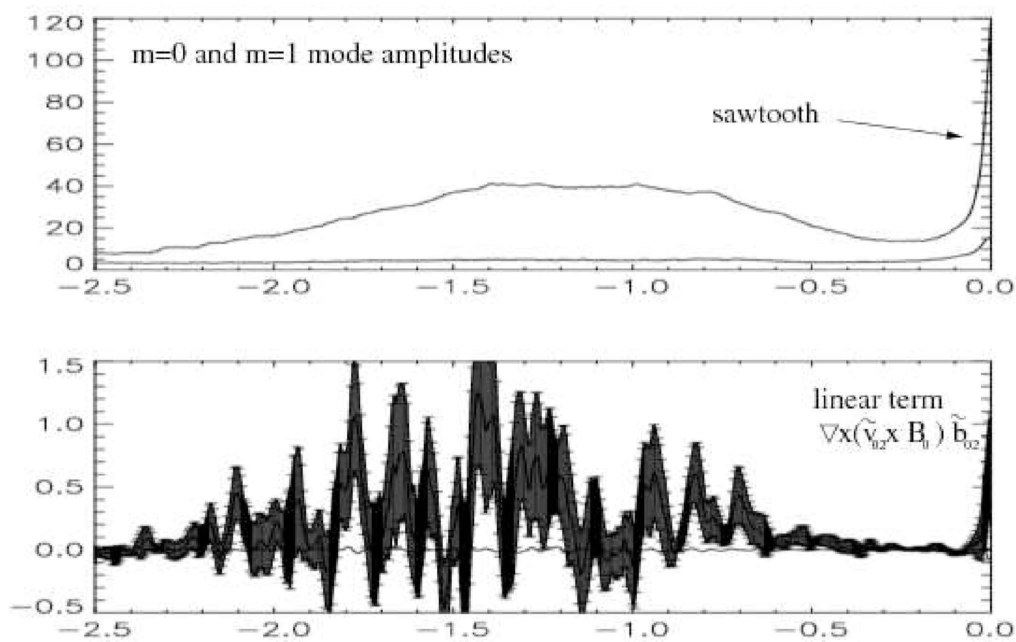

Figure 5.18 Triple tip Langmuir and $\dot{B}$ probe indicates m=0 mode may be unstable during bubble and definitely is during sawtooth.

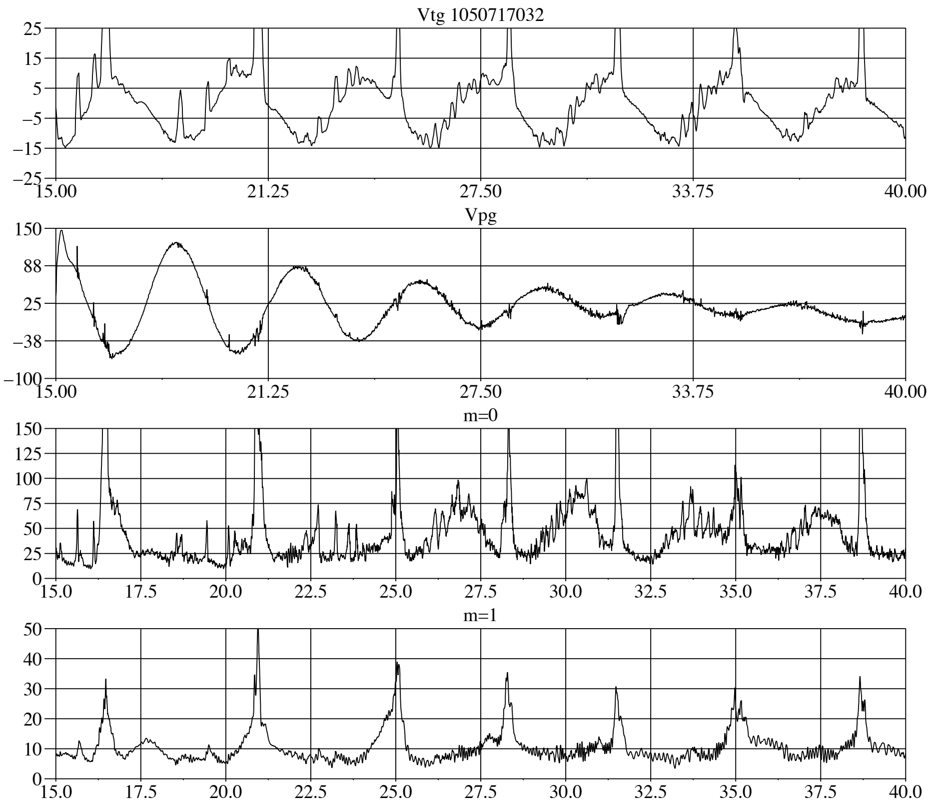

Figure 5.19 As the Bp oscillator ramps down the m=0 bubbles show up.

perturbation ($t_{osc} < \tau_H$ where τ_H is the hybrid time.) But the m=1 mode amplitude shows an unmistakable 530 Hz modulation. The triple tip probe used in 280 Hz OPCD was not available when we were running at 530 Hz, so we have little chance of studying this phenomenon further until programmable power supplies replace the ignitron oscillator [1].

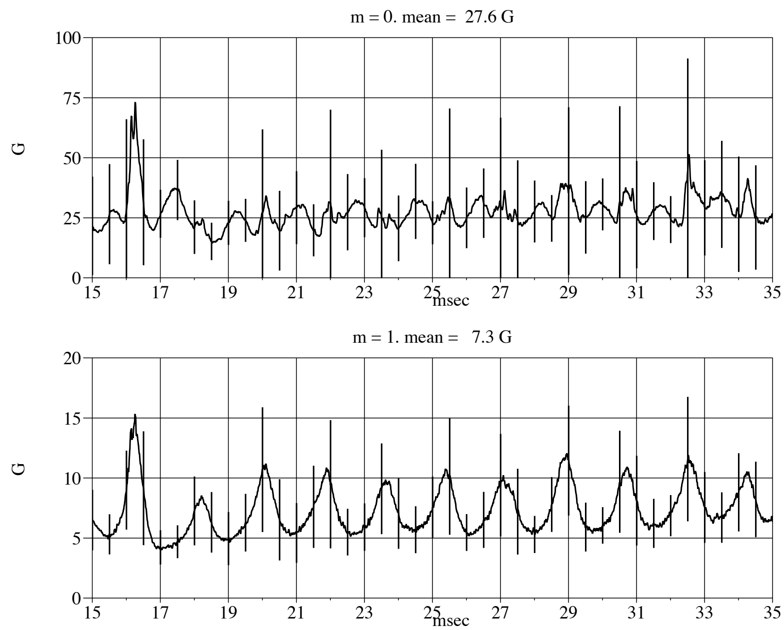

Figure 5.20 The m=0 and m=1 mode amplitudes during 530 Hz OPCD.

Figures 5.21 and 5.22 show the n spectra for the $m = 0$ and $m = 1$ modes. The distribution of energy amongst the $m = 1$ modes is not unlike it is in NOFCD. The 530 Hz modulation is visible up to $n = 10$. The modulation is also visible in the $m = 0$ spectrum. And again it is fairly flat.

5.1.3 Anomalous Ion Heating

One of the most intriguing effects we've observed in OPCD has been a large but hard to reproduce modulation of the deuterium ion temperature. Figure 5.23 shows three occasions where the modulation appeared. Each occured during a 530 Hz, 350 kA OPCD discharge. Each plot is an ensemble average of data taken by the Rutherford Scattering system about 16 cm from the magnetic axis. The temperature swing on the first occasion is about 80 eV. There has been only

[1] *another hint to the powers that be.*

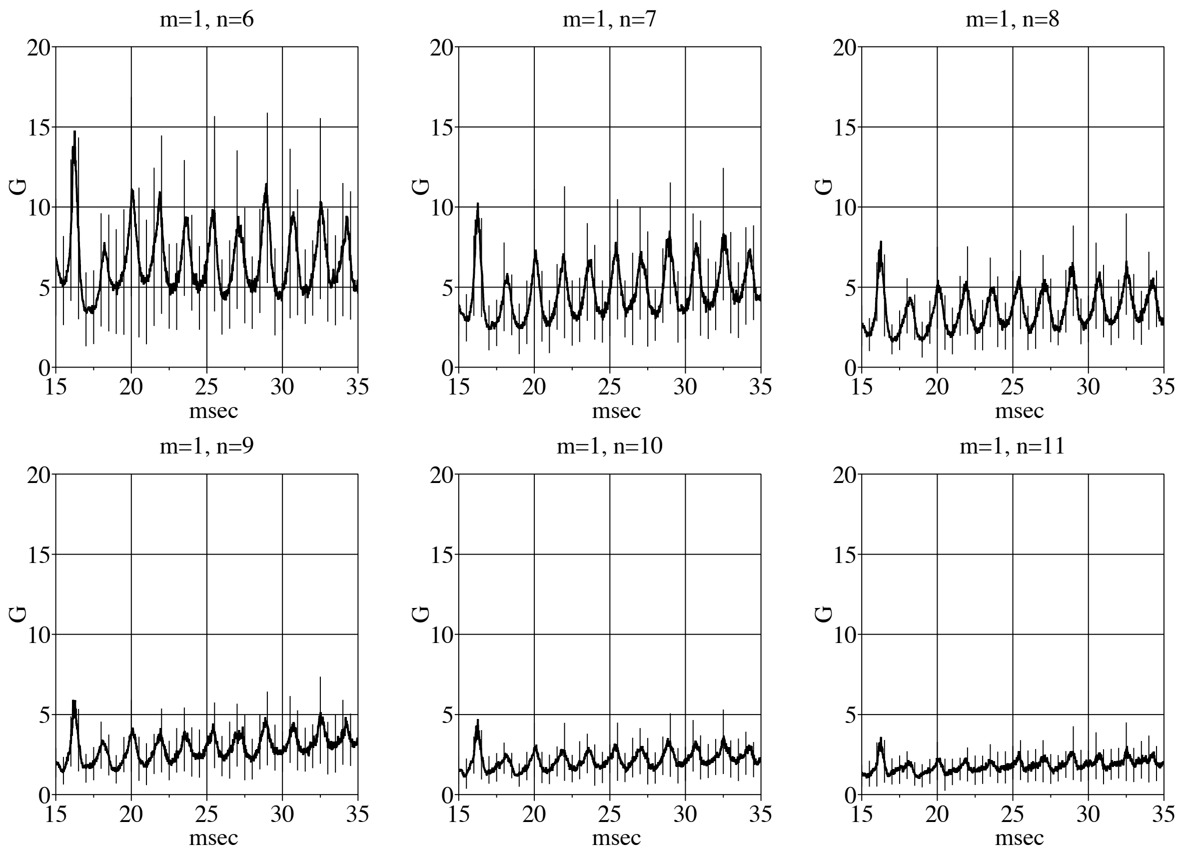

Figure 5.21 The $m = 1$ mode n-spectra during 530 Hz OPCD.

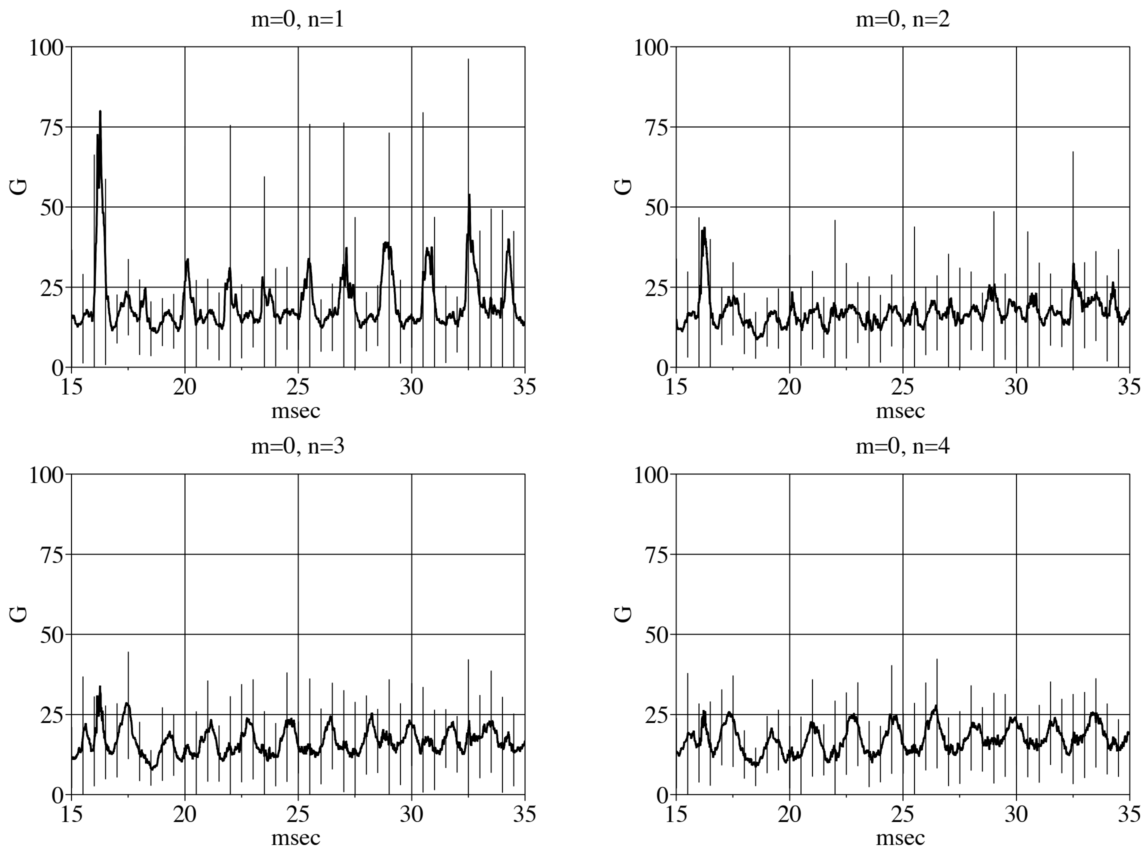

Figure 5.22 The $m = 0$ mode n-spectra during 530 Hz OPCD.

one attempt to find the OPCD modulation of T_i during 280 Hz OFCD. The diagnostic showed no modulation that day.

One possible explanation for the temperature swing is collisional heating via magnetic pumping, a combination of adiabatic compression/decompression and collisional equilibration. If the magnetic field in a plasma is slowly increased a gyrating particle will attempt to maintain it's magnetic moment $\mu = U_{\perp}/B$ where the perpendicular kinetic energy $U_{\perp} = \frac{1}{2}mv_{\perp}^2$. The only way to do so is to increase the gyration velocity $v_{\perp}$. If the particle were alone that would be it. As the field decreased (decompression) $U_{\perp}$ would relax to it's original value and no net heating would occur. But if collisions occur during compression, the perpendicular energy (with 2 degrees of freedom) will equilibrate with the parallel kinetic energy (with one degree of freedom) changing μ. Upon decompression μ is again conserved to a new value at the original magnetic field, keeping in mind that $U_{\|}$ is not subject to the conservation of μ. The transfer of energy from $U_{\perp}$ to $U_{\|}$ during compression yields a cycle average increase in temperature as long as the period of oscillation is much longer than the collision frequency. In MST the collision frequencies are $\nu_{ei} \simeq 100kHz$ for the electron-ion collisions and $\nu_{ii} \simeq 1kHz$ for ion-ion collisions. The governing equations are given by Berger, et al [1].

$$\frac{dU_{\perp}}{dt} = (\frac{1}{B}\frac{dB}{dt} - \frac{\nu}{2})U_{\perp} + \nu U_{\|} \tag{5.1}$$

$$\frac{dU_{\|}}{dt} = \frac{\nu}{2}U_{\perp} - \nu U_{\|} \tag{5.2}$$

Where $B = B_0 + B_1 sin(\omega t)$ and $\frac{U_{\perp}}{2} + U_{\|} = kT_0$. Relaxed state modelling of OPCD shows that the field at r=16 cm is mostly toroidal and oscillates 160 Gauss (B_1) about a nominal value of 2377 Gauss (B_0.) Measurements show $kT_0 = 200eV$ at the start of the oscillation. Solving the above equations (for any collision rate ¿ 1kHz) numerically shows a temperature swing of 20 eV, which is comparable to at least some of the observations. But for days that saw temperature swings of 80 eV other dynamics must be at play.

You'd think such a large effect would be easy to reproduce. It isn't. We've taken about a dozen ensemble sets over the last 6 years. It may be large and consistent on one day and absent 24 hours later. The effect appears in about half of the runs.

One corroborating diagnostic for ion temperature is the Ion Doppler Spectroscopy (IDS) system which measures the temperature of impurity ions. The impurity ion temperature should equilibrate with the bulk ions so a modulation on one should show up on the other. Of the few days we had both IDS and Rutherford scattering diagnostics both running we saw no modulation of the impurity temperature. We have confidence that both are working since they give the right values immediately before the oscillator kicks on.

We've tried to find anything, anything at all that coincides with the appearance of the ion temperature modulation. Figure 5.24 shows the results of that effort. Each cluster of bars corresponds to some diagnostic. Each bar represents a run day. The first 5 bars (hopefully green) are those days for which the ion temperature oscillation appeared. The last 4 are days when it did not. The height of each bar is the amplitude of either the mean value or the appropriate frequency component (280 Hz or 530 Hz) (from an FFT) of that signal. The amplitudes are normalized by the amplitude observed on the first day we saw the modulation. For each diagnostic, if the 'on' bars are all high and the 'off' bars are all low then we can say there's a good correlation between whatever that diagnostic measures and our ion temperature modulation. No such luck. The closest contender is the appropriate frequency component of the pyrometer measurement. The pyrometer is just another gross measure of the temperature.

In a normal MST discharge (NOFCD) it is common to see the ion temperature jump during a sawtooth. The effect is at least consistent but, as in OPCD, the mechanism remains unexplained. Future studies of OPCD should shed light on whatever is heating the ions during a sawtooth.

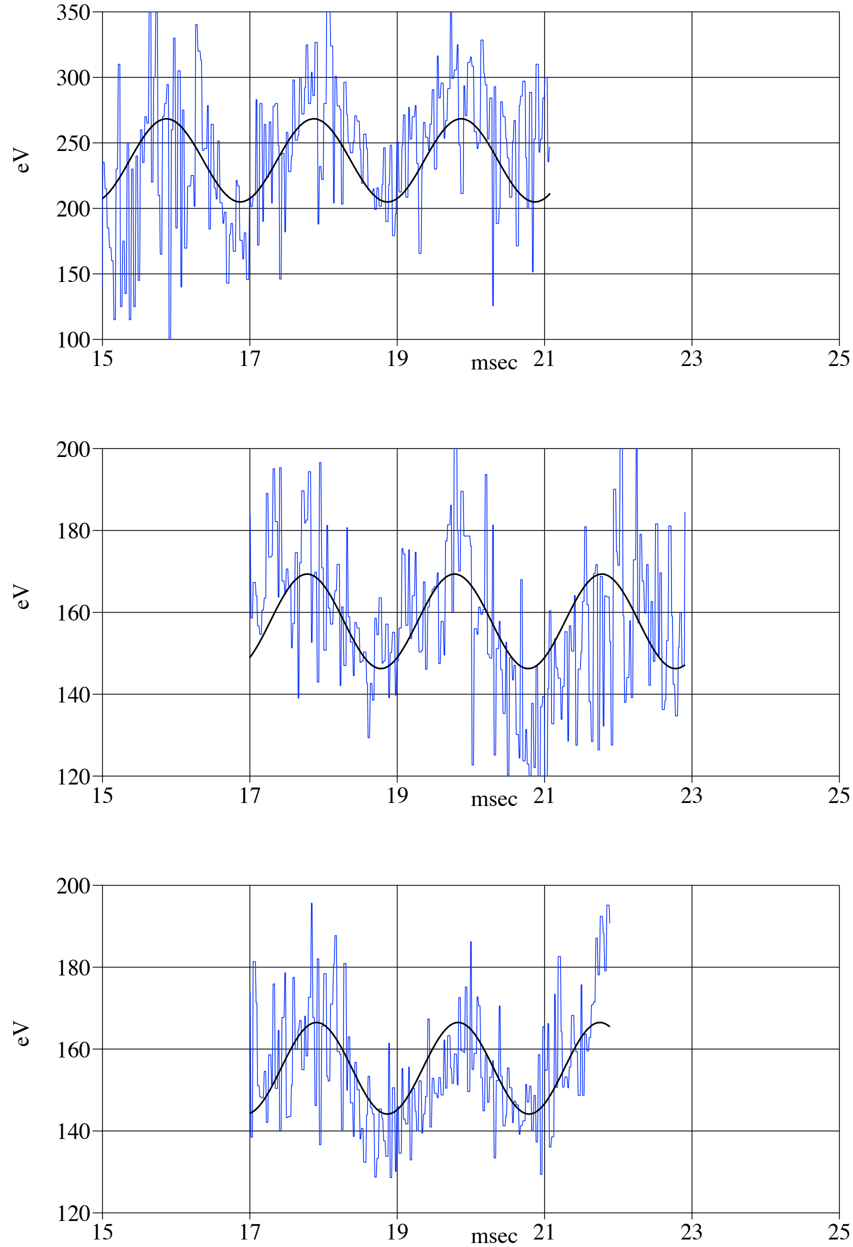

Figure 5.23 Ion temperature measurements for 3 different occasions.Temperature swing varies from 20 to 80 eV

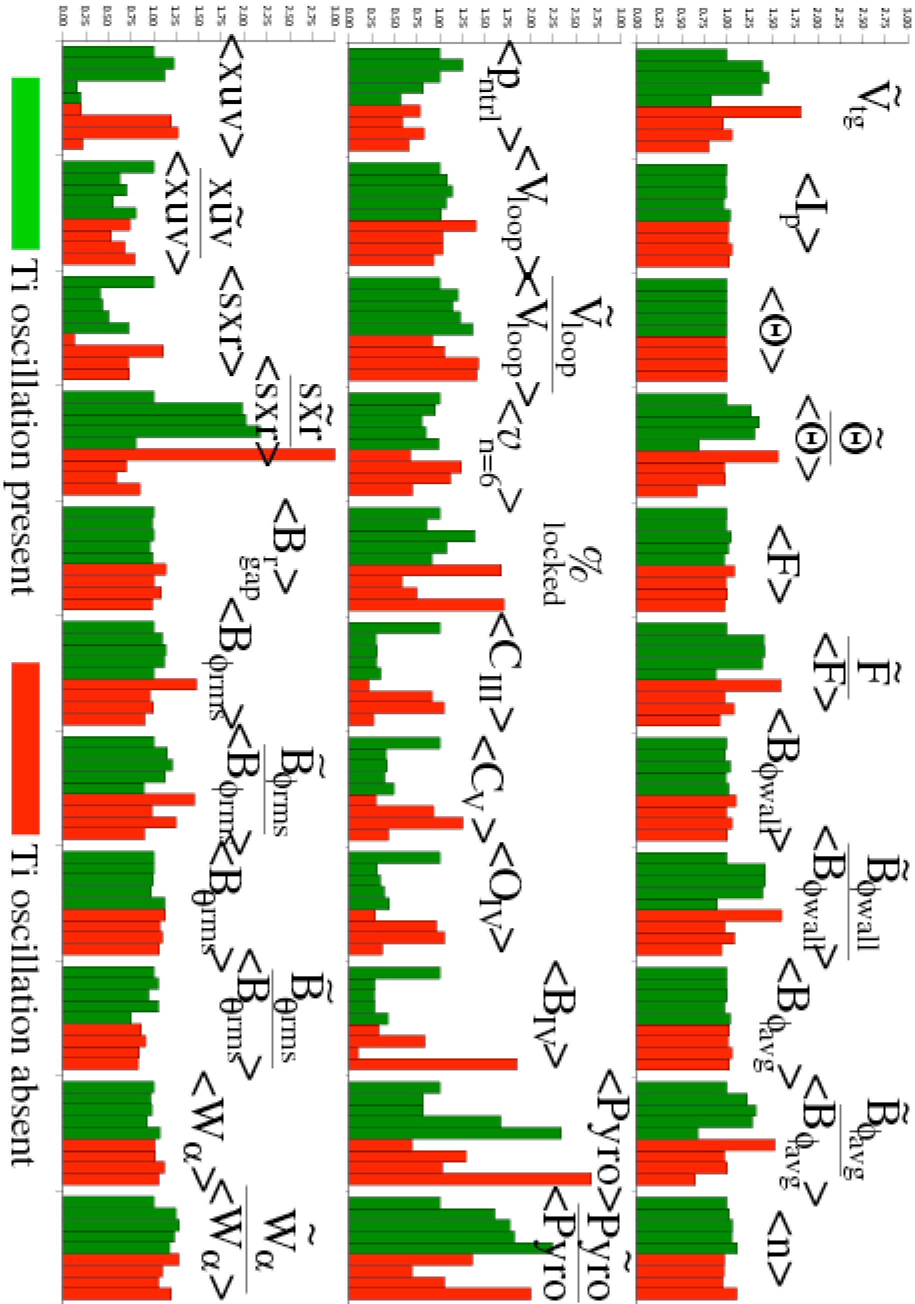

Figure 5.24 Nothing strongly correlates with the presence of Ti oscillation.

5.2 OTCD

In Oscillating Toroidal Current Drive (OTCD) only the toroidal edge loop voltage is oscillating. The magnetic field at the wall is mostly poloidal, so we don't expect to have a large effect on the parallel current profile. Then again, the applied oscillation is 10 times larger than the OPCD oscillation. Figure 5.25 shows the gap voltages for OTCD at 280 Hz with a nominal plasma current of 230 kA. The peak-peak amplitude on the poloidal gap is about 200 V. Looking at the toroidal gap voltage it appears the sawteeth are still at least somewhat entrained but less consistently than they were during OPCD and they usually appear in pairs. There also appears to be a slight oscillation on the toroidal gap voltage. The oscillating voltage on the poloidal gap is so large that, while the electric field is almost perpendicular to the magnetic field at the edge, there is still a small toroidal component. Apparently, it is enough to cause a small oscillating poloidal loop voltage as seen at the toroidal gap and to modulate the parallel current profile enough to create a weak OPCD-like entrainment of the sawteeth. The picture is different at 530 Hz as seen in figure 5.26. The peak-to-peak voltage is only about 70 Volts, less than half the amplitude at 280 Hz. If you look closely (and at a lot of shots) you can see that the sawteeth are well entrained to every other cycle. This is surprising since the higher frequency and lower voltage should have less impact on the current profile.

One unresolved concern the author holds is the effect of the wall on the radial displacement caused by the OTCD oscillator. Recall that the toroidal electric field crosses with the equilibrium poloidal magnetic field at the edge yielding a radial displacement velocity $V_{r00} = E_{z00} \times B_\theta / B_\theta^2$. For our experimental parameters this amounts to a few tens of meters per second. For an oscillation period of a few milliseconds this translates to a radial displacement of a few centimeters back and forth. The gap between the wall and the plasma is only about one centimeter so we're bound to hit the wall during one half of the cycle. Unresolved is the effect this asymmetric velocity will have on OFCD performance when both oscillators are turned on. Another concern is whether this plasma-wall interaction will knock impurities off the wall and into our plasma.

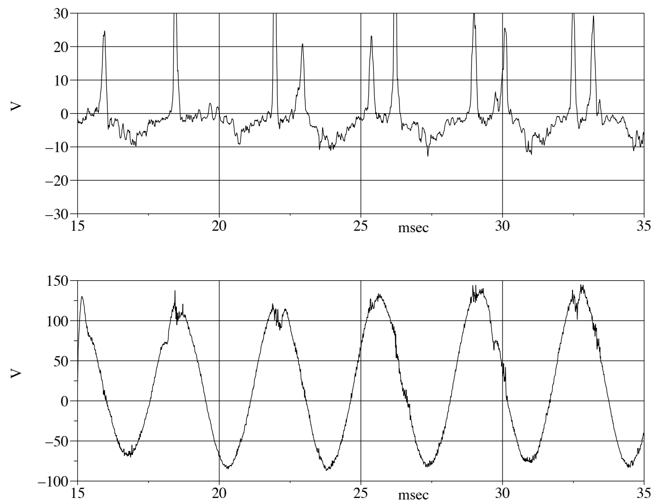

Figure 5.25 The gap voltages measured at the toroidal (top) and poloidal (bottom) gaps during 280 Hz OTCD.

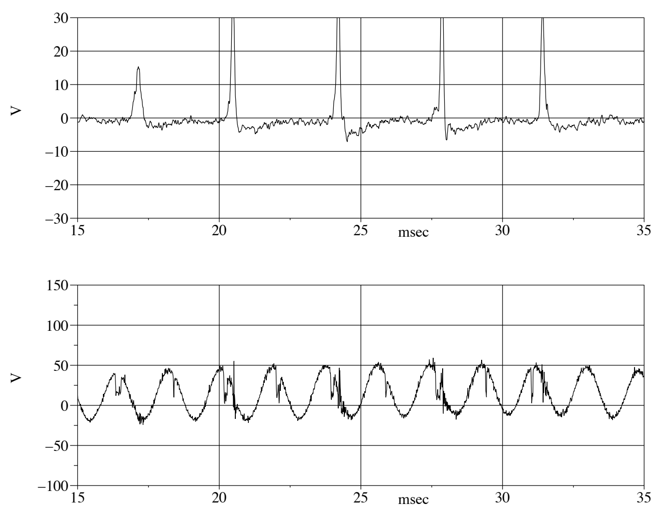

Figure 5.26 The gap voltages measured at the toroidal (top) and poloidal (bottom) gaps during 530 Hz OTCD.

Figure 5.27 shows the poloidal magnetic field at the wall. Since the NOFCD value of the poloidal field at the wall is so large to start with, the effect of OTCD is not as profound as the effect OPCD had on the toroidal field at the wall. This is reflected in the oscillation of the pinch parameter, Θ in figure 5.28

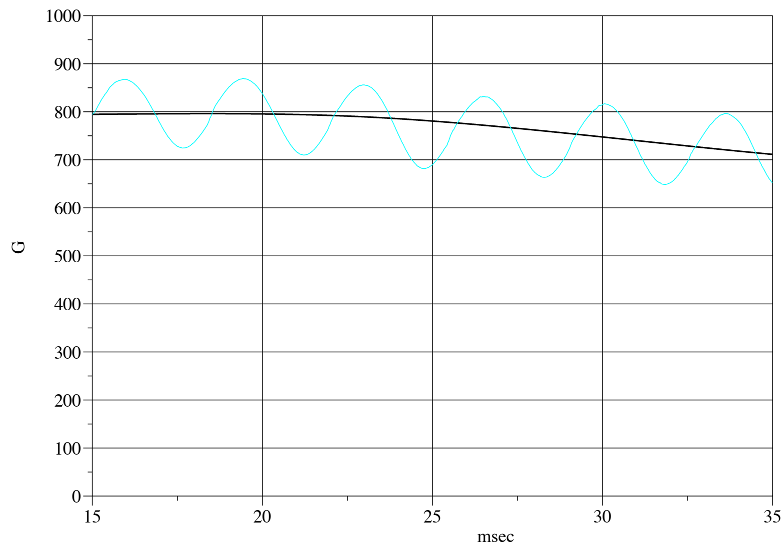

Figure 5.27 The poloidal field at the wall during 280 Hz OTCD.

The $F-\Theta$ trajectory in figure 5.29 does not come even close to following the theoretical curve. We shouldn't be too alarmed by this because the trajectory is still small since, again, the magnetic field at the wall is mostly poloidal. So we're only oscillating the small toroidal component of the parallel current density. So the trajectory should be nearly perpendicular to the OPCD trajectory as it appears to be (ish).

Since the OTCD edge current is nearly perpendicular to the edge magnetic field, the current that is induced should remain in the edge. An oscillating edge only current, cast in terms of the α model, implies the shape factor α should oscillate (which would shift the $F-\Theta$ trajectory back and forth) while the $\lambda_0 = J(0)/B(0)$ factor should be less affected since it describes the current in the core. Figure 5.30 shows both during 280 Hz 250 kA OTCD. α does indeed oscillate but no more that it did during OPCD. What's most surprising is the effect on λ_0. Extrapolating around the

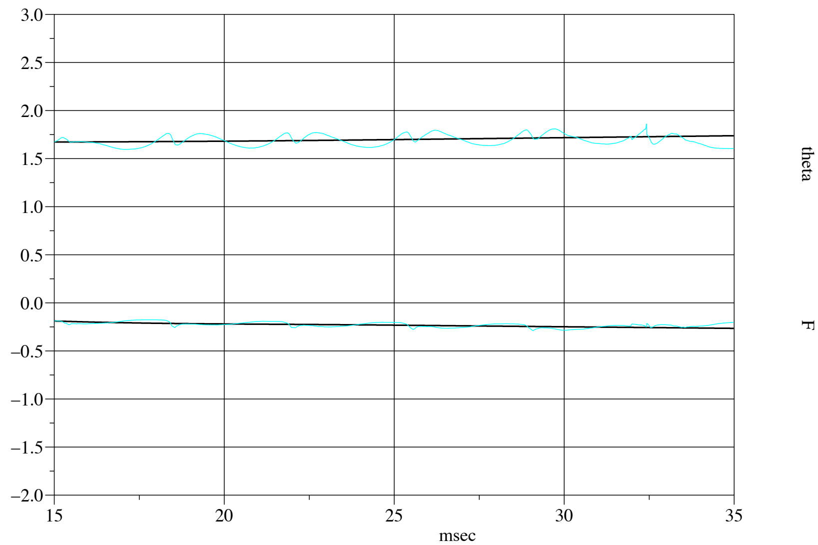

Figure 5.28 The reversal and pinch parameters during 280 Hz OTCD.

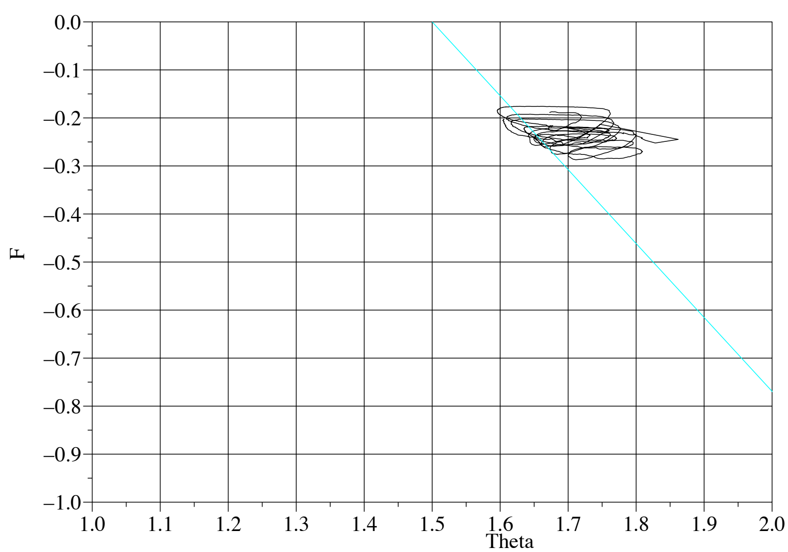

Figure 5.29 The F - Θ trajectory during 280 Hz OTCD. Also plotted is the ideal trajectory from the α-model with $\alpha = 4$.

sawteeth, λ_0 shows a pretty clear sinusoidal modulation. The magnetic field at the core is toroidal and λ_0 is the normalized current density at the core. This implies the oscillating electric field is rapidly penetrating into the core. This is encouraging since we'll need OFCD edge current to get into the core for the method to be viable.

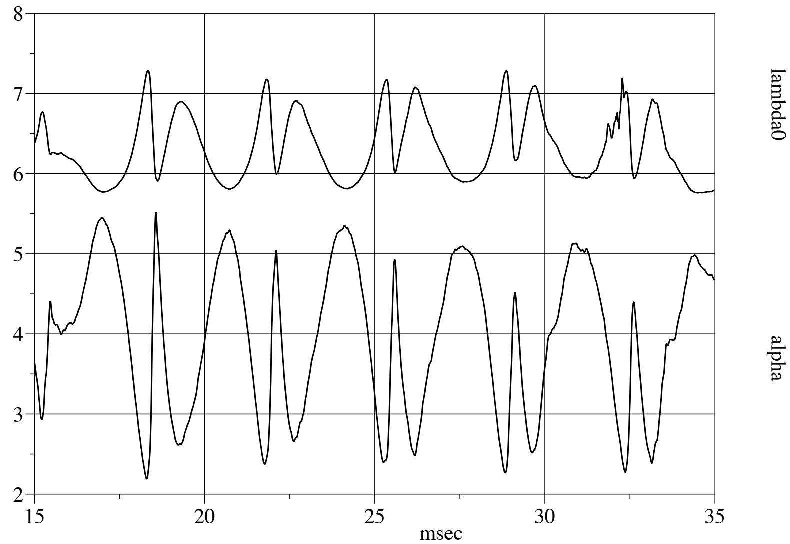

Figure 5.30 The scale factor λ_0 and shape factor α vs time during 280 Hz 250 kA OTCD

5.2.1 Mode Spectra

Because OTCD attempts to drive a current perpendicular to the magnetic field in the edge, we might not expect to have much effect on the m=0 and m=1 modes.

5.2.1.1 280 Hz

To study the effects of OTCD on the m=0 and m=1 modes we begin again at our preferred frequency. Figures 5.31 and 5.32 show the m=0 and m=1 mode amplitudes during 280 Hz OTCD with a nominal plasma current of 200kA. We see a familiar pattern between the sawteeth in the m=0 waveform. There are two lumps that look a lot like the m=0 bubbles we saw in OPCD. This is a large ensemble average. Take my word for it, the first bubble is just the second sawtooth of each cycle that we saw in figure 5.25. But the second appears to be the same phenomenon we saw during OPCD. This is likely due to the small toroidal component of the magnetic field at the edge. The OTCD voltage is so large that even though the toroidal field at the wall is small there is enough to yield a small OPCD effect. The n spectra of the m=0 and m=1 modes are shown in figures 5.32 and 5.33. The sawtooth doublets are more apparent but otherwise the distribution of energy is nothing unexpected. I only include it in case someone asks "but what about the n-spectra?" and to kill some ink.

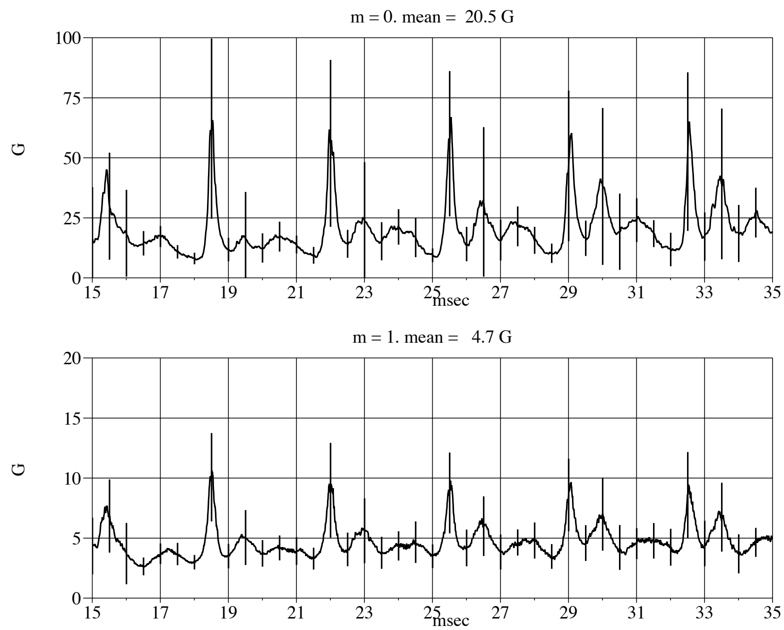

Figure 5.31 The m=0 and m=1 mode amplitudes during 280 Hz OTCD.

5.2.1.2 m=0 bubbles

We immersed our triple-tip probe a few centimeters into the plasma again to characterize the instabilities of the m=0, n=1 mode during the m=0 bubble. Unfortunately the effect is so small and grows so slowly that the probe yielded no results.

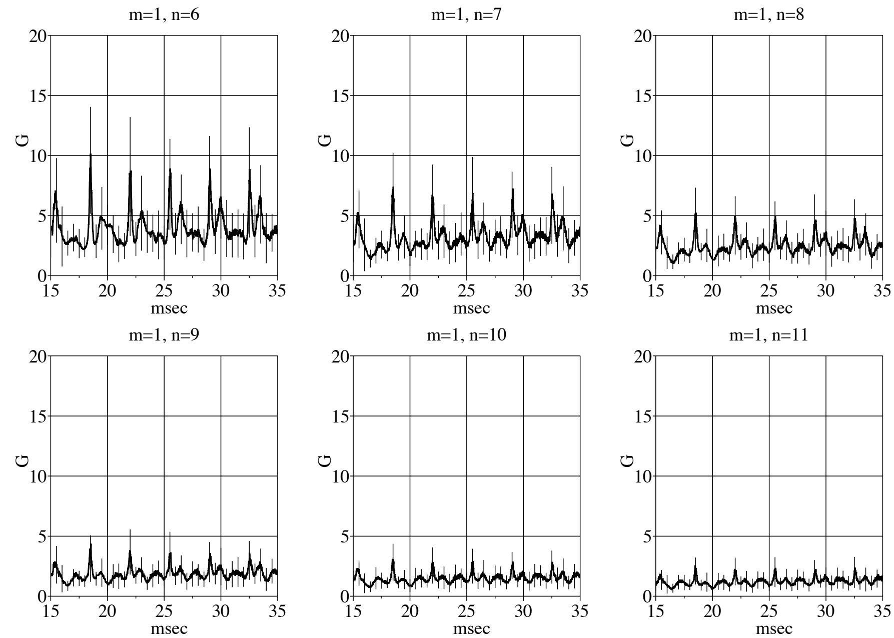

Figure 5.32 The m=1 mode n-spectra during 280 Hz OTCD.

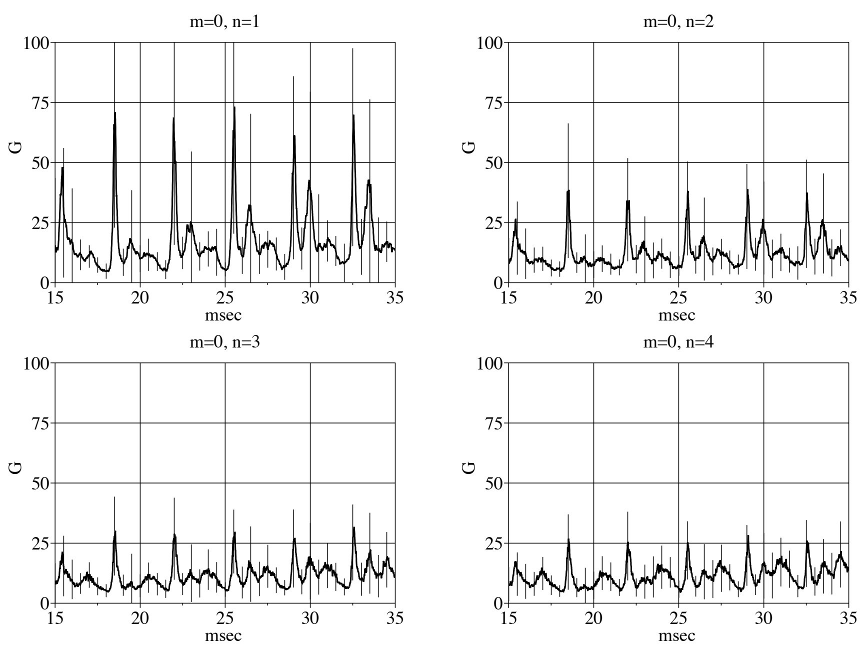

Figure 5.33 The m=0 mode n-spectra during 280 Hz OTCD.

5.2.1.3 530 Hz

At the higher frequency, the m=0 and m=1 modes behave more like a standard discharge as we'd expect them to. Figure 5.34 shows that the m=0 term jumps in sync with the m=1 mode so it looks like the m=0 mode is driven by coupling of the m=1 modes as nature intended. No m=0 bubbles appear. Nor do the m=1 bubbles that we saw during 530 Hz OPCD appear. But this unexpected lack of unexpected behavior may be due to the fact that, at 530 Hz, the OTCD voltage was less than half of what it was at 280 Hz. The n-spectra of each is blissfully uninteresting as well, as seen in figures 5.35 and 5.36.

5.3 OFCD

Finally, we get to what this experiment is really about, OFCD. Does it drive current? Will the wall interactions that tormented ZT-40 do the same to us? How do the bizarre behaviors seen in OPCD and OTCD combine when both oscillators are turned on?

We'll answer the most important question up front. Does partial sustainment OFCD drive current? The short answer is yes. But the behavior and possibly the very mechanism are not what we expected.

5.3.1 280 Hz

Figure 5.37 shows the gap voltages during 280 Hz OFCD with a nominal plasma current of about 250 kA. The OTCD and OPCD peak-peak voltage swings are 200V and 24V respectively, about the same as in the OPCD and OTCD experiments. From the toroidal gap voltage we can see that the sawteeth are still entrained.

The toroidal and poloidal fields at the wall are shown in figure 5.38. The oscillation of each is about what we saw in the OPCD and OTCD experiments. Figure 5.39 shows the reversal and pinch parameters are each modulated together as they were separately. So far so good.

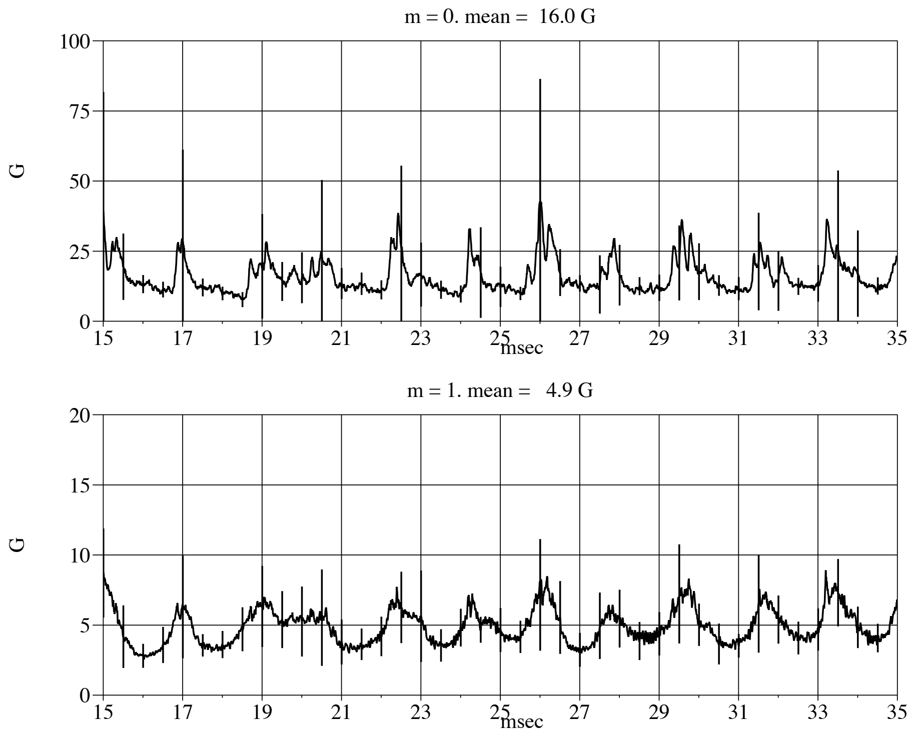

Figure 5.34 The m=0 and m=1 mode amplitudes during 530 Hz OTCD.

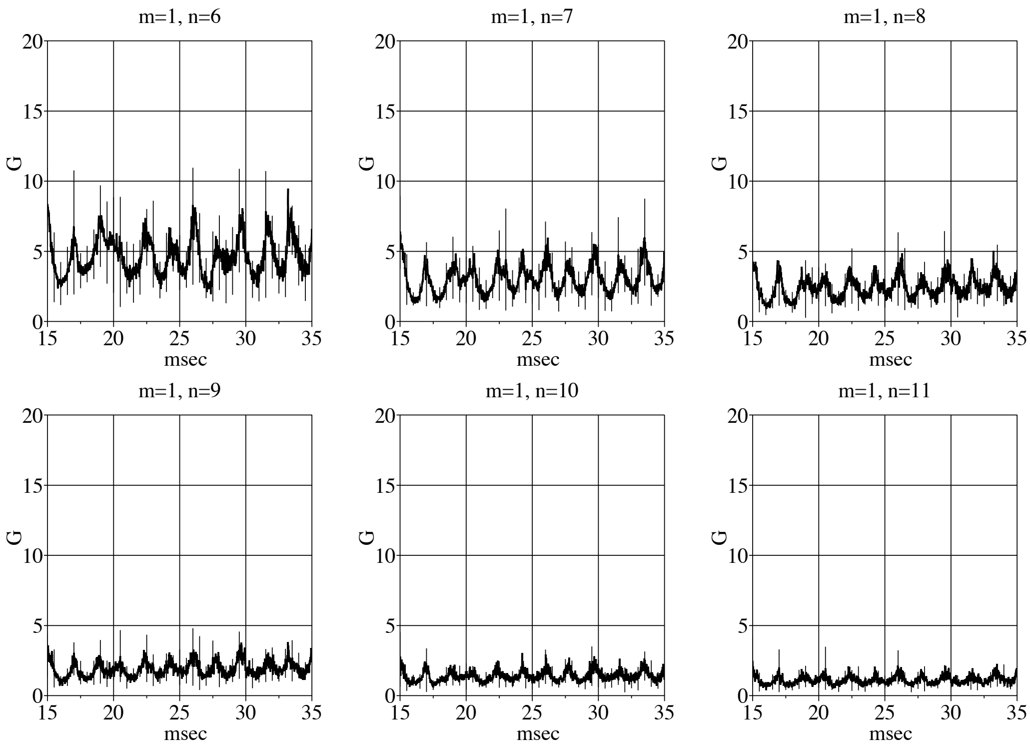

Figure 5.35 The m=1 mode n-spectra during 530 Hz OTCD.

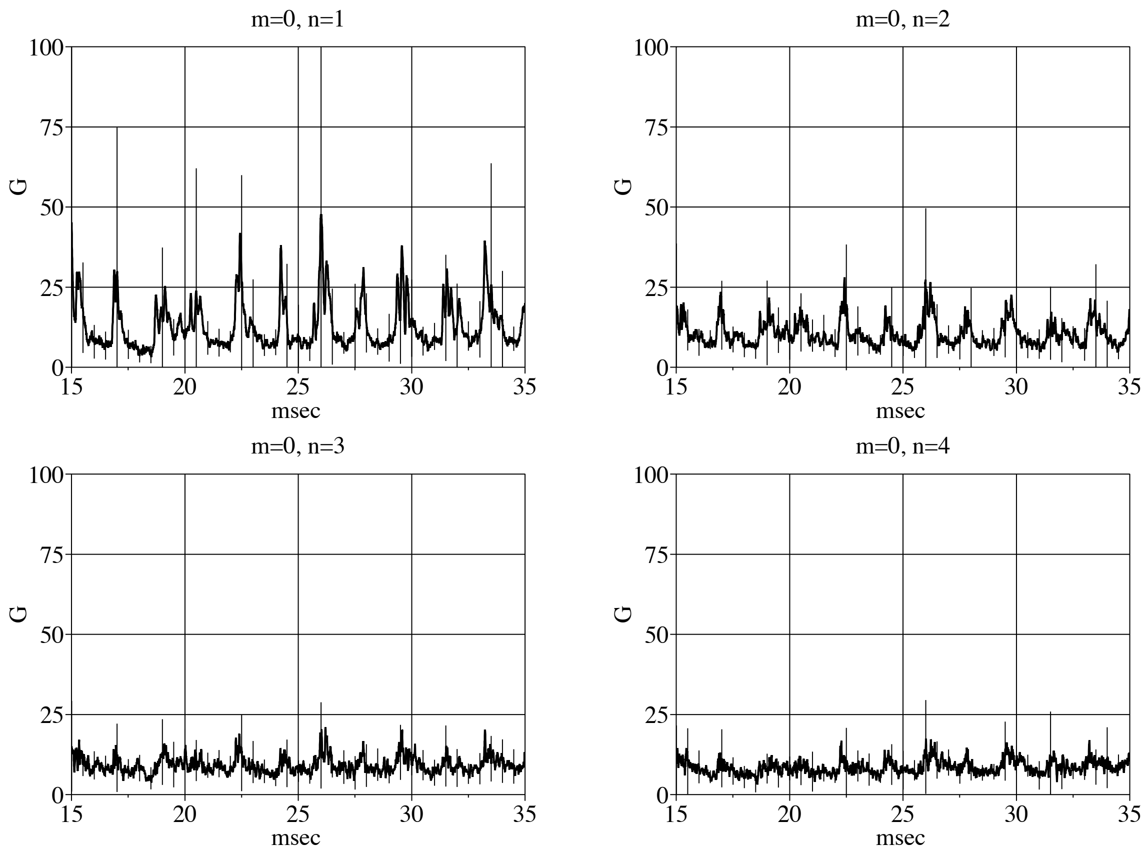

Figure 5.36 The m=0 mode n-spectra during 530 Hz OTCD.

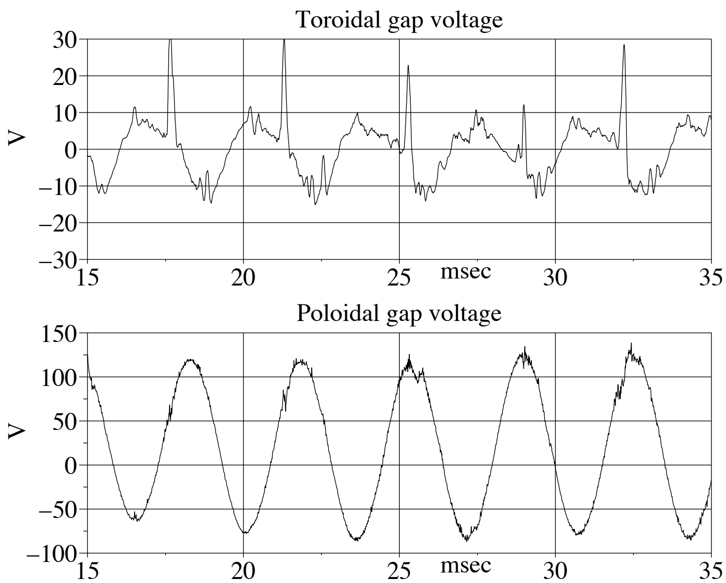

Figure 5.37 The gap voltages measured at the toroidal (top) and poloidal (bottom) gaps during 280 Hz OFCD.

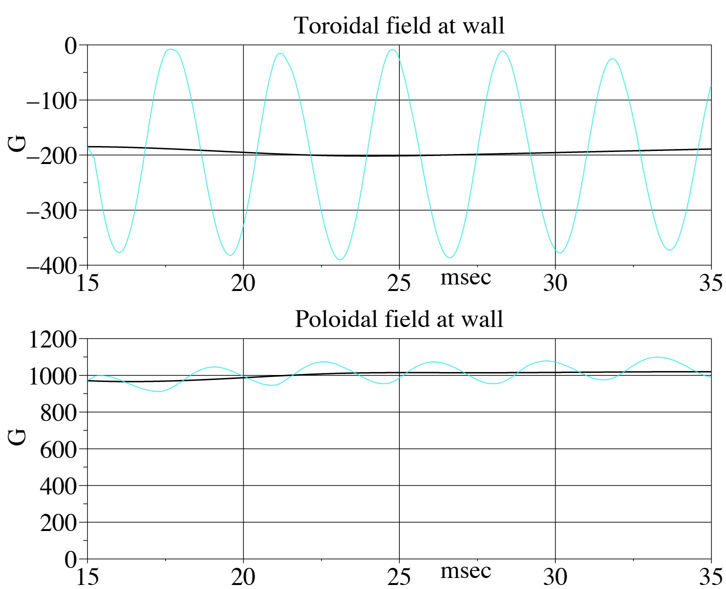

Figure 5.38 The toroidal and poloidal fields at the wall during 280 Hz OFCD. The thick curve is the cycle average.

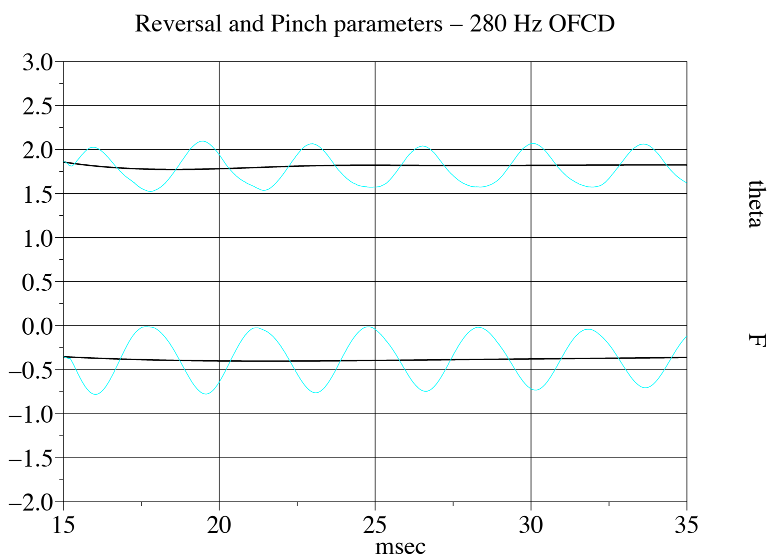

Figure 5.39 The reversal and pinch parameters during 280 Hz OFCD.

Figure 5.40 shows the very important $F - \Theta$ trajectory. While not as close to the theoretical perfectly relaxed curve as we saw in OPCD the excursion is still small enough that we can say the plasma is not much further from the pseudo-relaxed state of NOFCD.

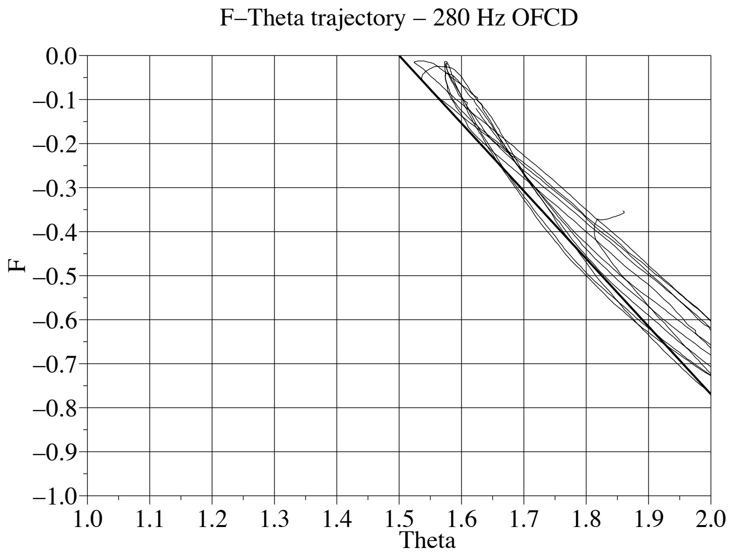

Figure 5.40 The $F - \Theta$ trajectory during 280 Hz OFCD. The dark line is the theoretical trajectory predicted by the α-model for $\alpha = 4$.

MSTFIT is a software package that finds an equilibrium profile that satisfies the Grad-Shrafonov equation (read a book) that fits the output of most of the MST diagnostics, including the FIR. One product of MSTFIT is $\lambda(r,t) = \mu_0 J_{\|}/B$, the normalized current profile. An accurate prediction of λ is important to OFCD since it (and the boundary conditions) fully describe the equilibrium magnetic field of a relaxed plasma. If we're to have any faith in any other predictions, the λ profile predicted by modeling must be a good match to experimental data. The λ profile (normalized by a) predicted by the 3D model is shown in figure 5.41 for 2 points in a cycle. t1 corresponds to the point that helicity ejection is maximum (v_z at minimum.) t2 corresponds to maximum helicity injection(v_θ at minimum.) It should be noted that the 3D simulation was performed at a slightly higher frequency than the experimental value. The λ profile from MSTFIT using nearly every diagnostic on MST is shown in figure 5.42. The match is not very good. Fishing for possible excuses, the experimental λ profile is not a raw measurement. It's a fit to an equation that makes a lot of assumptions about the plasma. MSTFIT assumes a plasma in equilibrium, which is never really true in MST. Of course, the 3D model has it's own set of assumptions, including a cylindrical geometry and a lower resistivity than is observed. It also assumes a static resistivity profile and does not take into account a host of realities like transport. It's just a question of which model is less presumptive. MSTFIT at least starts with real measurements so it should be a more accurate representation of the real plasma. Perhaps a better approach is to concentrate on the edge values predicted by modeling and what we can measure directly rather than debate what's going on inside the plasma. This is fine for most considerations, but not very useful for studying confinement, so we won't study confinement.

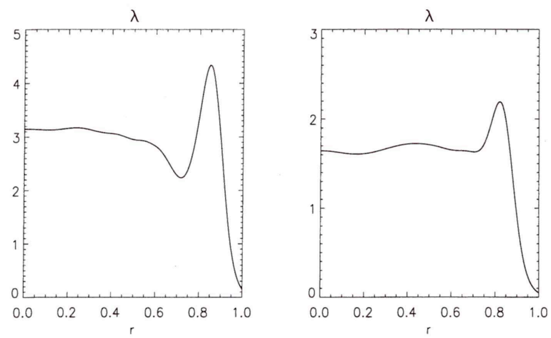

Figure 5.41 Lambda profile at 2 phases of oscillation during partial sustainment OFCD as predicted by the 3D model.

5.3.1.1 Current Drive

We start, as usual, at our preferred frequency, 280 Hz. Recall that there should be a phase difference between the oscillators that maximizes the added current drive (the drive phase.) There should also be a phase that maximizes the subtraction from the plasma current (anti-drive), presumably $180°$ from the drive phase. Figure 5.43 shows the maximum current drive, maximum antidrive, and the nominal NOFCD current. The current drive for this ensemble average is about 17 kA. The antidrive yields about -50 kA. The fact that one phase adds current and another subtracts current is encouraging by itself. It confirms theoretical expectations at least qualitatively.

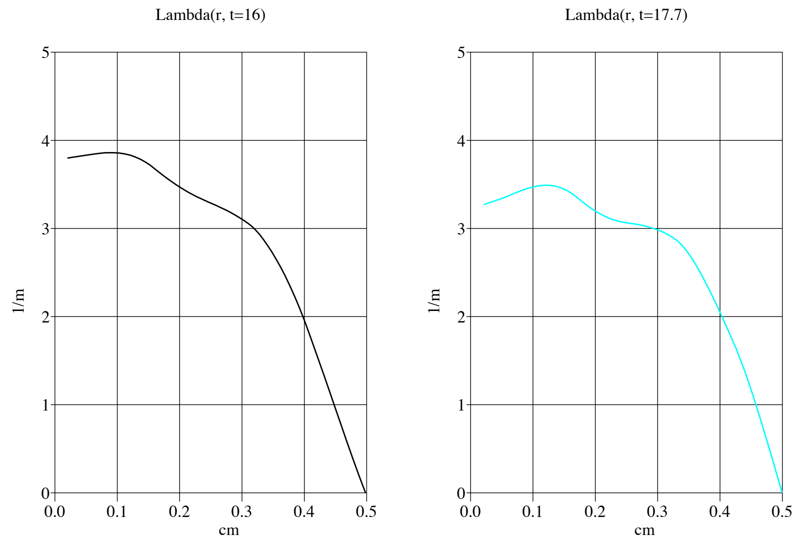

Figure 5.42 The $\lambda = \mu_0 J_{\|}/B * a$ profile for two points in a cycle according to MSTFIT.

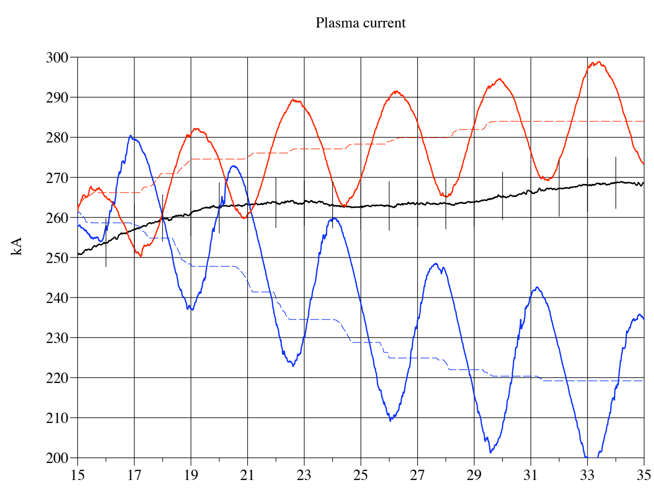

Figure 5.43 The cycle averaged current drive, antidrive, and nominal current during 280 Hz OFCD.

What was not expected was the phase dependence. The math and 1D model both say the helicity injection rate should vary sinusoidally with the phase difference. We presume current drive would do the same. The 1D relaxed state model showed a maximum current drive of 13 kA (5% referenced to 250 kA) at 90° phase difference and maximum antidrive current of -14 kA (6%) at -90°. 3D modeling saw maximum current drive of about 20 kA (8%) at 45° phase difference and antidrive of -40 kA (-16%) at -90°. Since the simulations take so long we dont yet have enough points from the 3D model for a detailed phase scan. Figure 5.44 shows that the actual phase dependence of current drive is not at all sinusoidal. The best fit curve is left to the readers imagination. This is probably the most unusual phenomena we've seen thus far. Nothing in the theory suggests such an ugly curve. The maximum current drive occurs at about 25° and is about 20 kA (8%) on top of the nominal value of 268 kA by the end of the shot. The maximum antidrive is -50 kA (-19%), enough to occasionally quench the plasma. The 1D model prediction of maximum current drive is within spitting distance of experimental results (albeit at a different phase.) The maximum antidrive of 14 kA predicted by the 1D model is not even close to the experimental value. Also plotted are 2 points from the 3D model. The 3D model did a much better job predicting antidrive current of -40 kA at -90°. More points from the 3D model are on order. The curve is distinctly asymmetric implying something beyond the classical OFCD dynamics is at play. Figure 5.45 shows the cycle averaged helicity injection rate from eqn 3.7 appears to have the expected sinusoidal dependence with a maximum injection rate at least close to the expected 90° and a maximum ejection rate at -90°. So maximum current drive does not occur during maximum helicity injection. But the curve is offset. The magnitude of the helicity ejection rate is larger than the largest injection rate. This could account for some of the large antidrive current.

Most unusual/disturbing is that it doesn't look like the result will be the same at $\pm 180^\circ$ unless the curve takes a sharp dive on the right or a U-turn on the left. A broader phase scan is needed. Looking back at figure 5.37 we see that the waveforms for the two oscillators are identical(ish) in that they start at the same absolute phase and they both start with a sharp transient. To shift the phase between the oscillators we start the OTCD oscillator before or after the OPCD oscillator. So, for up to 1.8 msec, one oscillator is running alone. The asymmetry of the current drive might be

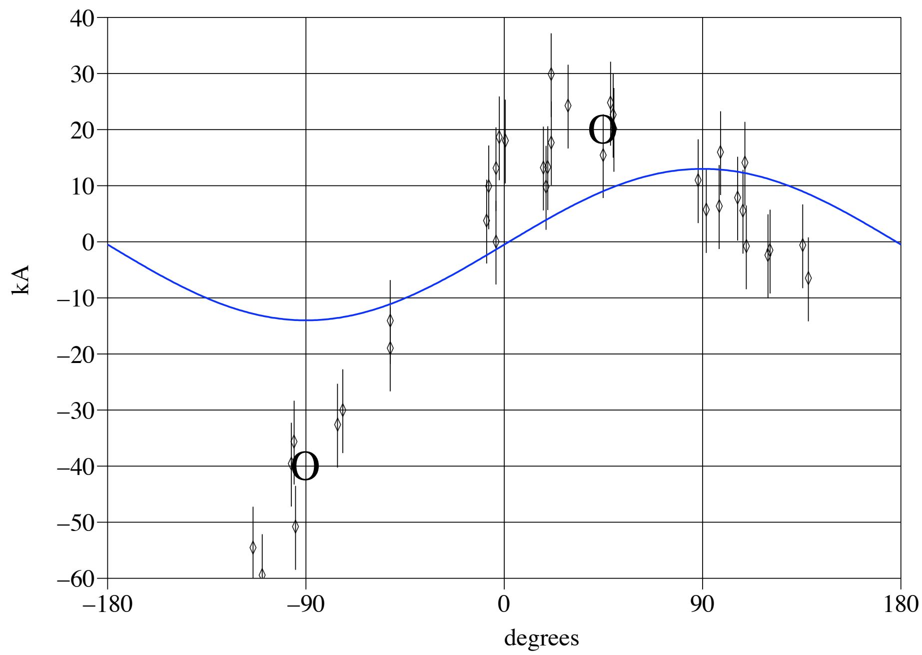

Figure 5.44 Current drive vs phase difference for 280 Hz OFCD. The blue curve is the prediction by the 1D model. The large circles are two points from the 3D model. The curve bears little resemblence to the sinusoidal dependence seen in the 1D model but is in good agreement with the 3D model for the two points available. Maximum current drive occurs at about $25°$

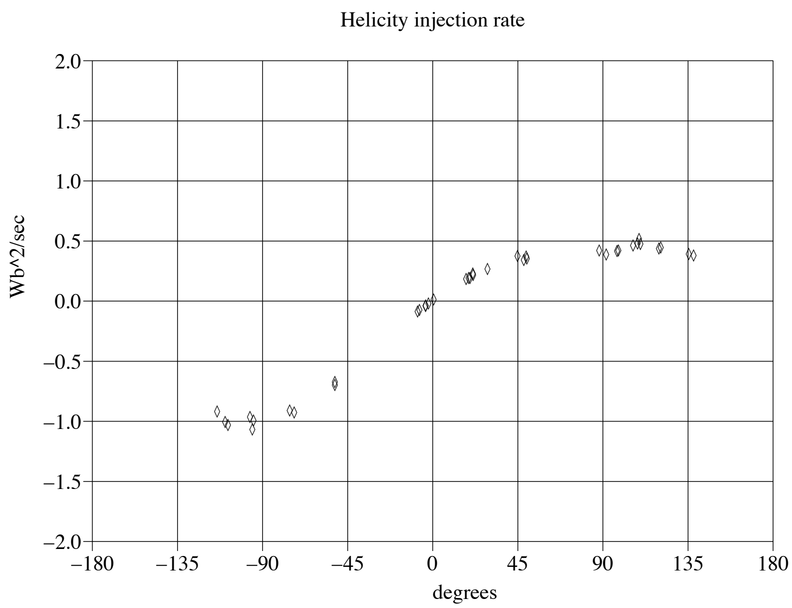

Figure 5.45 The cycle average helicity injection rate vs phase difference for 280 Hz OFCD

due to this timing difference instead of the phase difference. But for such a short time interval to have such a large effect implies that OPCD (or OTCD) has a far greater impact on the plasma than seen in the OPCD/OTCD experiments. Looking back at figure 5.6 we see that OPCD alone does indeed reduce the plasma current. But it takes 20 msec, not 1.8, to drive the current down 20 kA. The current degradation of figure 5.6 could be due to some monstrously deleterious and lasting effect of the large transient at the start of the waveform. It would be better if the two oscillators could be started at the same time but with truly different phases, at least as seen at the gap. There is a plan to try isolating the OPCD oscillator from the gap when it is first fired so that both oscillations appear at the gap at the same time but at different phases. The SCRs of the Bt crowbar bank will be used as a crude switch.

It was suggested that the shape of the curve might be influenced by the nominal plasma current. Figure 5.46 shows a phase scan with a nominal (NOFCD) current of 300 kA. There wasn't much data available and the frequency differences between the two oscillators is a few Hz larger, but the shape appears to be nearly the same, if not quite as asymmetric.

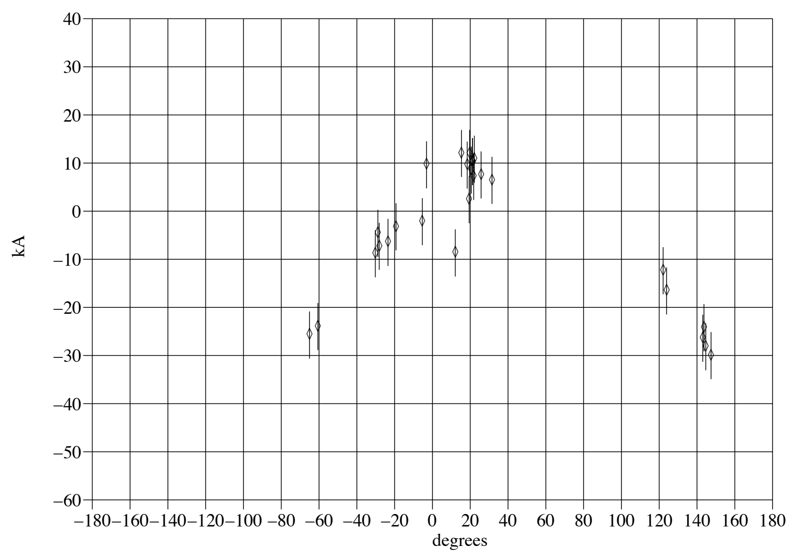

Figure 5.46 Current drive vs phase difference for a 300 kA nominal plasma current for 280 Hz OFCD.

To learn what is driving the phase dependence we'll look at how other plasma behavior depend on the phase difference between the oscillators.

Impurity levels The obvious first culprit to consider is the plasma-wall interaction. Impurities dumped into the plasma will raise the resistivity and thus hinder current flow. This is what hampered the ZT-40 OFCD attempts. Our only measure of wall interaction are the emissions from CIII, CV, OIV, BIV, and NIV (spectral lines of carbon, oxygen, boron, and nitrogen) measured by the impurity monochromater array (IMA.) This is not to say the IMA is a particularly good measure of wall interactions. Other factors like bulk ion temperature and density can affect the IMA results. The effective value of the charge factor, Z_{eff}, would be better but we don't have a Z_{eff} meter. The IMA is all we've got. Impurity emissions vary from day to day as probes and such are inserted and withdrawn from the plasma. So we use the difference between the OFCD and NOFCD waveforms.

Figure 5.47 shows how the mean value of each impurity measurement varies with the phase difference. Each point is the difference between the time-averaged values of the OFCD and baseline NOFCD waveforms. Again, the best fit curve is left to the imagination of the reader. Except for the carbon V line, each shows a vaguely parabolic shape with a minima right at (or very near) our maximum current drive phase. The telltale shape is most apparent in the boron IV line. Many of the probes are coated with boron. There is also a small amount of boron on the wall of MST. Note that the boron curve displays the same asymmetry as the current drive.

This correlation does not necessarily mean plasma-wall interactions are driving up the resistivity of the plasma. As mentioned before, the IMA is not a great measure of wall interactions. But if extraneous factors like confinement were driving the IMA waveforms we'd expect to see the same effect on each. When the one spectral line that happens to come from the most prevalent impurity on the wall shows such a familiar shape we have cause to be concerned. More study is needed here.

Mode amplitudes: The $m = 0$ and $m = 1$ mode amplitudes play an important role in confinement in MST. Confinement affects resistivity which obviously affects current drive. So we

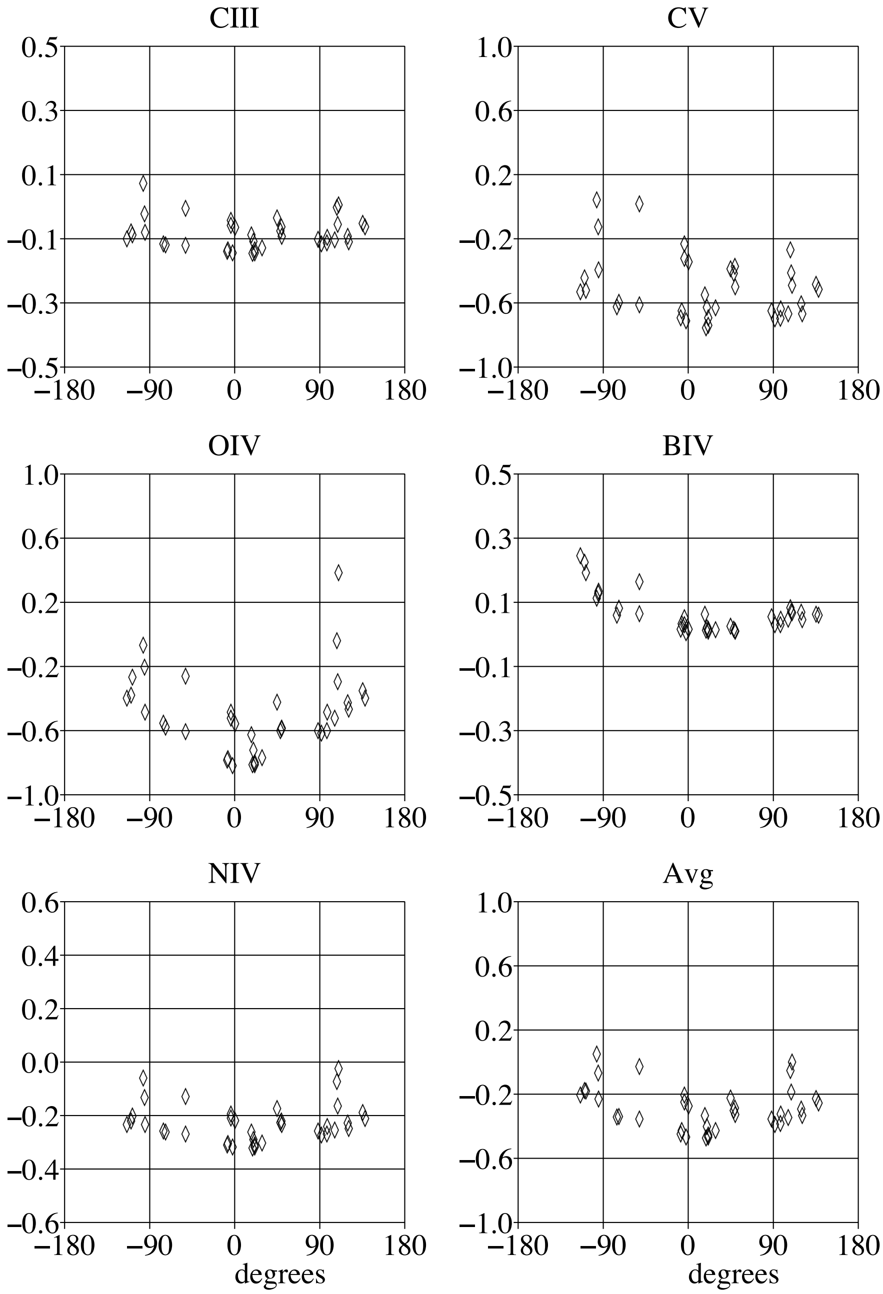

Figure 5.47 Mean value of impurity measurements vs phase difference of the oscillators for 280 Hz OFCD

need to know if the modes amplitudes vary with oscillator phase. Figures 5.48 and 5.49 show how the m=0 n=1..4, and m=1 n=6..11 vary with phase. Each point is the time-averaged value for one shot. The $m = 0$ curve shows the most obvious dependence, with a minima right where our maximum current drive occurs. The $m = 1$ curve shows a barely visible dependence, with a rough minimum in the same place. Reduced fluctuations mean better confinement which means increased core temperature which means lower resistivity which means increased current drive. This is likely a contributing factor to maximum current drive. Temperature measurements will be discussed shortly. Whether and how much confinement improves is a subject of ongoing research.

Pedestrian factors like temperature and confinement are beyond the OFCD dynamics you find in papers and what we've studied in 1D and 3D simulations. But these factors apparently depend on the phase of the oscillators and must be considered as at least possible conspirators in the odd shape in figure 5.44. The question then becomes *why* should *these* factors depend on phase? Which is cause and which is effect? How much of the current drive and antidrive we see is driven by classical OFCD dynamics and how much by factors like temperature and resistivity? And, most of all, how will all of this impact full-sustainment OFCD? These are all important questions that remain definitively unanswered as of this writing. There are at least three more doctoral theses in just these questions. But we have at least answered the most important question: Does OFCD drive current? The answer, at least for the partial sustainment case, is yes. But some aspects of the mechanism that makes it happen are unclear.

5.3.1.2 Mode Spectra

The m=0 and m=1 mode amplitudes are shown in figures 5.50 and 5.51 for the drive and antidrive phases of 280 Hz OFCD. Also shown are the NOFCD values, though the lack of sawteeth is only because sawteeth are randomly placed in NOFCD and average away in a large ensemble average. There's obviously a tremendous difference in the behavior of the tearing fluctuations in the drive and antidrive phases. In the antidrive phase the m=0 mode amplitude looks a lot like it did during OPCD, with enormous slow growing 'bubbles' of m=0 activity. Also recall that OPCD caused a lot of current degradation, nearly 20kA as seen in figure 5.6. Since the OPCD

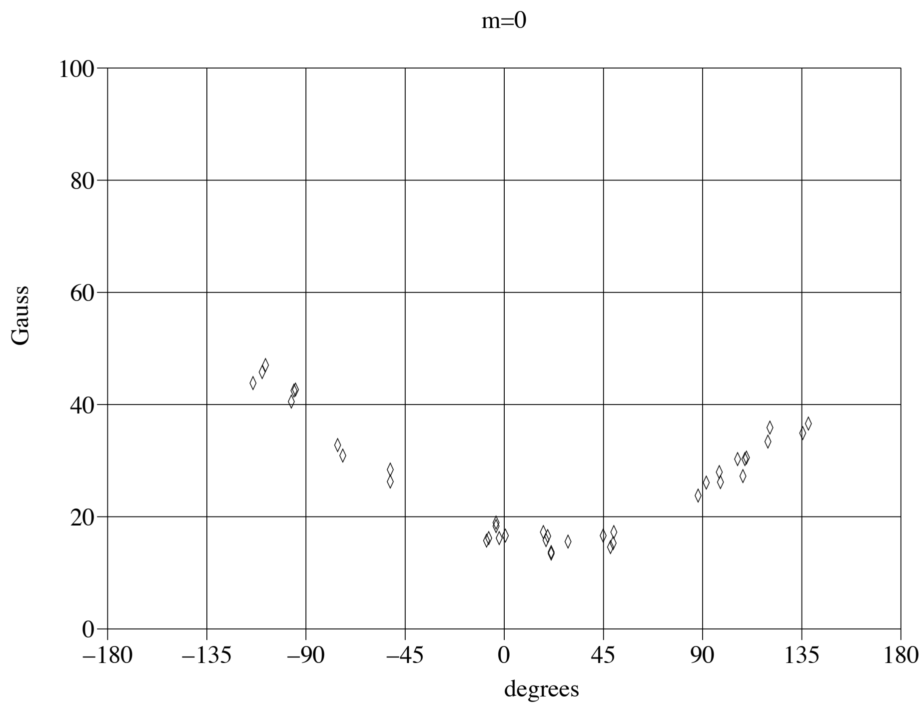

Figure 5.48 The time-averaged $m = 0$ mode amplitude vs oscillator phase.

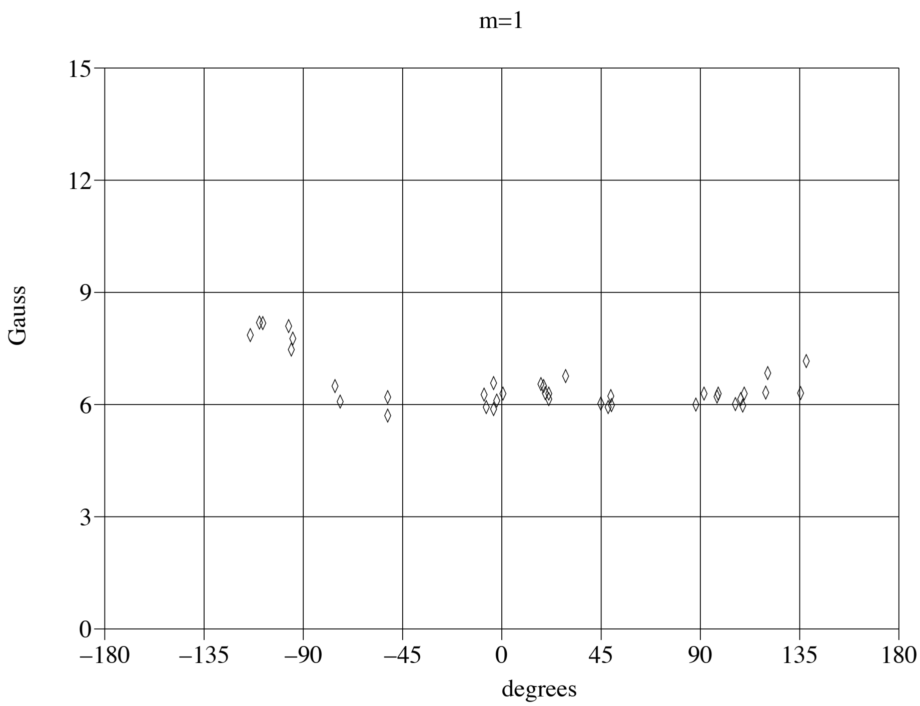

Figure 5.49 The time-averaged $m = 1$ mode amplitude vs oscillator phase.

oscillation is the dominant component in the edge, the strange shape of figure 5.44 may be due to a combination of classical OFCD dynamics plus the peculiar effects of OPCD. Further study of OPCD may yield the reason for the excess antidrive of OFCD. A programmable power supply will (hopefully) soon replace the OPCD ignitron oscillator. The tunability and capacity for other waveforms will no doubt be mighty useful for studying OPCD.

The n-spectra of the m=0 and m=1 modes for drive and antidrive are shown in figures 5.52 through 5.55. Note the larger scale for m=0 antidrive.

5.3.1.3 m=0 bubbles

As with OPCD and OTCD we immersed our triple tip Langmuir probe into the plasma to monitor the stability of the m=0, n=1 mode. Unfortunately, as explained in the OPCD section, the bubbles were too small and slow for us to detect any net positive or negative change in the energy of the mode.

5.3.1.4 Helicity dissipation

Harken back to chapter 3 and equation 3.2, the rate of change of global magnetic helicity injection,

$$\frac{\partial K}{\partial t} = 2v_z\Phi_z - 2\int \mathbf{E}\cdot\mathbf{B}dV \tag{5.3}$$

where v_z is the toroidal loop voltage (at the edge) and the volume integral is over all space. The first term on the right hand side is the helicity injection rate. The second term is the rate of helicity dissipation (through ohmic loss.) In this section we'll examine the second term. We'll reconstruct $\mathbf{E}$ and $\mathbf{B}$ as directly as we can from edge measurements. We'll assume, as we did in the 1D model, that the α model accurately describes the internal normalized parallel current ($J_{\|}/B$) profile.

$$\frac{J_{\|}}{B} = \Lambda(r) = \lambda_0(1-(\frac{r}{a})^{\alpha}) \tag{5.4}$$

From measurements of the toroidal magnetic field at the wall, the plasma current, and the toroidal flux we can find the values of α and λ_0 that best fit these edge measurements. From α, λ_0,

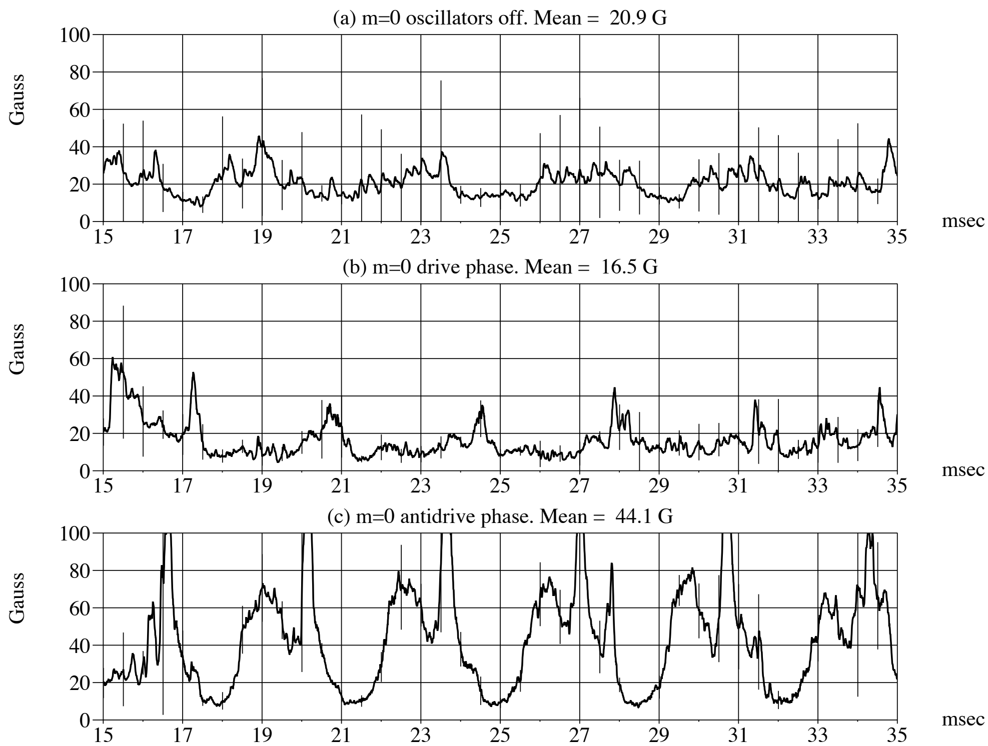

Figure 5.50 The m=0 mode amplitudes for 280 Hz OFCD for: (a) NOFCD (b) OFCD maximum current drive phase, (c) maximum antidrive phase.

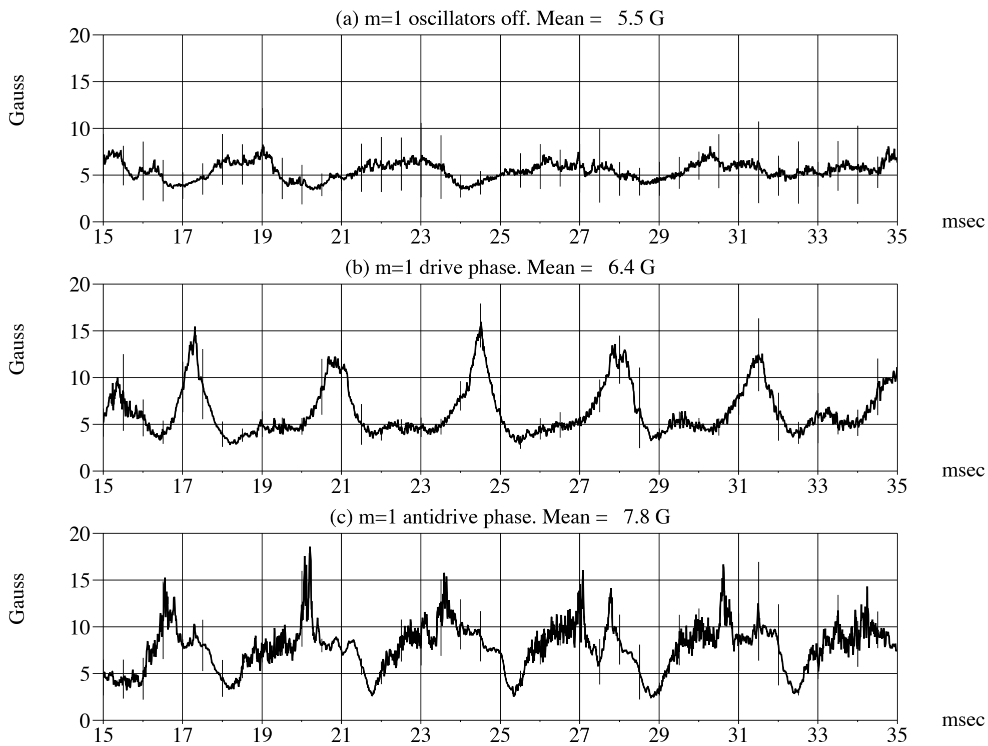

Figure 5.51 The m=1 mode amplitudes for 280 Hz OFCD for: (a) NOFCD (b) OFCD maximum current drive phase, (c) maximum antidrive phase. The NOFCD curve is smoothed by the ensemble average and random placement of the sawteeth.

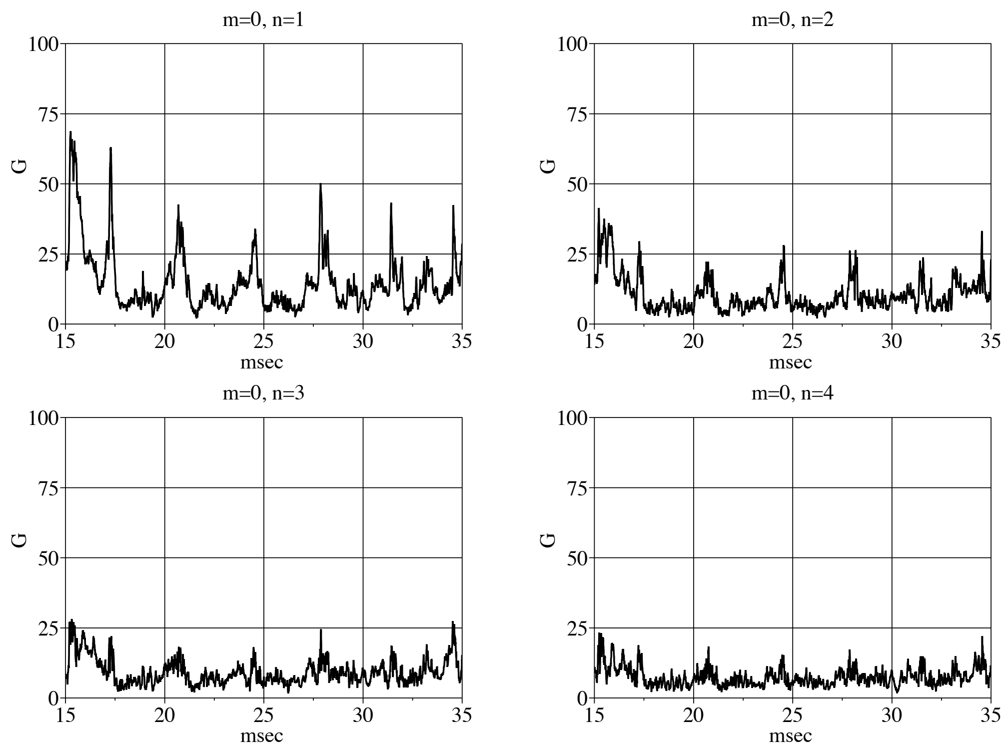

Figure 5.52 The n-spectra of the m=0 mode during 280 Hz OFCD. Oscillator phase difference set for maximum current drive. The vertical spikes are error bars.

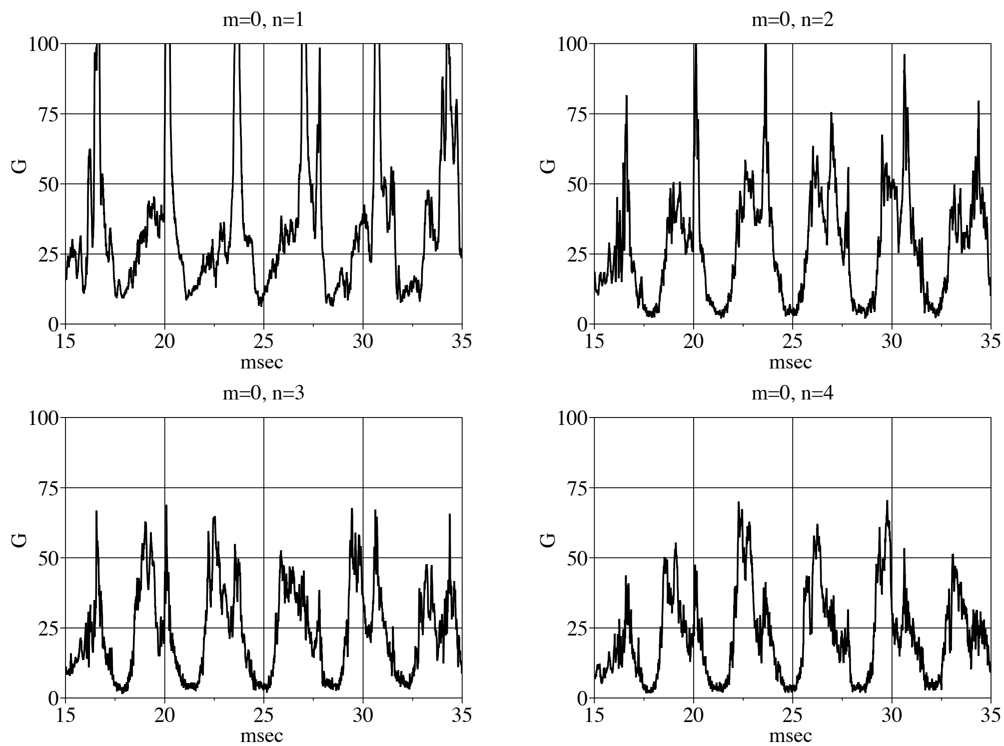

Figure 5.53 The n-spectra of the m=0 mode during 280 Hz OFCD. Oscillator phase difference set for maximum current antidrive. The vertical spikes are error bars.

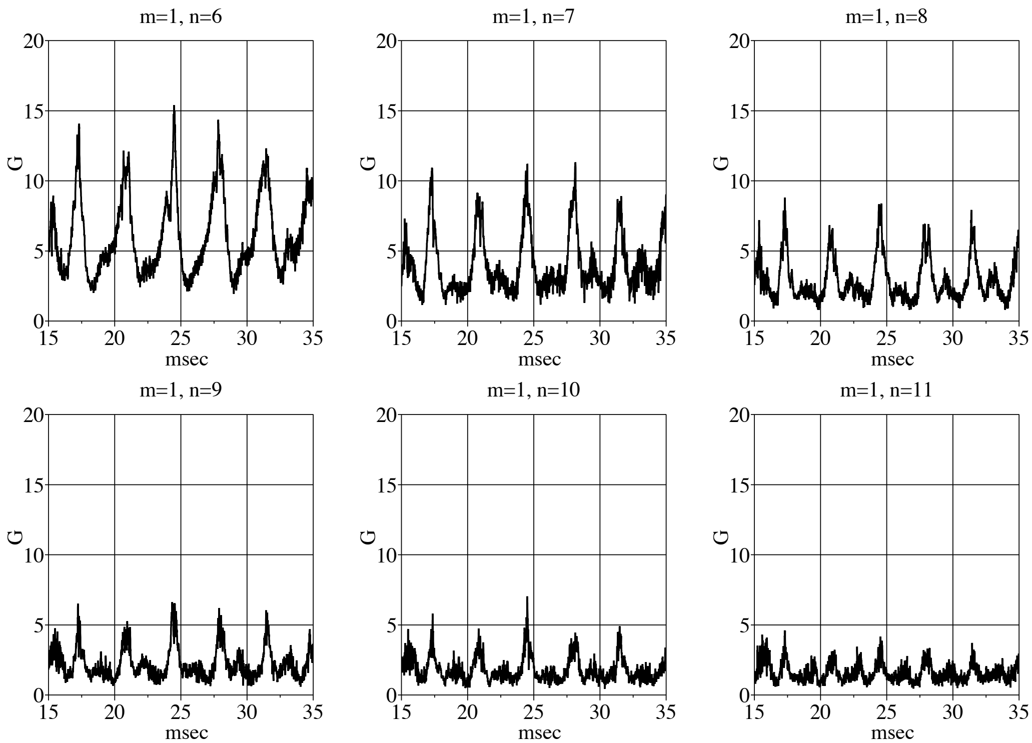

Figure 5.54 The n-spectra of the m=1 mode during 280 Hz OFCD. Oscillator phase difference set for maximum current drive. The vertical spikes are error bars.

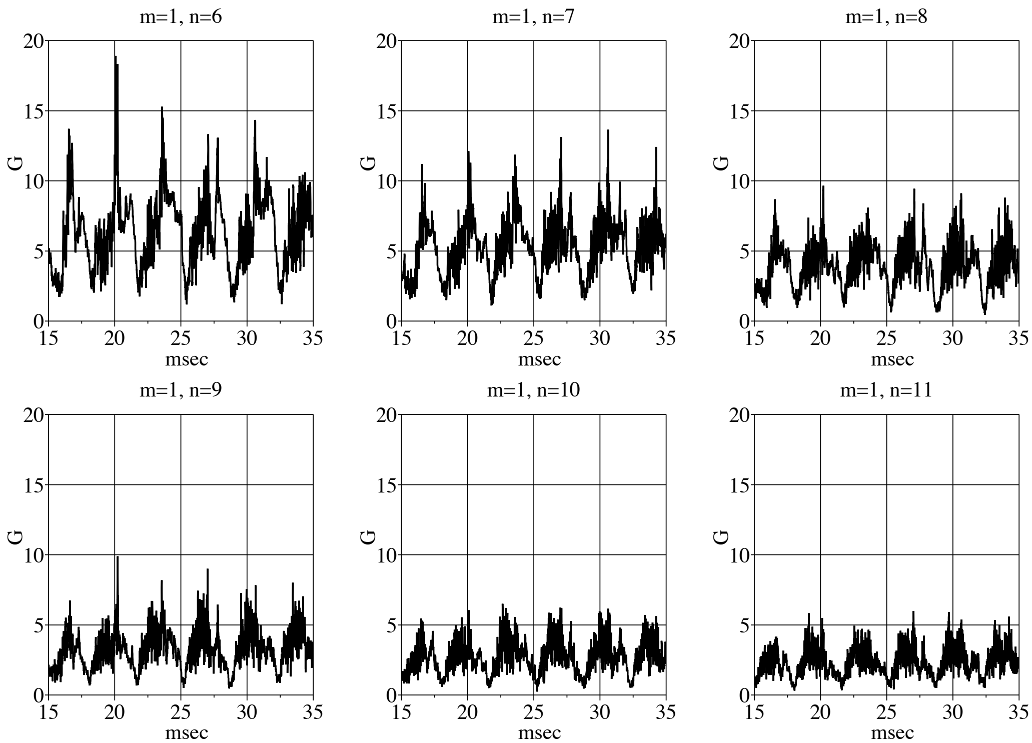

Figure 5.55 The n-spectra of the m=1 mode during 280 Hz OFCD. Oscillator phase difference set for maximum current antidrive. The vertical spikes are error bars.

and the toroidal flux we can reconstruct the magnetic field profile by solving

$$\nabla \times \mathbf{B} = \Lambda(r)\mathbf{B} + \frac{\mathbf{B} \times \nabla p}{B^2} \tag{5.5}$$

in cylindrical coordinates. The pressure profile is assumed parabolic with a poloidal $\beta = 0.07$.

From the time varying values of $\mathbf{B}$ we can get the electric field profile using Faradays law

$$\nabla \times \mathbf{E} = -\frac{\partial \mathbf{B}}{\partial t} \tag{5.6}$$

taking care to include the poloidal magnetic flux from the central iron core that threads the center of MST. This boils down to two integrals for the two components of $\mathbf{E}$.

$$E_z(r,t) = \frac{v_z}{2\pi(R_0 - a)} - \frac{1}{R_0 - r}\int_r^a \dot{B}_\theta(r',t)(R_0 - r')dr' \tag{5.7}$$

$$E_\theta(r,t) = -\frac{1}{r}\int_0^r \dot{B}_z(r',t)r'dr' \tag{5.8}$$

where R_0 and a are the major and minor radii of the torus. In MST v_z is measured at the poloidal cut in the vacuum vessel.

The helicity dissipation and injection rates are

$$\frac{\partial K_{diss}}{\partial t} = 2\int \mathbf{E}\cdot\mathbf{B}dV = \int_{r=0}^{a}\int_{z=0}^{2\pi R_0}\int_{\theta=0}^{2\pi}(E_zB_z + E_\theta B_\theta)rdrdzd\theta \tag{5.9}$$

$$\frac{\partial K_{inj}}{\partial t} = 2v_z\phi_z = 2v_z(2\pi)\int_{r=0}^{a} B_z r dr \tag{5.10}$$

Figure 5.56 shows the helicity injection and dissipation rates during a normal (NOFCD) MST discharge. We can see that the dissipation rate slightly exceeds the injection rate, implying helicity is being lost to ohmic dissipation. Figure 5.57 shows the two rates with the OFCD oscillators on and the phase difference between them set for maximum current drive. The thick curves are the cycle average values. We see that the cycle average injection rate closely matches the dissipation rate implying that OFCD does a slightly better job sustaining helicity than do the standard discharge power supplies. Finally, figure 5.58 shows the rates with OFCD on and the phase difference set for antidrive of -40 kA. There are more extreme antidrive cases but the plasma is often literally snuffed out by those phases. The chosen phase and current drive closely matches the antidrive case studied in the 3D model. For the antidrive phase there is clearly more dissipation than injection. The final value of the dissipation rate is nearly double the final value in the drive phase. The injection rate is also decreased. This isn't too surprising. As antidrive OFCD decreases the plasma current, the plasma runs cooler so the resistivity is increased.

5.3.2 530 Hz

The higher frequency experiments were conducted earlier in the OFCD program. Back then the oscillators were horribly unreliable. The failure rate was over 90%. So we didn't have enough data for a decent phase scan. We were able to get only the two extremes: drive and antidrive shown in figure 5.59. At this high frequency, no appreciable current is driven in the drive phase. In fact, there may be a slight degradation. The antidrive phase yields a subtraction of 30 kA from the drive phase at the end of the shot. This lackluster performance is what inspired us to lower the frequency to 280 Hz even though it means fewer cycles within the shot.

Figures 5.60 and 5.61 show the m=0 and m=1 mode amplitudes for NOFCD, drive, and antidrive. The only noteworthy feature here is that the difference between the m=0 amplitudes during drive and antidrive phase is not nearly as pronounced as the difference at 280 Hz. This may be because the higher frequency oscillation does not penetrate the plasma deep enough to excite the mode.

5.3.3 Anomalous Ion Temperature Modulation

As in OPCD experiments, the ion temperature measured by the Rutherford scattering diagnostic can show a significant modulation at our oscillator frequency. But with OFCD we have one more knob to turn - the phase between the oscillators. Figure 5.62 shows the ion temperature vs time for 4 phases: $-90, 0, 45, 90°$. $45°$ is closest to the maximum current drive phase and $-90°$ is closest to the maximum antidrive phase. Also plotted are the best fit sinusoids near 280 Hz as found with a DFT. There's little apparent difference between the drive and antidrive cases. In fact, it's debatable whether the modulation exists for antidrive. But the modulation is most apparent between these two cases, at $0°$ and $90°$. We might be inclined to read something into this. But this

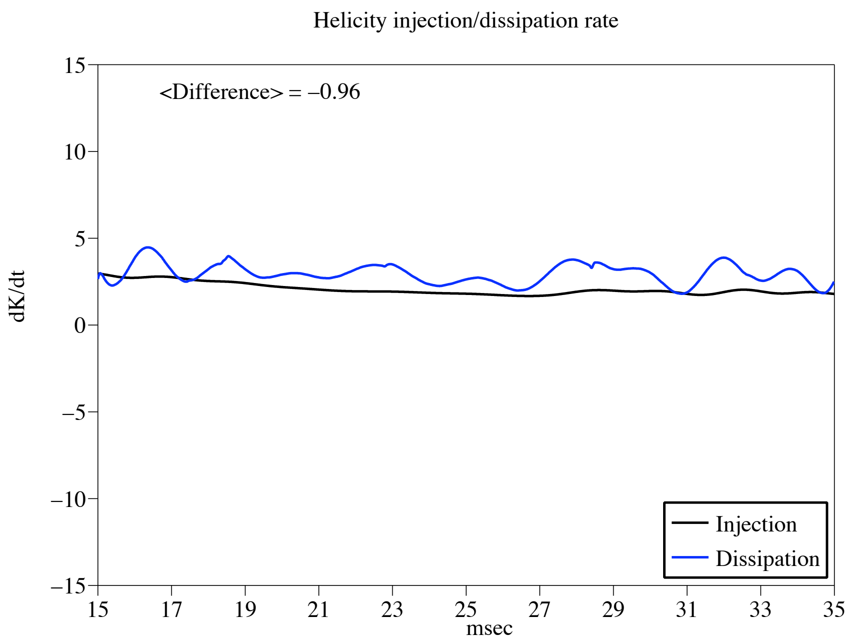

Figure 5.56 Helicity injection and dissipation rate during a standard 250 kA discharge. Helicity dissipation slightly exceeds the injection rate, implying helicity is slowly being lost.

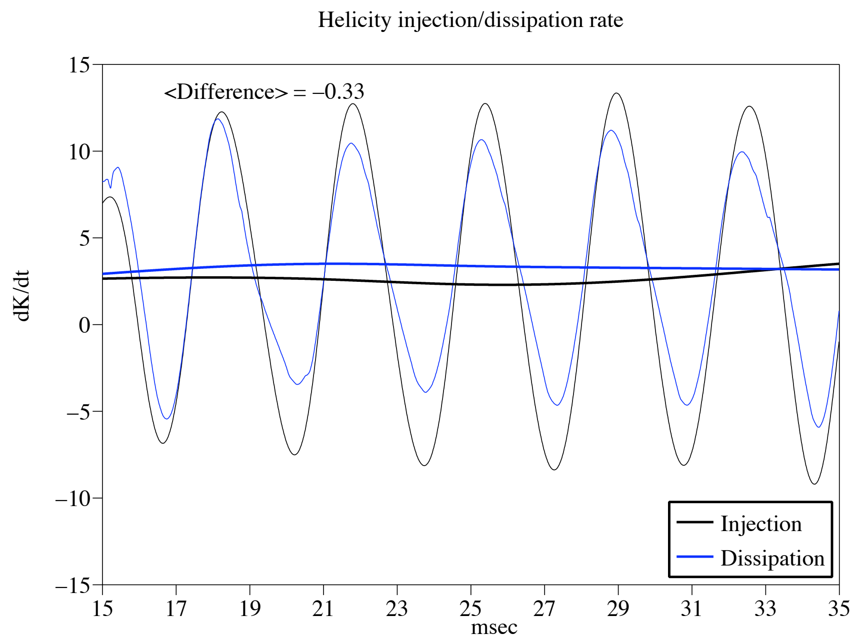

Figure 5.57 Helicity injection and dissipation rate during 280 Hz 250 kA OFCD. The oscillators are set for maximum current drive. Cycle averaged helicity injection rate closely matches dissipation rate, implying helicity is being conserved.

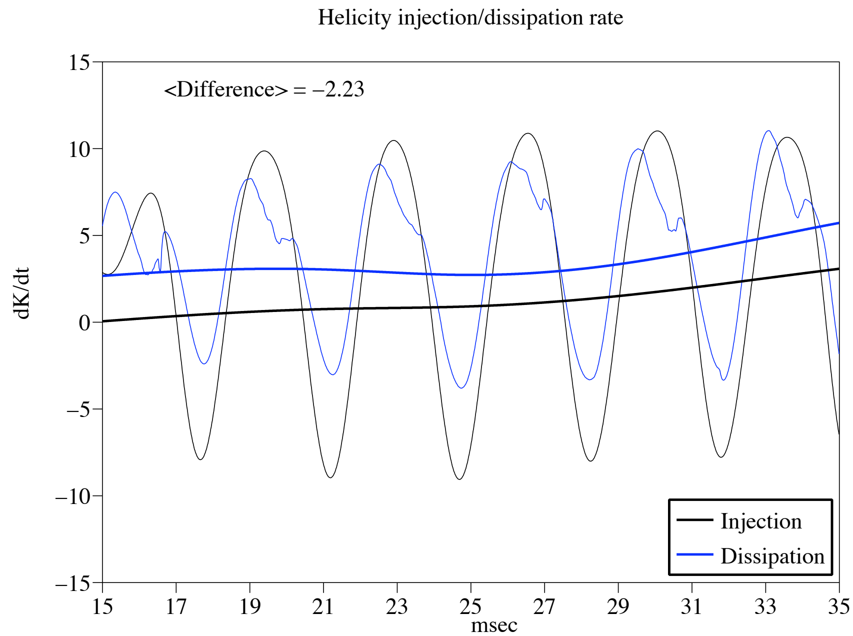

Figure 5.58 Helicity injection and dissipation rate during 280 Hz 250 kA OFCD. The oscillators are set for maximum current antidrive. Cycle averaged helicity dissipation rate greatly exceeds the injection rate, implying helicity is rapidly being lost.

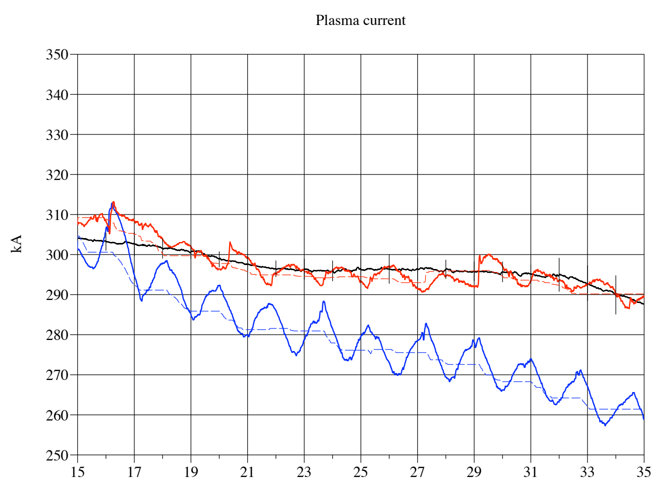

Figure 5.59 Off, Drive, and Antidrive plasma current for 530 Hz OFCD.

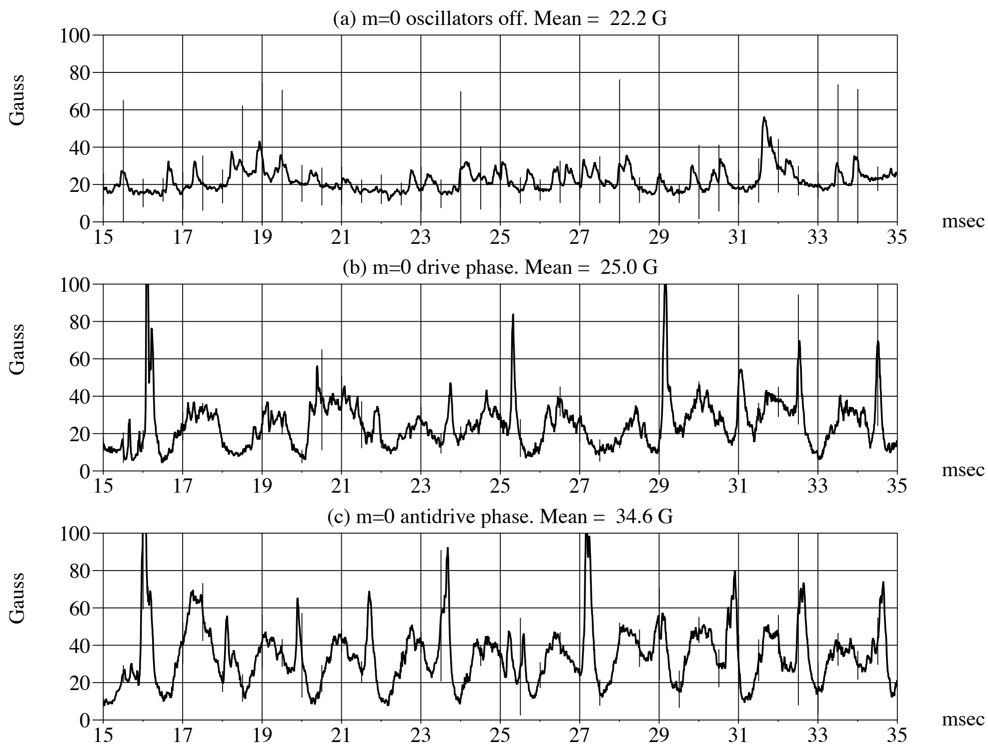

Figure 5.60 The m=0 mode amplitudes for (a) NOFCD, (b) drive, and (c) antidrive for 530 Hz OFCD. The NOFCD curve is smoothed by the ensemble average and random placement of the sawteeth.

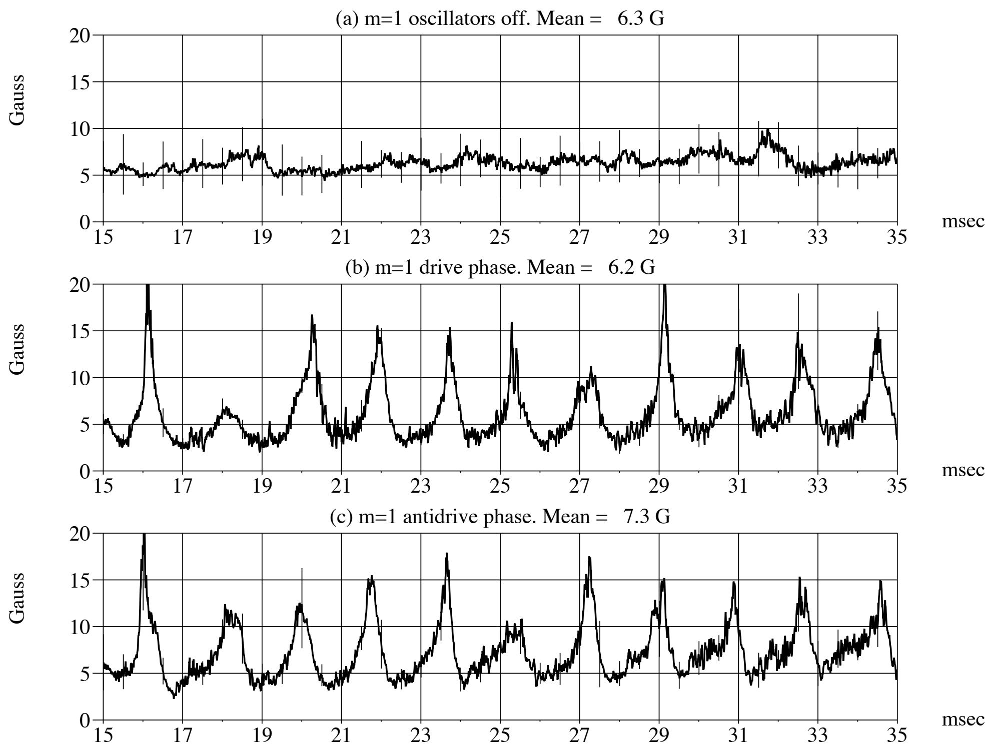

Figure 5.61 The m=1 mode amplitudes for (a) NOFCD, (b) drive, and (c) antidrive for 530 Hz OFCD. The NOFCD curve is smoothed by the ensemble average and random placement of the sawteeth.

temperature modulation has been so sporadic that we really need to repeat this experiment several times to say with confidence that there is a phase dependence in the ion temperature modulation. Looking at the best fit sinewaves, notice that the phase of the modulation is always the same (or nearly so) even between the extreme phase differences $+90°$ and $-90°$. To set the phase difference between the two oscillators we fix the OPCD oscillator start time and change the OTCD oscillator start time. The fact that the phase of the modulation stays put for each phase difference indicates that the ion temperature modulation is driven almost entirely by the OPCD oscillator. This isn't too surprising. Since the magnetic field is mostly poloidal at the edge, we'd expect the oscillator that drives poloidal current to have the greater influence, whatever the mechanism. Look back at the section on Anomalous Ion Heating in the OPCD section for more on this.

5.3.4 Temperature profiles

The electron temperature profile is measured with the Thomson scattering diagnostic, which takes a snapshot of the temperature profile at several different chords. Electron temperature is particularly important to OFCD since current drive goes with resistivity and resistivity (according to Spitzer) goes with $T_e^{-1.5}$. Changes in T_e vs time and phase difference could explain the unusual phase dependence in figure 5.44. Figure 5.63 shows the temperature profile for 3 time points in one cycle for drive and antidrive modes of operation. Figures 5.64 shows the electron temperature vs time for 3 different radii, the core (r=0), the m=1 n=6 resonant surface, and the reversal surface for drive and antidrive phases.

Evidence of a sinusoidal modulation is not easy to see until the 9 chords are put together in the contour plot shown in figures 5.65 and 5.66. The horizontal axis is time. Shown underneath are various waveforms. In the maximum current drive phase, the closest correlation to the temperature appears to be the helicity injection rate. In antidrive it appears to be the plasma current. The latter is believable since the temperature is (mostly) driven by ohmic dissipation of the toroidal current. Why T_e should be correlated with dK/dt in the drive phase is unclear, especially considering the phase difference for maximum current drive is not the phase difference that maximizes helicity

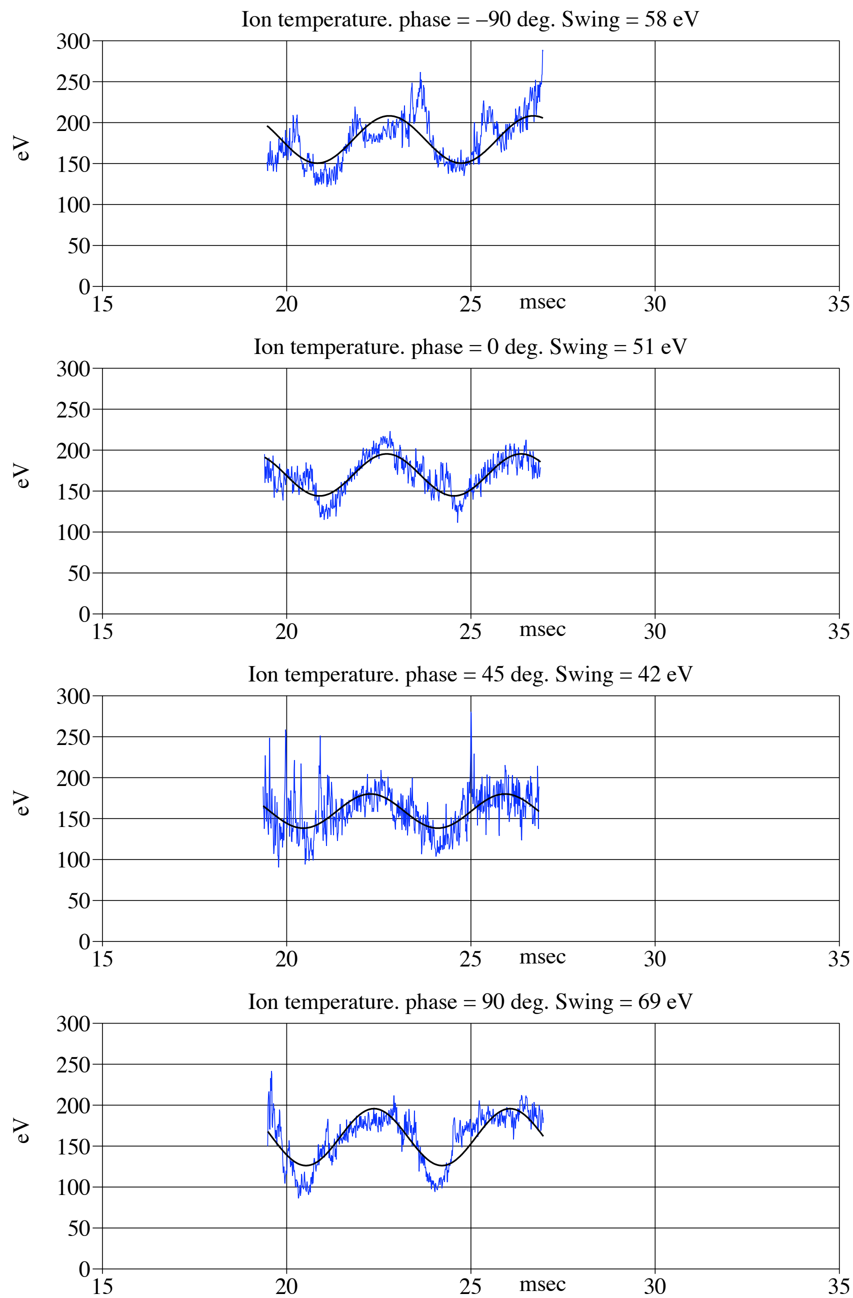

Figure 5.62 Ion temperature for 4 oscillator phases during 280 Hz OFCD.

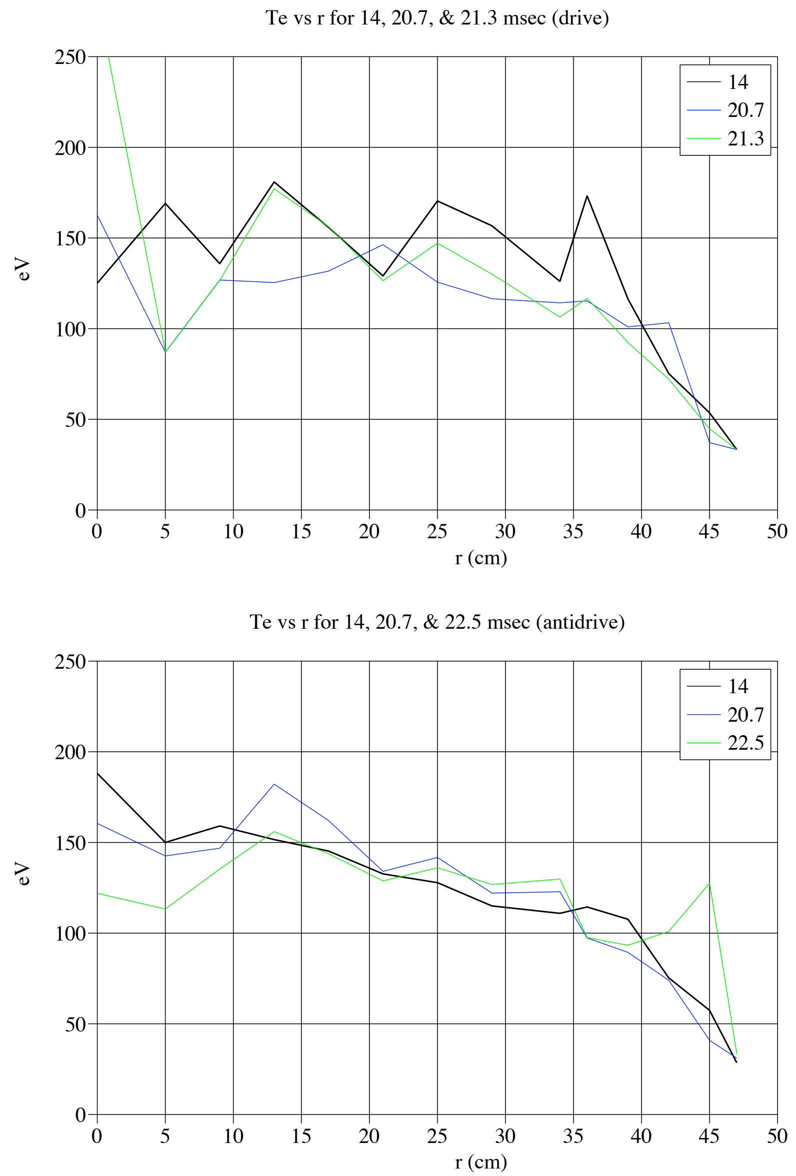

Figure 5.63 Electron temperature profile during 280 Hz OFCD. The three curves correspond to 3 time points. The first is at 14 msec before the oscillators turn on. For the top plot oscillator phasing is set for maximum current drive. For the bottom plot phasing is set for maximum antidrive.

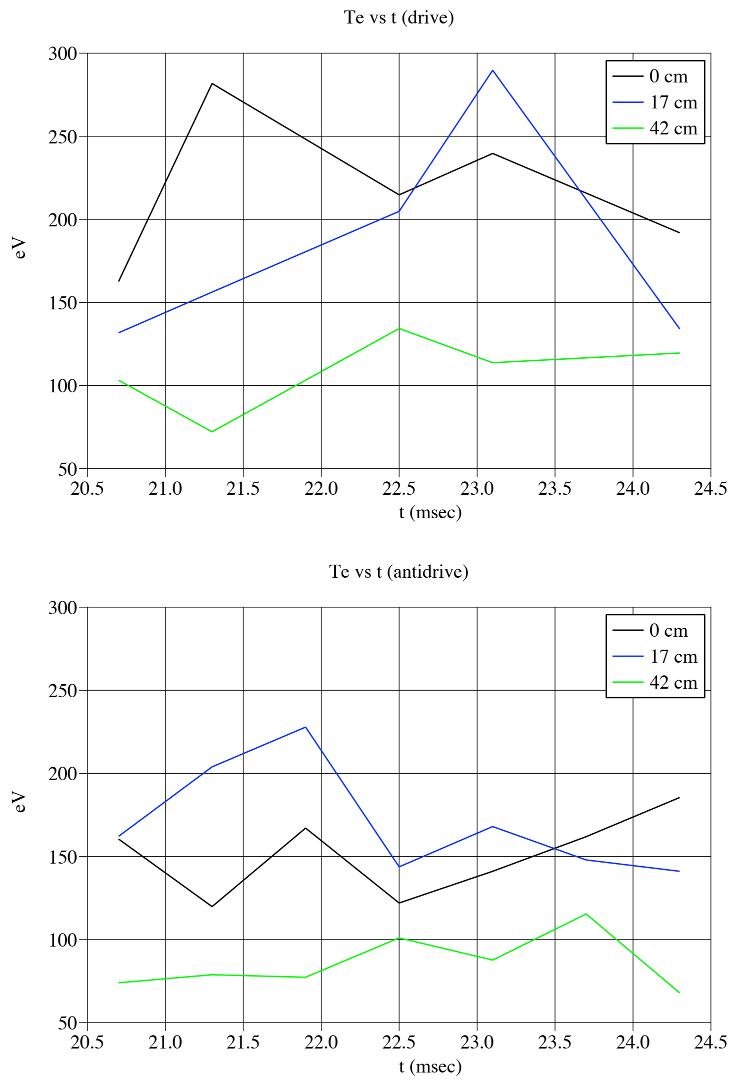

Figure 5.64 Electron temperature vs time for three different radii: r=0 (the core), r=17 cm (the m=1,n=6 resonant surface,) and r=42 cm (the reversal surface) during 280 Hz OFCD. In the top plot the oscillators are phased for maximum current drive. In the bottom plot they are set for maximum antidrive.

injection. Confounding this effort to find a corelation is the fact that whatever the driving force, the temperature response is probably going to be delayed, especially near the core.

Whatever the temperature does or what it correlates with is not as important to OFCD as what it means for the resistivity.

5.3.5 Resistivity profile

Given the electron temperature profiles we can get a measure of the resistivity of the plasma vs time. The Spitzer equation is used along with an effective value of the atomic number Z that varies with radius.

$$\eta(r) = \frac{\pi Z_{eff}(r) e^2 m^{1/2}}{(4\pi\epsilon_0)^2 (kT_e)^{3/2}} ln\Lambda \tag{5.11}$$

Where $ln\Lambda$ is the Coulomb logarithm and is about 10 for most plasmas. $Z_{eff}(r)$ is an offset sinusoid with an average value of 3, $Z_{eff}(r) = 2.5 + sin(2\pi r/2)$. The shape of Z_{eff} is a neoclassical correction provided by Anderson[24]. The bulk resistance, R_p, the volume integral of the resistivity, is shown in figure 5.67 along with the gap voltages and plasma current (all normalized for easy comparison.) With a little imagination we can say the resistance in the top plot vaguely resembles a sinusoid. But it doesn't fall in phase with either of the gap voltages or the plasma current. We'd expect the resistance to depend on the plasma current since higher current means more dissipated power means higher temperature means lower resistivity. The time difference may be because the oscillating current deep in the core, where resistance is lowest, might be slightly out of phase with the total current measured by the Rogowski coil at the edge of the plasma.

5.3.6 Penetration

The current generated by OFCD in the edge has got to find its way into the core to be a candidate for full sustainment. We expect this to happen via the same dynamo action that MST normally uses to drive current into the edge, only backwards. The Far InfraRed interferometer yields a measure of the toroidal current density and poloidal magnetic field profiles. From these the parallel current density is derived. Figure 5.68 shows the parallel current density $J_{\|}$ at various radii. Our oscillation

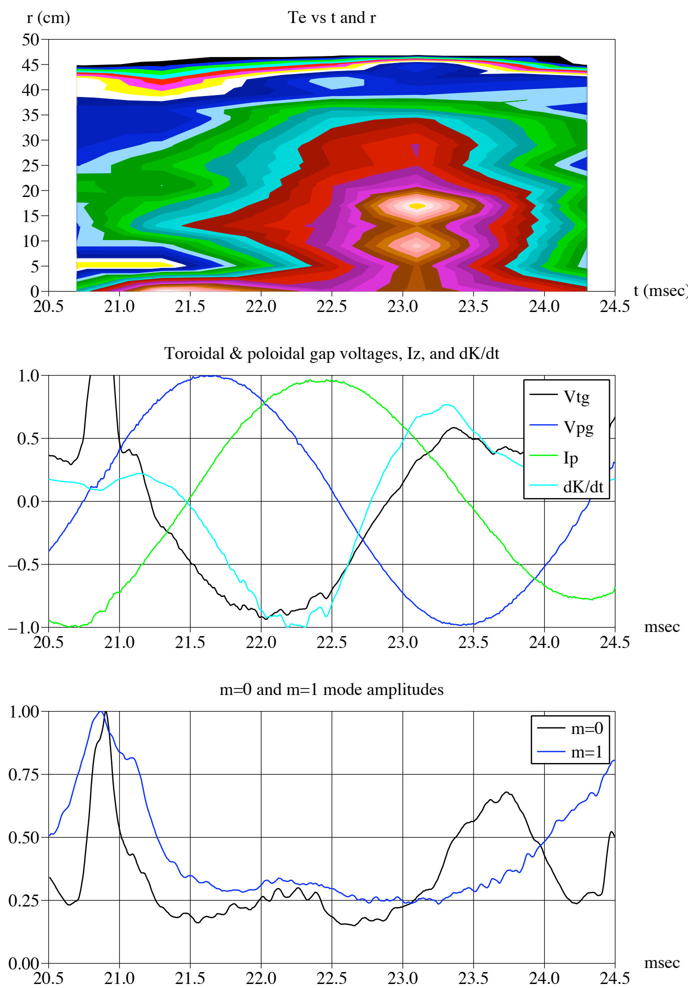

Figure 5.65 Electron temperature vs radius and time. In the contour plot at the top, the horizontal axis is time in msec and the vertical axis is radius. The middle plot shows the normalized gap voltages, the plasma current, and the helicity injection rate. The bottom plot shows the normalized m=0 and m=1 mode amplitudes. The oscillator phase difference is set for maximum current drive.

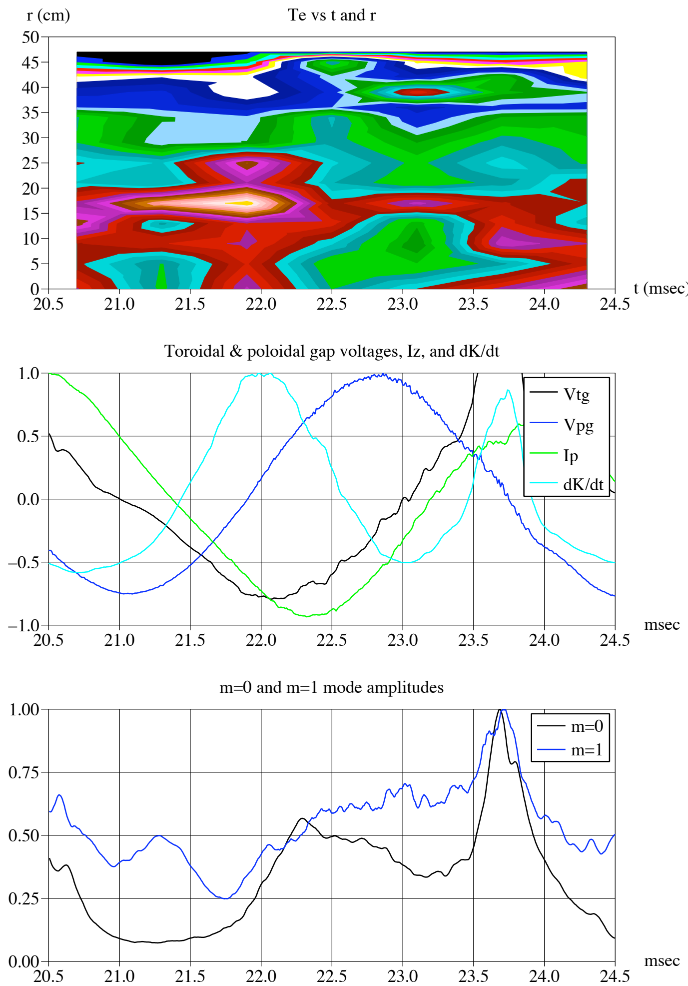

Figure 5.66 Electron temperature vs radius and time. In the contour plot at the top, the horizontal axis is time in msec and the vertical axis is radius. The middle plot shows the gap voltages, the plasma current, and the helicity injection rate. The bottom plot shows the m=0 and m=1 mode amplitudes. The oscillator phase difference is set for maximum current antidrive.

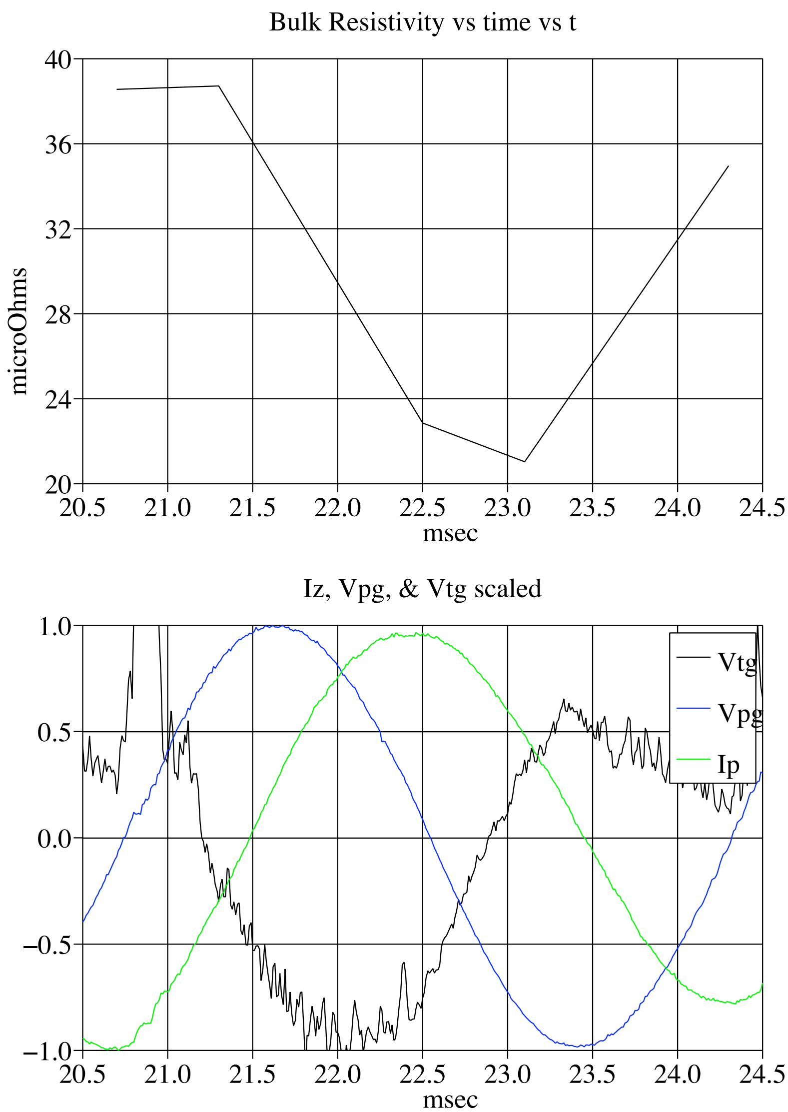

Figure 5.67 The top plot shows bulk resistivity of the plasma. The bottom plot shows the gap voltages and plasma current. The resistance appears to oscillate out of phase with applied voltages and plasma current.

is obvious. The oscillators start at 15 msec. We see a sizable modulation of the current near the core and almost no current at the edge.

There is a puzzling feature in the very last plot in figure 5.68. It shows very little current density near the edge. The conductivity of the plasma goes to zero at the very edge of the plasma so we expect the current to go to zero at r=a. But we should see a sizable current at least *near* the edge. The standard OFCD picture is an edge current driven by $\mathbf{V}_{00} \times \mathbf{B}_{00}$ that finds its way into the core by dynamo action, presumably during discrete sawtooth events. A relaxation mechanism that is marked by a sawtooth normally takes about 100 usec to redistribute current from the core to the edge of MST during a normal discharge. We had expected the same mechanism would carry our edge current to the core on the same time scale. When a sawtooth occurs, there would be sudden drop in the edge current and jump in the core current. Instead, it looks like the oscillating current appears almost immediately in the core. The edge current holds steady near zero and the core modulation holds steady at $0.5MA/m^2$ peak-to-peak while the cycle average value gradually rises up from $1.25MA/m^2$ to $1.5MA/m^2$. So the mechanism that carries current into the core appears to be a gentle continuous process unlike the usual violent method of current redistribution durring a sawtooth.

This what we expected to see in the 1D relaxed state model because it assumes the plasma is always relaxed. But we dismissed this part of the 1D results and emphasized long time-scale predictions just because we expected the current redistribution to occur in discrete events during sawteeth. The results of the 1D model are included in figure 5.68. The agreement is very good, especially near the edge. So, even on a short time scale, our simple 1D relaxed state model is better than we expected.

Bellan [10] suggested that the edge current in OFCD was not as Shoenberg and company had suggested but was instead the product of a compressional Alf́ven mode and a resistive diffusion mode ($\tilde{V}_{alf} \times B_{res}$) rather than from any relaxation dynamics. He did, however insist that relaxation was required to get current from the edge into the core. Bellan may have been right but in the wrong region. He assumed B had no radial component. The field in MST is stochastic throughout most of the cross sectional area. So an Alf́venic mode driven in the edge could propagate into the core and beat with modes in or near the core and driving current modulated by our oscillators. That would explain the large oscillation in the core and small oscillation in the edge. It would also explain why the core oscillation starts so quickly. But Bellan also predicted more current drive at higher frequencies. We've seen just the opposite.

Whatever the mechanism, this is all very encouraging for future prospects like full sustainment. The usual mechanism that reorganizes current in MST is brief and violent. Any violence is bound to have nasty effects on a plasma. For MST, a sawtooth is accompanied by a sudden loss of confinement. If the mechanism that distributes OFCD current across the plasma is continuous and gentle, a plasma fully sustained by OFCD may have no sawteeth at all.

Finally, figure 5.68 shows the parallel current density profile for 6 points in one cycle of the helicity injection rate. Also plotted are the profiles predicted by the 1D model. Again, agreement is very good. Note that the FIR curves are only so smooth because of the fitting routine used by the FIR team.

5.3.7 What happens if $F > 0$?

Looking back at the 1D model results we see that, for full sustainment, the reversal parameter is positive for a small portion of each cycle. Positive F has ominous implications for MST; it means we've lost the R in RFP. MST would, albeit briefly, look more like a poorly designed tokamak than an RFP. When the plasma goes out of reversal the stabilizing effect of shear is weakened. As F cycles up and down the m=0 resonant surface alternately enters and leaves the plasma, and we expect the m=0 mode amplitude to fluctuate as it does. To measure the potential impact of briefly losing reversal, the standard parameters of MST were modified to increase F enough that the plasma was able to come out of reversal for about $120°$ of a cycle. Figure 5.70 shows F and Θ and the $F - \Theta$ trajectory for 280 Hz OFCD with a density of $0.5 \times 10^{13}/cc$ and a starting current of about 230 kA. It's clear that the plasma is out of reversal for a significant portion of each cycle.

Despite having only a third of the cycle above zero the effect on the plasma is pronounced. Figure 5.71 shows the m=0 and m=1 mode amplitudes for a normal case where F is always below zero. Figure 5.72 shows what happens when F goes positive. First notice that the m=0 mode

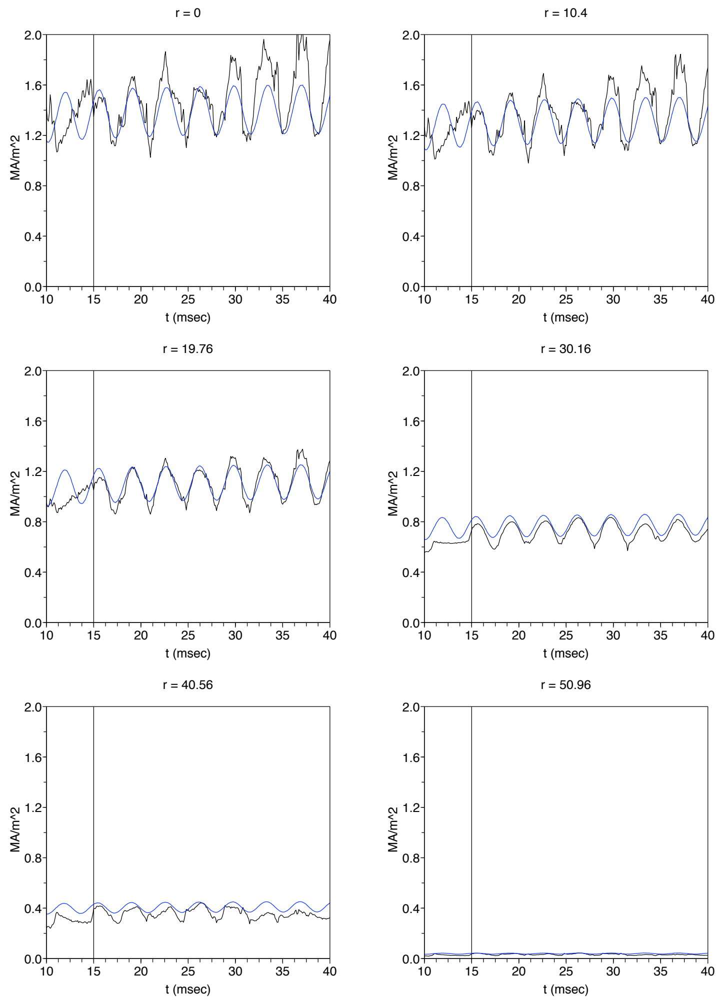

Figure 5.68 Parallel current density at various radii during 280 Hz OFCD. Oscillators begin at 15 msec. Penetration appears to occur within 1 msec. Also shown (in blue) is prediction of $J_{||}$ by the 1D relaxed state model.

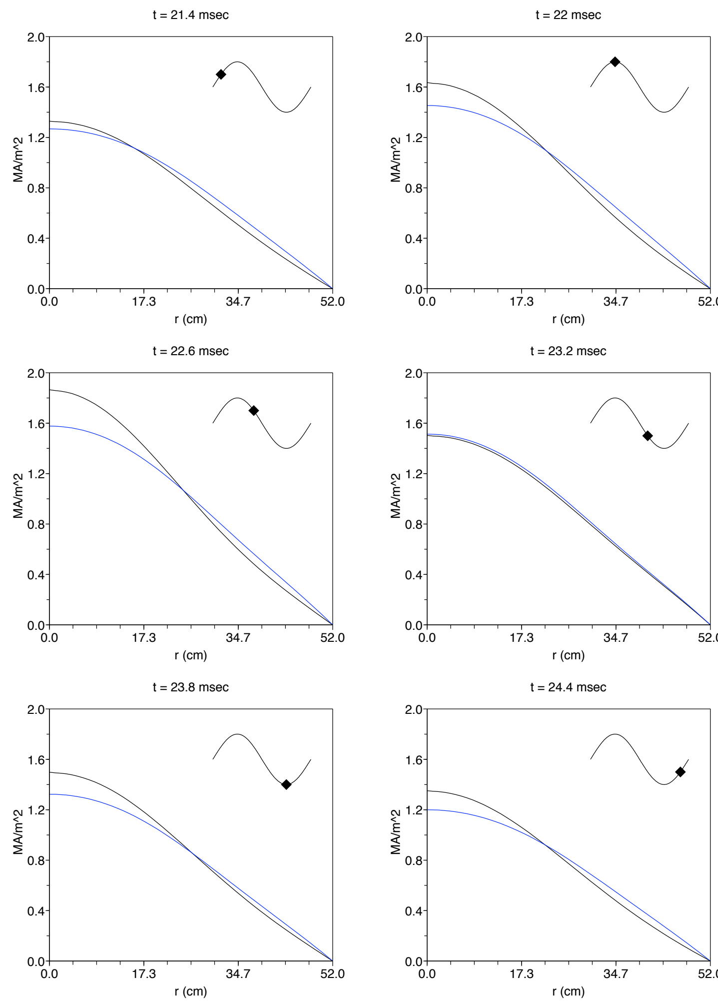

Figure 5.69 Parallel current density profile during 280 Hz OFCD. Each plot is a point on one cycle of the helicity injection rate. Also shown (in blue) is prediction of $J_{\|}$ by the 1D relaxed state model.

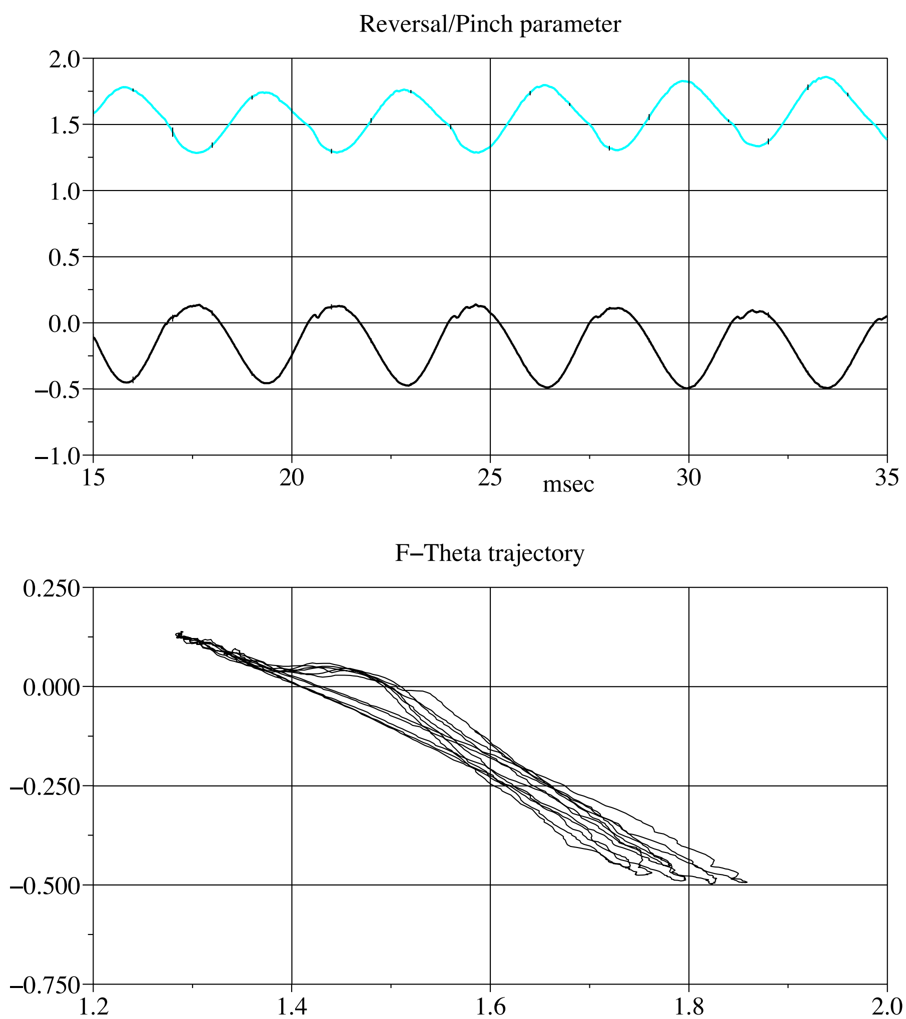

Figure 5.70 The reversal and pinch parameters during 280 Hz OFCD. The plasma conditions have been changed to allow F to go above 0 for a portion of each cycle.

amplitudes are significantly reduced when F is above 0. This is because the m=0 resonant surface is outside the plasma. Without a resonant surface the m=0 mode amplitudes are understandably reduced. The most dramatic effect is on the m=1 mode amplitude. The plot is an ensemble average so some of the finer details were averaged out, namely the rapid-fire sawteeth group that appears on the downhill side of the applied poloidal loop voltage. The ensemble averaging mushes them together into the square shapes seen in the plot. The mean value of the m=1 mode has increased 50%. This is going to reduce energy confinement and probably increase the resistivity of the plasma. Figure 5.73 shows the mean value of the m=1 mode amplitude vs the maximum value of the reversal parameter. There are only 7 points, but the trend is unmistakable.

Figure 5.74 shows the first 5 toroidal components (n=5 to 9) of the m=1 mode amplitude for the case where F is positive during part of the cycle. Since the q profile is raised and flattened the n=5 mode is probably resonant in the plasma so it is included. We can see that the n=5 component is comparable to the n=6 component. Other than that, the spectrum decays away at higher n as it normally does.

Most disturbing of all is the effect on current drive. Figure 5.75 shows the plasma current for a normal OFCD data set (F ¡ 0.) At this density and starting current the current drive is about 7 kA. Figure 5.76 shows the effect of letting F go positive. Our 7 kA current drive became -11 kA of antidrive. This is obviously unacceptable. There is hope however. All the data shown thus far in this section have been at a plasma density of $0.5 \times 10^{13}/cc$. Figure 5.77 shows the plasma current for a nominal density of $1 \times 10^{13}/cc$. The 5 kA of drive is still far below the 20 kA we usually get ($F < 0$) at this density, but at least it's positive. The lesson learned from all this is that, for full sustainment OFCD to work, the density should be as high as possible and, if possible, reversal should be maintained throughout each cycle. The excursion of F is due almost entirely to the OPCD oscillator, which is due to be replaced with a programable power supply. With the flexibility to create arbitrary waveforms, the solution may be simply to lop off the top of the OPCD voltage to forcibly maintain reversal.

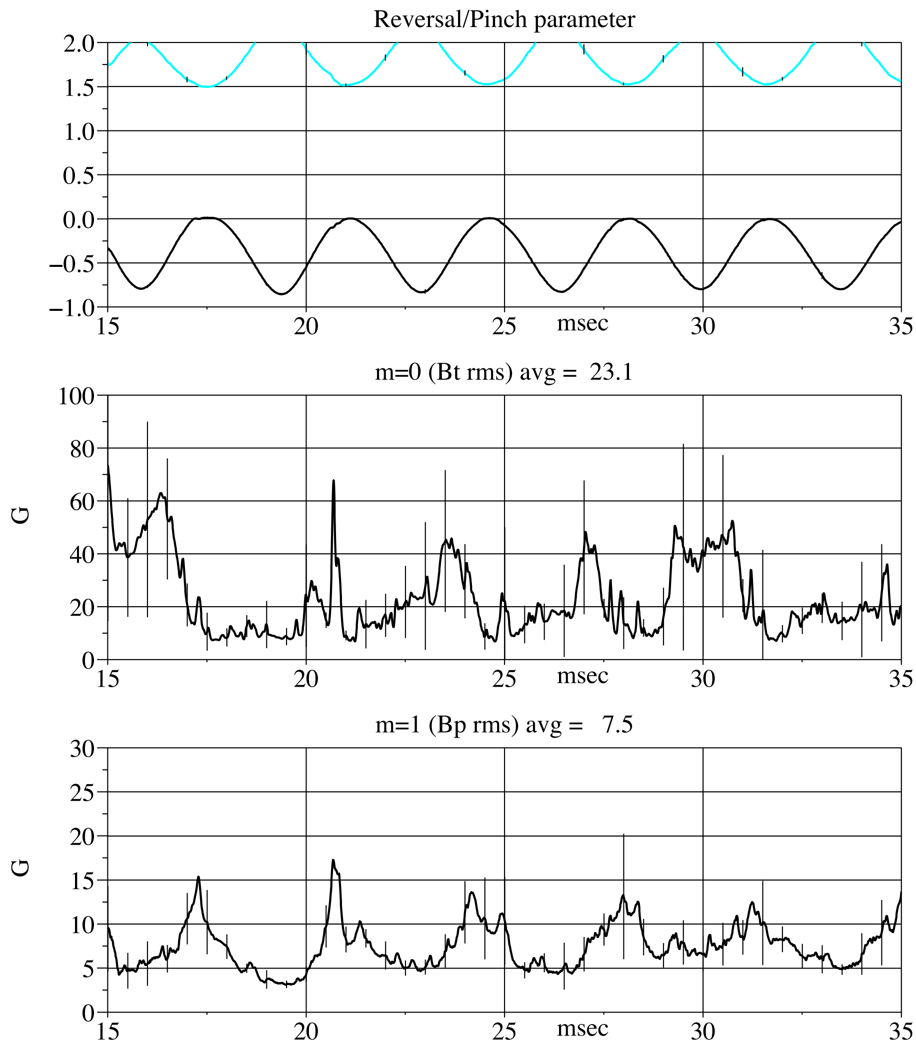

Figure 5.71 The m=0 and m=1 mode amplitudes during a normal 280 Hz OFCD with F always negative.

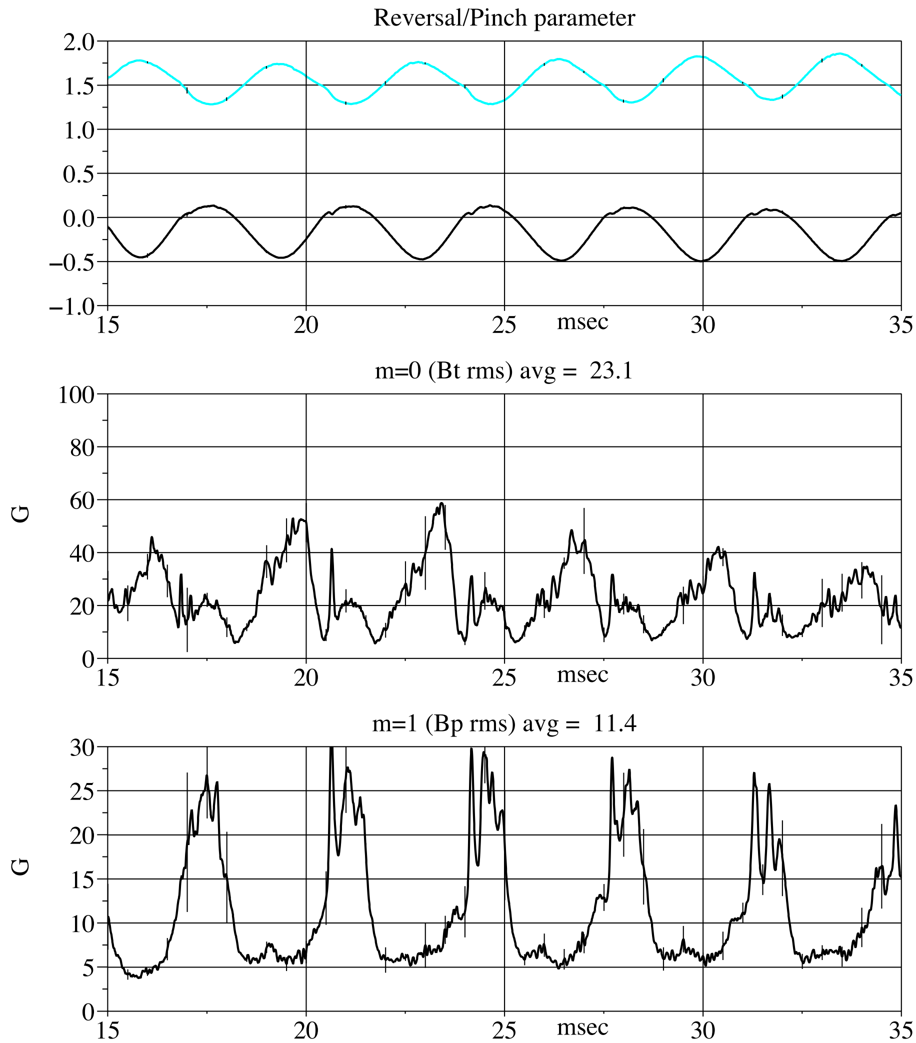

Figure 5.72 The m=0 and m=1 mode amplitudes during 280 Hz OFCD. Letting F go positive for even a portion of the cycle causes the m=1 mode amplitude to significantly increase.

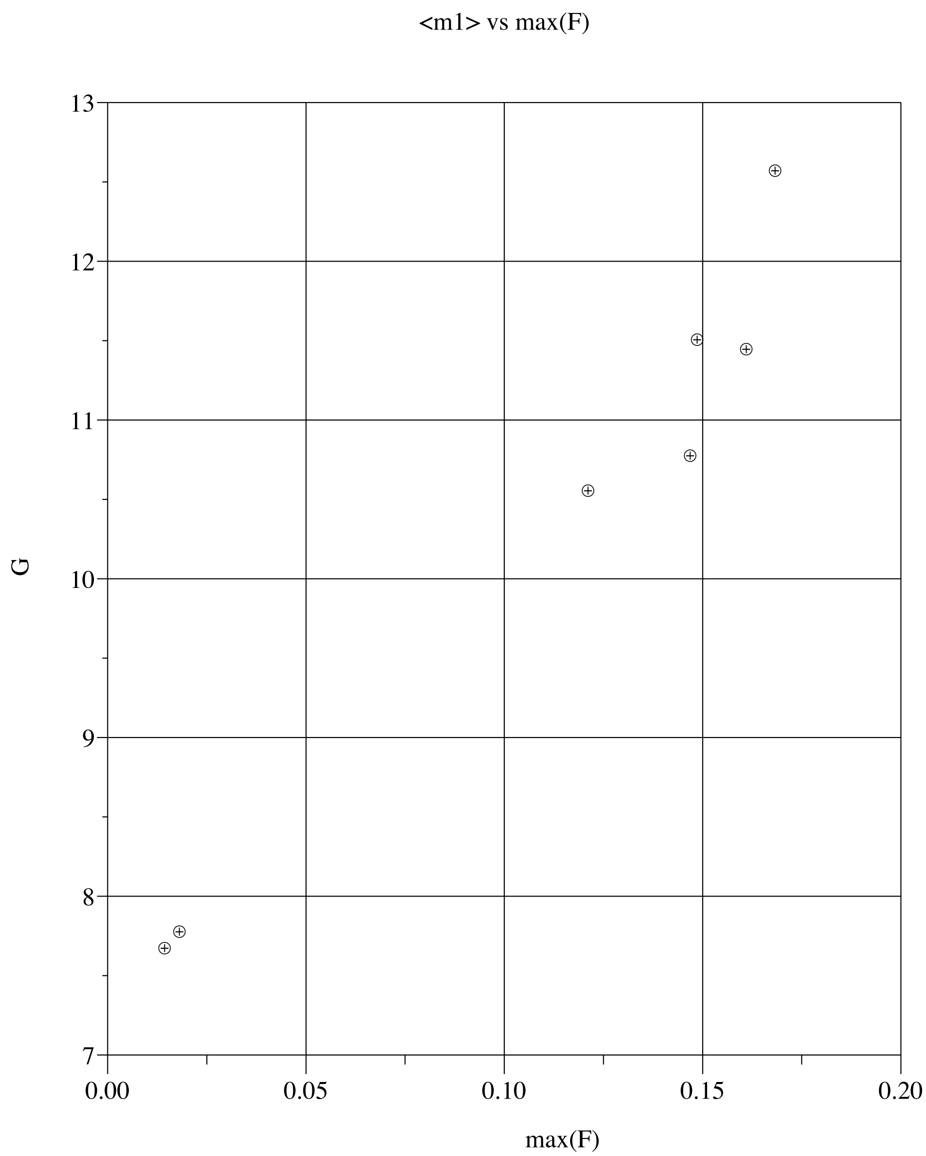

Figure 5.73 The mean value of the m=1 mode amplitude increases dramatically as the plasma is allowed to go further out of reversal.

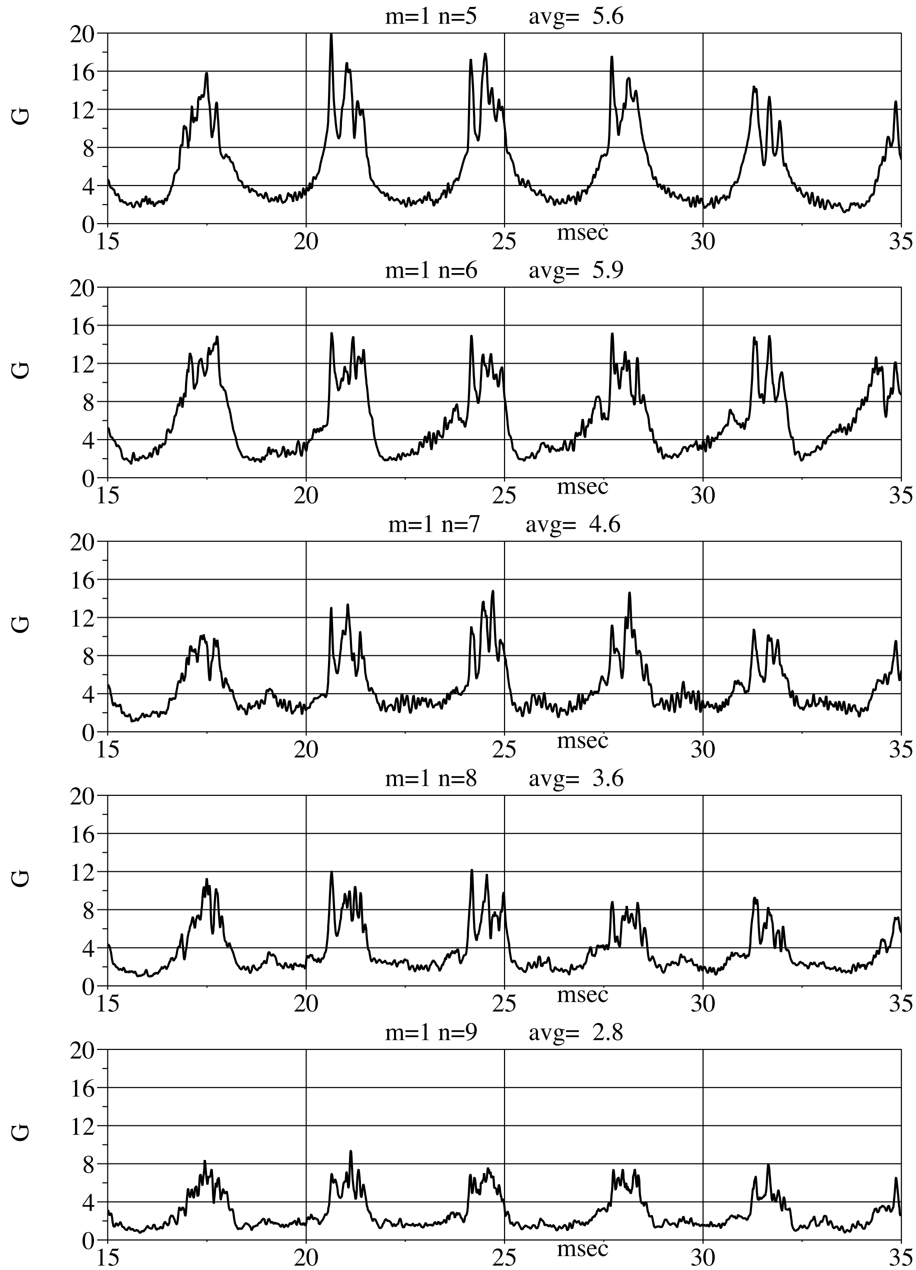

Figure 5.74 The toroidal n spectrum for the m=1 mode vs time during 280 Hz OFCD. Letting F go positive brings the m=1,n=5 resonant surface into the core of the plasma.

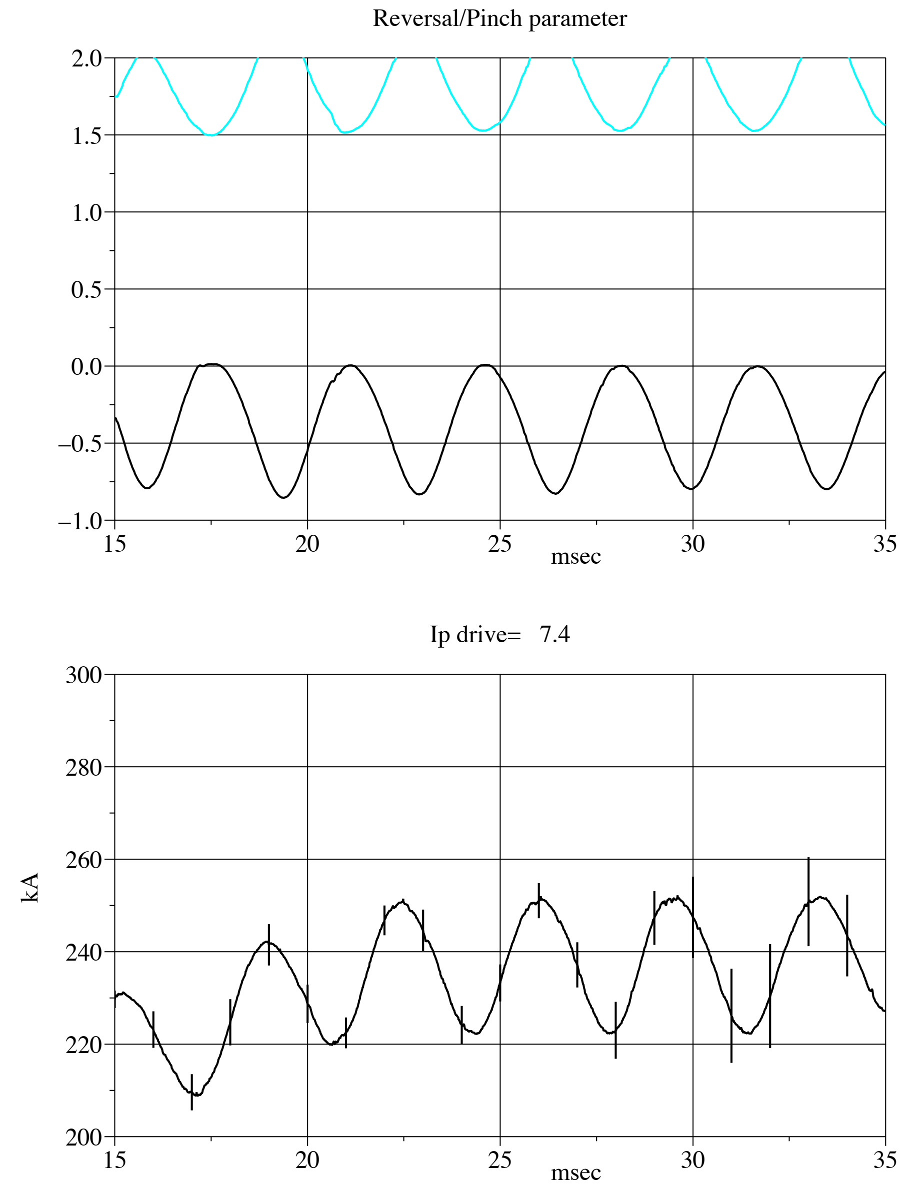

Figure 5.75 The plasma current during a normal (F¡0) 280 Hz OFCD. The nominal density is $0.5 \times 10^{13}/cc$. The vertical spikes are error bars.

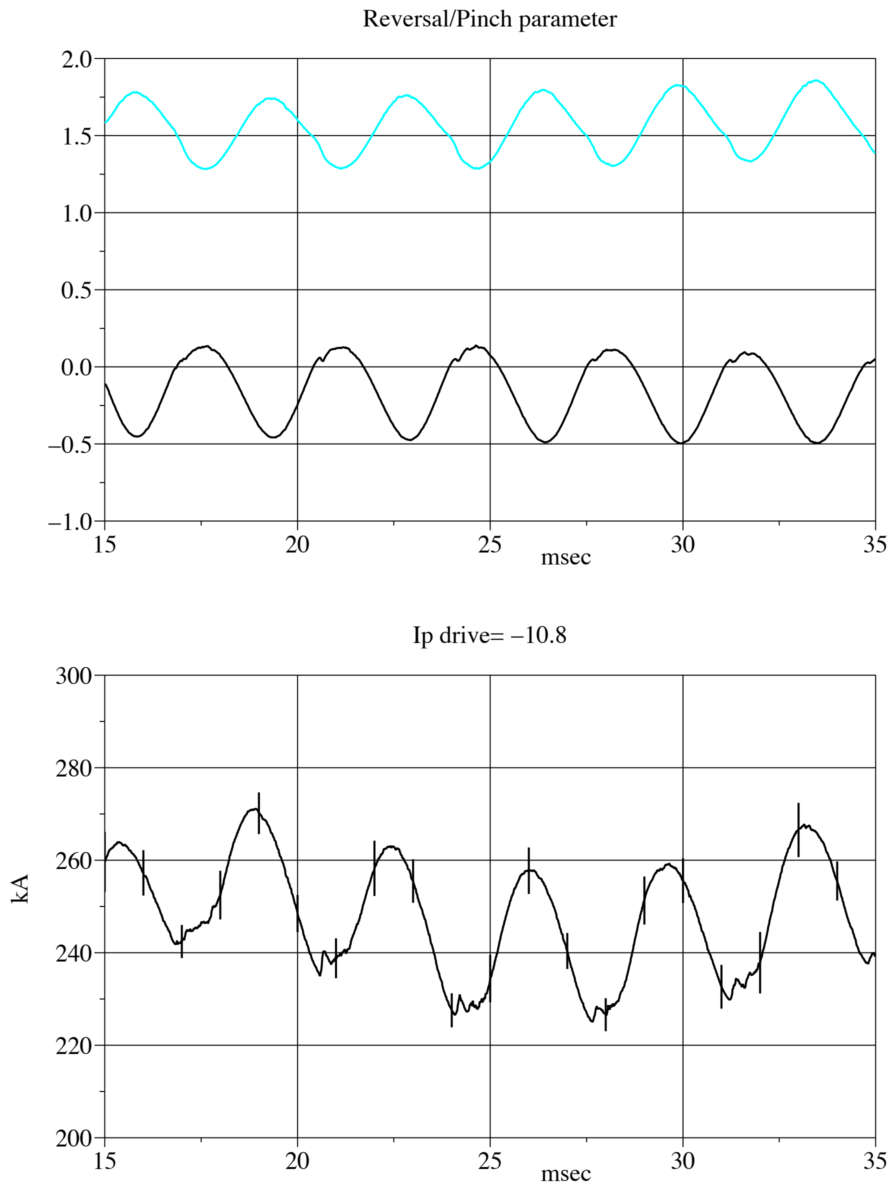

Figure 5.76 The plasma current during an abnormal 280 Hz OFCD. F is positive for a portion of the cycle. 18 kA of current drive has been lost. The nominal density is $0.5 \times 10^{13}/cc$. The vertical spikes are error bars.

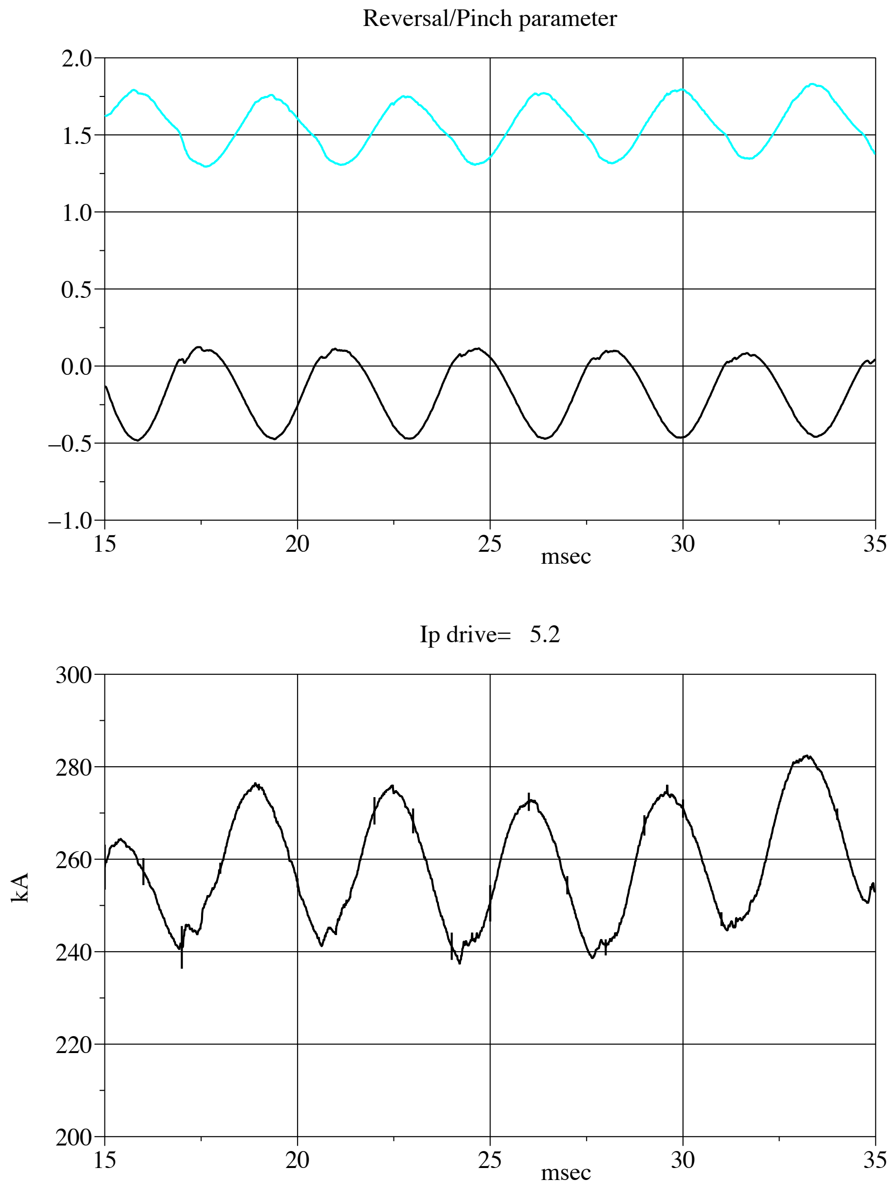

Figure 5.77 The plasma current during a normal 280 Hz OFCD with higher density. F is positive for a portion of the cycle, but there is still positive current drive. The nominal density is $1 \times 10^{13}/cc$. The vertical spikes are error bars.

Chapter 6

Summary and Conclusions

The first phase of Oscillating Field Current Drive (OFCD) experiments has been conducted on MST and compared to numerical predictions. A low-power system was built and integrated with the toroidal and poloidal circuits of the MST main power supplies to provide two oscillating toroidal and poloidal loop voltages on top of the usual supply voltages. The oscillators consist of a Pulse Forming Network feeding a resonant LC tank driven by two temperamental commutating ignitrons. The oscillator that supplied an oscillating loop voltage was labeled OTCD (Oscillating Toroidal Current Drive) and the other was labeled OPCD (Oscillating Poloidal Current Drive.)

A simple one dimensional model was used to make long term cycle averaged predictions of the current drive as well as other macroscopic parameters like power dissipation and field reversal. The model employs only energy balance and an assumed shape of the $J_{\|}/B$ profile. Several variations of the model were studied and each yielded comparable results. The model used for predictions and optimization was the relaxed state model, where a shape factor of the $J_{\|}/B$ profile was held constant and a scale factor was free to roam. The model predicted that current would be maximized when the helicity injection rate was maximized which occurs when the toroidal oscillator is $+90°$ out of phase with the poloidal oscillator. It also predicted the current drive would exhibit a sinusoidal dependence on the phase difference and that a maximum negative current would be driven in the plasma when the oscillators were $-90°$ out of phase. The model predicted that with decreasing frequency the current drive would increase but the power dissipated in the plasma and the modulation of the reversal parameter would rise rapidly. The model predicted current drive would immediately appear in the core but that result was dismissed because of the simplicity and assumptions built into the model. On that score, the 1D model's prediction proved to more closely match experimental results than any other prediction it made.

The model was used to optimize the amplitude, frequency, and waveform shape of the applied voltages. For partial sustainment, the criterion for the optimal frequency was that the plasma never go out of reversal. The optimization of the waveform shape proved fruitless because of the filtering effects of the plasma and the helicity injection process. The model did provide the optimal relative voltage amplitudes. The results of the optimization effort using the 1D relaxed state model was that the optimum frequency should be about 280 Hz, the phase difference between the oscillators should be $+90°$, and the applied toroidal loop voltage should be about 10 times larger than the applied poloidal loop voltage. Using these parameters and the voltage levels attainable with available hardware, the model predicted a supplementary current drive of 13 kA (5%) in MST for the partial sustainment case where OFCD is superimposed on the usual power supplies. It predicted a maximum antidrive current of -15 kA if the oscillators were phased for it. It also predicted that full (OFCD only) sustainment was achievable at this frequency if the voltages were increased by a factor of 3 but that the plasma would go out of reversal for a small fraction of each cycle.

Where available, results of a prior study using a 3D MHD model were compared to both the 1D model and to experimental results. The 3D model predicted maximum supplementary current drive would occur when the phase difference between the oscillators was about $+45°$, which proved to be closer to the experimental results than the prediction by the 1D model. The 3D model also predicted the sawteeth events in MST would be entrained to the applied oscillation, which also proved to be true. It also predicted that current drive would decrease with increasing frequency, as predicted by the 1D model and verified in the experiments.

To isolate the effects of each oscillator, initial experiments were conducted with one of the two oscillators turned off (usually because it hadn't been built yet.) The results of the OPCD experiments included a significant but difficult to reproduce modulation of the ion temperature. The ion temperature modulation can be at least partially explained by collisional heating by magnetic pumping though the results of some experiments greatly exceeded this predictor. Also observed was a very large excitation of the $m = 0$ modes accompanied by little or no excitations of the $m = 1$ modes. The modulation of the current profile by the OPCD oscillator caused an entrainment of the sawteeth events that mark an ordinary MST discharge. These effects all proved useful to other MST experiments for studying the MHD dynamo. The most extensive of these experiments were edge probe studies designed to determine the stability of the $m = 0$ modes. The results of that study suggest that the $m = 0$ mode might be linearly unstable during those intervals where OPCD excites the $m = 0$ modes, though the error bars of that experiment were too large to make any decisive judgement. OTCD experiments were also conducted and similar behavior was observed, but the effects were much weaker than observed in OPCD.

When both oscillators came online, OFCD experiments were conducted at two frequencies and a variety of plasma conditions. The most important question, 'Does OFCD drive current?', has been answered. Supplementary current of about 8% was consistently observed - more than predicted by 1D modelling and about what was predicted by 3D modelling- though there are still open questions about the mechanism of that current drive. The amount of supplementary current exhibited little or no dependence on the nominal (oscillators off) current. Current drive was dependent on density, higher densities being preferred.

While current drive did display a dependence on the phase difference of the oscillators, the shape of that dependence was not the sinusoid predicted by modelling. Maximum current drive does not occur when the phase difference is set to maximize the helicity injection rate. Whereas helicity injection rate is maximized at a phase difference of $+90°$, the current was maximized at about $+30°$. Nevertheless, the amount of positive current drive was comparable (within a factor of 2) to that predicted by both 1D and 3D numerical studies. When the phase difference between the oscillators was set to maximize negative helicity injection, the amount of negative current driven (that is, current subtracted from the nominal value) was much larger than predicted.

It is unclear how much of the observed current drive was due to classical OFCD dynamics and how much was due to modification of nominal plasma parameters like confinement. The $m = 0$ and $m = 1$ fluctuation amplitudes exhibited a significant dependence on the phase between the oscillators. Greater fluctuation levels usually mean less confinement. More pedestrian factors like plasma-wall interactions may also be contributors. Emisions from impurities did exhibit a visible dependence on the phase between the oscillators.

Why the mode amplitudes and impurity emisions should depend on the phase difference between the oscillators as they do is an unanswered question as is the peculiar shape of the current drive dependence. But from an engineering perspective, the conclusion from the experimental phase dependence studies is that the phase difference between the oscillators should be about $+30^\circ$ to maximize performance.

One objective of the experiments was to optimize the frequency of the applied oscillations. Higher frequencies mean more cycles within the duration of the MST plasma, so experiments were conducted first at 530 Hz. It was determined that 530 Hz was too high for the relaxation dynamics OFCD relies upon to have the desired effect. Lower frequency experiments at 280 Hz proved more fruitful as predicted by the 1D model. Adequate current penetration well past the reversal surface was observed in keeping with predictions by both the 1D and 3D model, though the measured current profiles differed substantially from the predictions of the 3D model. It was a pleasant surprise to find that the current drive penetrated to the core much faster than expected by intuition. It appears the mechanism that redistributes OFCD current from the edge to the core was more continuous than the discrete and violent method the MST plasma normally employs to redistribute current from the core to the edge.

The helicity injection and dissipation rates were 'measured' using the α-model fitted to experimental edge data. Just enough positive helicity injection to balance dissipation was observed for maximum drive phase OFCD. Dissipation substantially outpaced injection during antidrive experiments.

Also studied was the effect of allowing the plasma to travel briefly out of reversal as it is expected to do in future full sustainment experiments. The effects of allowing even brief intervals on nonreversal were pronounced. The m=1 mode amplitudes nearly tripled at their peak values. The effect greatly hindered current drive, eliminating it altogether at low densities. The damage is somewhat alleviated by higher densities. Some means of maintaining reversal would be preferred.

A programmable power supply may offer hope. Increasing the frequency of oscillation should also help but it would come at the expense of current drive.

6.1 Future plans

Future experiments will focus on explaining the strange phase dependence of current drive and extrapolating what we can to full sustainment OFCD. Of particular interest will be the plasma-wall interactions that confounded the ZT-40 experiments. Also of interest are the effects on confinement and stability when the plasma is pressed out of reversal by future higher power experiments.

We will continue to take advantage of our ability to isolate the effects of the OPCD and OTCD oscillators. We hope to determine whether the OPCD ion temperature oscillation is real or a problem with the Rutherford scattering diagnostic. If the diagnostic proves true, we hope to determine the mechanism that drives such an enormous temperature oscillation and why it doesn't show up in corroborating diagnostics like IDS and why it's appearance is so sporadic.

The reliability of the ignitron oscillators has improved but is still not as good as we hoped for some seven years ago. The failure rate of the ignitrons has been our greatest impediment to progress in this experiment. Some diagnostics, like Rutherford scattering and probe work require enormous ensembles. Every shot counts at 1 O'clock in the morning. Work continues in preventing ignitrons that are supposed to stay on from turning off and ignitrons that are supposed to switch off from staying on. The author would prefer that all ignitrons be gathered from the four corners of the earth, forcibly if necessary, and either thrown into the sun or buried deep with nuclear waste.

The next generation medium power oscillators will likely be beefed up versions of the current ignitron oscillator design. By using bigger ignitrons, we hope to double or even triple our available power. This will get us closer to a full sustainment system with minimal investment. The only risk is blowing up what we already have, a win-win scenario either way.

Also in the works are programmable power supplies that will allow arbitrary waveforms (within some bandwidth) supplementing the existing supplies. The flexibility of programmable supplies will broaden OFCD experiments considerably. We can play with sine waves, square(ish) waves, triangles, whatever. One experiment of particular interest to the author is a chirped sinewave that sweeps across some frequency band during the discharge, accommodating long term changes in the plasma. Only the toroidal field supply (OPCD) will be implemented first. But we've seen that OPCD has greater impact on the plasma than OTCD so OPCD studies should yield insights into what to expect with programmable supplies in each circuit.

Someday, God willing, the entire MST power supply system will be replaced with megapower programmable supplies with enough juice to attempt full-sustainment OFCD. By that time the medium power experiments should have yielded enough results to predict the viability of full-sustainment.

I might even graduate by then.

LIST OF REFERENCES

[1] J.M. Berger, W.A. Newcomb, J.M. Dawson, E.A. Frieman, R.M. Kulsrud, A. Lenard, Phys. Fluids **1** 301 (1958)

[2] J.B. Taylor, Physical Review Letters **33** 1139 (1974)

[3] M.K. Bevir, J.W. Gray, *Proceedings of the Reversed Field Pinch Theory Workshop*, Los Alamos Report LA-8944-C, (1981)

[4] K.F. Schoenberg, R.F. Gribble, J.A. Phillips, Nuclear Fusion **22**, 1433 (1982)

[5] K.F. Schoenberg, C.J. Buchenauer, R.S. Massey, J.G. Melton, R.W. Moses, R.A. Nebel, J.A. Phillips, Phys. Fluids **27**, 548 (1984)

[6] K.F. Schoenberg, R.F. Gribble, D.A. Baker, J. Appl. Phys. **56**, 2519 (1984)

[7] T.H. Jensen, M.S. Chu, Phys. Fluids **27**, 2281, (1984)

[8] M.K. Bevir, C.G. Gimblett, G. Miller, Phys. Fluids **28**, 1826 (1985)

[9] P.M. Bellan, Physical Review Letters **53**, 1381 (1985)

[10] P.M. Bellan, Physical Review Letters **54**, 1381 (1985)

[11] J.M. Finn, Phys. Fluids **29**, 2630 (1986)

[12] R.A. Nebel, K.A. Werley, R.A. Scardovelli, G.H. Miley, D.S. Harned, H.R. Strauss, D.D. Schnack, Z. Mikić, Paper IAEA-CN-47/D-V-12, *Plasma Physics and Controlled Nuclear Fusion Research*, Vol II p 701 (1986)

[13] D.S. Harned, D.D. Schnack, H.R. Strauss, R.A. Nebel, Phys. Fluids **31** 1979 (1988)

[14] K.F. Schoenberg, J.C. Ingraham, C.P. Munson, P.G. Weber, D.A. Baker, R.F. Gribble, R.B. Howell, G. Miller, W.A. Reass, A.E. Schoefield, S. Shinohara, G.A. Wurden, Phys. Fluids **31**, 2285 (1988)

[15] J.C. Sprott, Physics of Fluids **31**, 2266 (1988)

[16] J.B. Taylor, M.F. Turner, Nuclear Fusion **29**, 219 (1989)

[17] M.R. Brown, P.M. Bellan, Phys Rev Lett, **64** 2144 (1990)

[18] J.C. Sprott, Internal Report PLP 1084, (1991)

[19] W. Shen, J.C. Sprott, Physics of Fluids B **3**, 1225 (1991)

[20] A.A.E.van Blockland et al, Rev. Sci. Instrum. **63** (1992)

[21] R. Dendy, Plasma Physics - An Introductory Course, Cambridge Univ Press (1993)

[22] F. Ebrahimi, S.C. Prager, J.S. Sarff, J.C. Wright, Physics of Plasmas Vol 10, No 4, pp 999 (2003)

[23] F. Ebrahimi, PhD Thesis

[24] J. Anderson, PhD Thesis

[25] S. Choi, PhD Thesis

[26] A.J. Redd et al, Proceedings of the APS division of Plasma Physics conference, 2005. Poster GP1.00090

[27] D.J. Holly et al, Proceedings of the APS division of Plasma Physics conference, 2005. Poster BP1.00039

[28] S. Ortolani, D. Schnack, Magnetohydrodynamics of Plasma Relaxation, World Scientific Publishing. (1993)